PhD Grant FRH/BD/62273/2009
Project FCOMP-01-0124-FEDER-027894

FCT
Fundação para a Ciência e a Tecnologia
MINISTÉRIO DA EDUCAÇÃO E CIÊNCIA

POPH
PROGRAMA OPERACIONAL POTENCIAL HUMANO

QREN
QUADRO DE REFERÊNCIA ESTRATÉGICO NACIONAL
PORTUGAL 2007.2013

UNIÃO EUROPEIA
Fundo Europeu de Desenvolvimento Regional

COMPETE
PROGRAMA OPERACIONAL FACTORES DE COMPETITIVIDADE

Intensified Bioprocess for the Anaerobic Conversion of Syngas to Biofuels
Filipa Maria Rodrigues Pereira
UMinho | 2014

Universidade do Minho
Escola de Engenharia

Filipa Maria Rodrigues Pereira

Intensified Bioprocess for the Anaerobic Conversion of Syngas to Biofuels

julho de 2014

Universidade do Minho
Escola de Engenharia

Filipa Maria Rodrigues Pereira

Intensified Bioprocess for the Anaerobic Conversion of Syngas to Biofuels

Tese de Doutoramento em Engenharia Química e Biológica

Trabalho efetuado sob a orientação da
Doutora Diana Z. Sousa
do
Doutor Nuno M. Reis
e da
Doutora M. Madalena Alves

julho de 2014

Acknowledgments

At the end of this intensive scientific experience, I want to thank all the people that somehow contributed to this PhD, by helping me in achieving great scientific and personal accomplishments. So, in the next paragraphs I address some simple and sincere words of gratitude and appreciation to those who were essential for me in getting this far.

I grateful and deeply acknowledge my supervisors, Dr Diana Sousa, Dr Nuno Reis, and Dr Madalena Alves, who acting as my scientific "godfathers", gave me the opportunity to start this PhD and shared with me their experience and knowledge. I thank you for your wise advices and for believing in me since the very first moment we made contact, for supporting me in the moments I needed, and most of all, for opening my eyes in those moments when confidence and determination seemed to loose strength inside me.

Diana, agradeço-te por me teres desafiado a iniciar este PhD, pelo teu apoio desde o início e por teres partilhado comigo o teu fascínio pela investigação. Nunca esquecerei o entusiasmo que sempre colocavas em cada discussão científica ou mesmo em simples tarefas no laboratório, e em muitos outros momentos completamente alheios à investigação. Obrigada por sempre encontrares um tempo livre para ouvires e responderes às minhas questões, quaisquer que fossem, e por sempre me fazeres olhar para o meu trabalho com optimismo e confiança.

Nuno, your way of working, thinking, and getting deep inside research, and your attitude in many other aspects outside research, were a wonderful inspiration for me. Under your guidance I experienced the best moments of this PhD. For me, you will always be a model of strength, determination, and honesty, with both professionalism and friendship. Thank you for constantly defying my limits with stimulating challenges, and for being always willing to discuss anything about my work and my personal interests.

Madalena, agradeço-te por me teres recebido no antigo grupo LBA, mesmo antes de começar este PhD, e por toda a confiança e expectativa que puseste em mim e nas minhas capacidades. Ainda recordo o modo como me disseste que eu seria a pessoa certa para começar e "enfrentar" os desafios deste novo tópico de investigação no BRIDGE. Agradeço principalmente a confiança depositada, nos momentos em que não se via a "luz ao fundo do túnel".

Thanks to my supervisors, I had the unique opportunity of working and spending time, in 3 renowned universities: Minho (PT), Cambridge (UK), and Loughborough (UK); places where I met wonderful people (colleagues, friends, and staff), which somehow also take part in the success of this PhD. I want to leave here a grateful acknowledgment to all, and particularly to some of those with whom I worked and related more closely, during these 4 years.

To all CEB colleagues, LBA people, Bridge group members, and Doctoral Program colleagues, I thank you for your help, presence, and concern, since I started working in CEB. Agradeço, especialmente, à Joana Alves, com quem comecei esta "aventura" do syngas. Joana, podes não estar ciente disso, mas a tua ajuda e presença em alguns momentos particulares (mesmo nos mais pequenos detalhes) foram muito importantes para mim. Agradeço também àqueles que de uma maneira particular, deram pequenos mas essenciais contributos, durante esta fase: Sónia, Sérgio, José Carlos, Andreia, Ângela, Roberto, Liliana, Vânia, Pedro, Marta Simões e Marta Neto. Agradeço ainda a preciosa ajuda técnica da Madalena Vieira e do Sr Manuel Santos.

Cambridge was my first big challenge during this PhD. The "unofficial" co-supervision of Professor Malcolm Mackley was very important in getting familiar with OFM technology and principles. To the person and the scientist I want to express my sincere acknowledgment for what I have learned from him. Many other people from the Dept of Chem Eng and Biotech, including former Polymer Fluids group members, gave me very important assistance. I specially mention Arjan Abeynaike, Ben Taylor, Simon Butler, Lee Pratt, Gary Chapman, and Amanda Taylor. I also thank Mariana Domingos, Fernando Abegão, Hugo Oliveira, Paul Rogers, and Five Alive Music group members, for the friendship and kindness shown in all moments we shared together.

Staying in Loughborough was the second big challenge and the greatest way to finish this PhD "adventure". I acknowledge all the fantastic people I met at the university, in Reis Lab research group and in Chem Eng Dept. I thank specially, Sean Creedon for entirely trusting in my "thoroughness and professionalism" (as you told me), particularly in relation to safety, but also Graham Moody, Jorgelina Farias, Tony Eyre, Jim Muddimer, Terry Neale, Paul Izzard, Rob Bentham, Dave Smith, Kim Robertshaw, Toby Vye, and Gianluca Li Puma. I want to thank all the friends I made there and office/lab mates, in special, Ana Castanheira, Ana Barbosa, Marco Lucas, Raffaella, Plaski, Elena, Karmen, Aydin, and Chiara, for making me feel and be the best I can be. To my PH "family" I also thank all your support and affection, during this amazing period of my life. Ana, Nayia, Winta, Yen Te (aka Clark), Ovo, Andrei, Patrick, and Ele, thank you for everything you gave me and made possible to happen. Loughborough will never be the same without you all. I also acknowledge Sarantos Kyriakopoulos and Dr Cleo Kontoradvi, from the Imperial College London, for their insightful, kindly, and essential scientific support provided for performing the FBA work.

This PhD came after a wonderful 5-year graduation along with many other colleagues. Some of them also boarded in this PhD "adventure", being very close to me, sharing the same desires, frustrations, uncertainties, expectations, fears, achievements, hesitations, successes and much more. Às amigas, Ana Cristina Martins, Ana Isabel Bourbon, Liliana Santos e Vânia Ferreira, obrigada pela vossa presença, apoio e amizade em todos os momentos (mesmo os menos bons!) que partilhamos e vivemos juntas até hoje, e por tudo o que aprendi convosco. À família Reis (Nuno, Cassilda, Ema, e Edgar), obrigada pela vossa amizade, pelo apoio em alguns momentos importantes, e por me proporcionarem algumas oportunidades únicas na vida. Aos meus amigos mais próximos no sector juvenil do MMF, obrigada pela amizade e pela partilha na FÉ, ajudando-me a compreender a forma maravilhosa como Ciência e Religião caminham lado a lado. Em memória do amigo Frei Carlos Furtado, que sempre recordarei com muito carinho por tudo o que aprendi dele. A todas as pessoas da minha paróquia com quem convivo de forma mais próxima, obrigada pela compreensão, apoio, e orações, especialmente, em todas as vezes que tive de "partir", pois razões mais fortes exigiam a minha atenção total.

Finally, I thank my family, for being always here, there, everywhere, beside me. Aos "Primos Rodrigues", obrigada por serem os melhores primos do mundo; ao meu pai Virgílio, pelo orgulho que sempre teve em mim; aos tios e tias, por me animarem em cada dia; ao meu irmão Pedro e "irmã" Ana, por sempre me mimarem e se interessarem com "aquelas coisas estranhas" que investigo; e em memória do meu padrinho Domingos, que via reflectido em mim o seu gosto e desejo pelo estudo. Acima de tudo e todos, agradeço à minha mãe Agostinha, por ser o meu amparo e exemplo, e me ajudar a ser a pessoa que hoje sou.

Dedication

In honor of Jesus, King of All Nations
Em honra de Jesus, Rei de Todas as Nações
Mary, Mediatrix of All Graces
de Maria, Medianeira de Todas as Graças
and my Holy Guardian Angel
e do meu Santo Anjo da Guarda

The work presented in this thesis was financially supported by the Portuguese Foundation for Science and Technology (FCT) and European Social Fund (POPHQREN) through a research grant (ref. SFRH/BD/62273/2009) and by the FEDER funds through the project FCOMP-01-0124-FEDER-027894, financed under the Operational Competitiveness Programme (COMPETE), and by national funds through the Portuguese Foundation for Science and Technology (FCT).

Summary

In the last decades, biological conversion of syngas has been studied and explored, in order to become an environmental friendly biotechnological alternative for the chemical route. Lignocellulosic biomass and other recalcitrant residues are a widely available feedstock that can be easily converted to syngas through gasification. Anaerobic microorganisms are able to use this syngas mixture, mainly composed by carbon monoxide (CO), hydrogen (H_2) and carbon dioxide (CO_2), as energy and carbon source to produce biofuels and other valuable chemicals. In this thesis, new routes for process intensification of biological syngas conversion were explored, addressing innovative aspects for enhancing gas-liquid mass transfer and overall process efficiencies based on enhanced gas-liquid contacting using oscillatory flow mixing and biological mixed cultures. The prospection for methane (CH_4) production and other alternative products during anaerobic syngas conversion was initially studied in batch incubations, using mesophilic mixed cultures. The effect of process controlling parameters, such as medium pH, syngas total pressure, and CO partial pressure, in the efficiency of the process was investigated. Complete consumption of CO and H_2 was obtained in all conditions, in less than 72 h at 1.0 atm syngas. Methanogenic-inhibited biomass was able to produce volatile fatty acids (VFA), alternatively to CH_4 with a maximum specific production of 27.3 mM VFA atm^{-1} (at pH 6.9 and 1.0 atm). In a second approach, consumption rates of CO and H_2 were determined, achieving 0.77 and 1.64 mmol d^{-1} as the maximum values, respectively (at 2.5 atm syngas). Methane production rates were also determined, being 0.39 mmol d^{-1} the maximum obtained (at 1 atm with 60 % of CO). Methane production rate variation with dissolved CO concentration in the liquid behaved as a typical Monod kinetics, describing inhibition effect above a certain CO concentration, for experiments at higher syngas pressures. In those conditions VFA accumulation as high as 23 mM was also achieved and related with CO inhibition.

In order to design a bioreactor capable of performing intensified syngas bioconversion, gas-liquid mass-transfer performance was studied in a multi-orifice oscillatory baffled column (MOBC), using CO_2 as model gas. Different baffle configurations with varying orifice diameters (d_o) in the range of 6.4–30 mm and relative baffle open area (α) of 15–42 % were used. Bubble size distributions (BSDs) and the overall volumetric CO_2 mass transfer coefficient (K_La) were experimentally evaluated for a range of gas flow rates (0.01–0.1 vvm) and fluid oscillations (f = 0–10 Hz and x_0 = 0–10 mm). Flow visualisation and bubble tracking experiments demonstrated that a small d_o of 10.5 mm combined with small α = 15 % generates sufficient, strong eddy mixing capable of trapping an extremely large fraction of microbubbles in the column. This resulted in increased interfacial area yielding maximum K_La values of 65 ± 12 h^{-1} obtained at 0.1 vvm, representing an up to 3-fold increase in comparison to CO_2 dissolution rate in the un-baffled, steady column. A modified oscillatory Reynolds number (Re_o) and Strouhal number (St) were also presented to assist the scale-up of gas-liquid systems in oscillatory baffled columns.

The anaerobic syngas conversion initially studied in batch incubations was then investigated in the oscillatory baffled system optimised to enhance gas-liquid mas transfer. Here, the novel 10 L multi-orifice oscillatory baffled bioreactor (MOBB), was fed in batch and continuous mode with a syngas mixture composed of 60 % CO, 10 % CO_2, and 30 % H_2 (v/v), and operated under oscillatory flow mixing. The effect of mixing intensity and inlet syngas flow rates was experimentally assessed in respect to CH_4 production. Under discontinuous syngas injection, enhancement in the uptake rates of CO and H_2 (up to 6-fold and 3-fold, respectively) were obtained, showing strong positive correlation with Re_o. At the same conditions, CH_4 production rate was found to be insensitive to Re_o, suggesting that the biological methanogenic reaction controls the process, which represents a major bottleneck to batch syngas conversion using mixed anaerobic microorganisms that cannot be overcome by improving the dissolution or uptake rates of syngas components. Surprisingly, continuous syngas injection in the MOBB has resulted in up to 27-fold enhancement on CH_4 production rates and up to 8-fold in CO and H_2 uptake rates. The use of continuous gas flow led to increase reaction rates, by acting as a driving force in the kinetics of the process. The reaction rates showed strong correlation with CO loading rates assuming Monod type kinetics behaviour, changing from first order to order zero by increasing CO loading rates.

Finally, a preliminary approach of flux balance analysis was used to characterise the preferable metabolic pathways during syngas microbial conversion by mixed anaerobic cultures, showing potential for helping in enhancing process efficiency.

Resumo

Nas últimas décadas, a conversão biológica do gás de síntese tem sido explorada, visando tornar-se uma alternativa biotecnológica e ecológica à via química. A biomassa lignocelulósica e outros resíduos recalcitrantes são uma matéria-prima largamente disponível que pode ser facilmente convertida a gás de síntese, através de gasificação. Há microrganismos anaeróbios capazes de usar esta a mistura de gás, composta sobretudo por monóxido de carbono (CO), hidrogénio (H_2) e dióxido de carbono (CO_2), como fonte de carbono e energia para produzir biocombustíveis e produtos químicos. Nesta tese são exploradas novas vias para intensificação de processo da conversão biológica do gás de síntese, com melhoria da transferência de massa gás-líquido e eficiências globais do processo, explorando os benefícios do uso de mistura de fluxo oscilatório e culturas biológicas mistas. O potencial para produção de metano (CH_4) e outros produtos alternativos, durante a conversão anaeróbia do gás de síntese foi inicialmente estudada em ensaios descontínuos, usando culturas mistas mesofílicas. Estudou-se o efeito de parâmetros processuais, como o pH, a pressão total do gás e a pressão parcial de CO, na eficiência do processo. Em menos de 72 h, obteve-se consumo total de CO e H_2 em todas as condições, a 1.0 atm. A biomassa com actividade metanogénica inibida foi capaz de produzir ácidos gordos voláteis (AGV), em alternativa ao CH_4, com produção máxima específica de 27.3 mM AGV atm^{-1} (a pH 6.9 e 1.0 atm). Numa segunda abordagem, determinaram-se as taxas de consumo de CO e H_2, atingindo valores máximos de 0.77 and 1.64 mmol d^{-1}, respectivamente, a 2.5 atm, e as taxas de produção de CH_4, com 0.39 mmol d^{-1} como máximo obtido a 1 atm com 60 % de CO. A variação da taxa de produção de CH_4 com a concentração de CO dissolvida no líquido obedeceu à cinética típica de Monod, mostrando efeito de inibição acima de um certo nível de concentração de CO, para os ensaios a pressões mais elevadas de gás de síntese. Nessas condições, atingiu-se uma acumulação de AGV (até 23 mM), relacionada com a inibição de CO.

Para desenvolver um reactor biológico capaz de intensificar a conversão biológica do gás de síntese, estudou-se a transferência de massa gás-liquido numa coluna oscilatória com anteparos de múltiplos orifícios (COAMO), usando CO_2 como gás modelo. Usaram-se anteparos com distintos diâmetro de orifício (d_o = [6.4–30] mm) e área aberta (α = [15–42] %). A distribuição do tamanho de bolhas (DTB) e o coeficiente volumétrico global de transferência de massa de CO_2 (K_La) foram avaliados numa gama de caudal de gás (0.01–0.1 vvm) e oscilação de fluido (f = 0–10 Hz, x_0 = 0–10 mm). Observações do fluxo e rastreamento das bolhas demonstraram que um pequeno d_o (10.5 mm) combinado com um pequeno α (15 %) gera mistura de vórtices capaz de reter uma fracção grande de microbolhas na coluna. Isto resultou no aumento da área interfacial produzindo um K_La máximo de 65 ± 12 h^{-1} obtido a 0.1 vvm, representando um aumento até 3 vezes em comparação com a taxa de dissolução de CO_2 na coluna sem anteparos. Apresentaram-se, ainda, modificações aos números de Reynolds oscilatório (Re_o) e de Strouhal (St) que auxiliam o aumento de escala de colunas oscilatórias com anteparos em sistemas gás-liquido.

A conversão anaeróbia de gás de síntese foi também investigada no sistema oscilatório com anteparos optimizado para melhorar a transferência de massa gás-liquido. Aqui, o novo reactor biológico oscilatório com anteparos de múltiplos orifícios (RBOAMO), foi alimentado em modo descontinuo e contínuo com mistura de gás de síntese composta por 60 % CO, 10 % CO_2 e 30 % H_2 (v/v), e operada mistura de fluxo oscilatório. O efeito da intensidade de mistura e dos caudais de entrada de gás de síntese sobre a produção de CH_4, foram experimentalmente avaliados. Em modo descontínuo, obtiveram-se taxas de consumo de CO e H_2 superiores (até 6 e 3 vezes, respectivamente), mostrando uma forte correlação positiva com o Re_o. Às mesmas condições, o Re_o não teve efeito sobre a produção de CH_4, sugerindo que o processo é controlado pela reacção metanogénica, representando uma limitação à conversão descontínua do gás de síntese usando culturas mistas que não conseguem superar a melhoria das taxas de dissolução ou consumo dos substratos. Surpreendentemente, a injecção contínua de gás de síntese no (RBOAMO) resultou num aumento na taxa de produção de CH_4 até 27 vezes e até 8 vezes nas taxas de consumo de CO e H_2. A utilização de fluxo continuo de gás levou ao aumento das taxas de reacção, actuando como força motriz na cinética do processo. As taxas de reacção mostraram um forte correlação com a carga de CO assumindo um comportamento típico da cinética de Monod, mudando de ordem um para zero com o aumento da carga de CO.

Finalmente, usou-se uma abordagem preliminar de análise do balanço de fluxo para caracterizar as vias metabólicas preferenciais durante a conversão microbiológica do gás de síntese por culturas anaeróbias mistas, tendo mostrado potencial para auxiliar na melhoria da eficiência do processo.

Table of Contents

List of Abbreviations

2D	2-dimensional
AD	Anaerobic digestion
ALR	Air-lift reactor
BC	Bubble column
BES	2-bromoethanesulphonate
BSD	Bubble size distribution
CH_4	Methane
CO	Carbon monoxide
CO_2	Carbon dioxide
CSTR	Continuous stirred tank reactor
DoE	Design of experiments
EtOH	Ethanol
FBA	Flux balance analysis
FID	Flame ionization detector
fps	frames per second
FTS	Fischer-Tropsch Synthesis
FVA	Flux variability analysis
GLPK	GNU linear programming kit
H_2	Hydrogen
H_2O	Water
H_2S	Sulphur gas
HEPES	4-(2-hydroxyethyl)-1-piperazineethane-sulfonic acid
HFM	Hollow fibre membrane
HPLC	High performance liquid chromatography
LB	Lower bound
MeOH	Methanol
MES	2-(N-morpholino)ethanesulfonic acid
MOBB	Multi-orifice oscillatory baffled bioreactor
MOBC	Multi-orifice oscillatory baffled column
n-BuOH	n-Butanol

N_2	Nitrogen
Na_2S	Sodium sulphide (reducing agent)
NO	Nitric oxide
OBC	Oscillatory baffled column
OF	Objective function
OFM	Oscillatory flow mixing
RMW	Relative molecular weight
rpm	rotations per minute
SCFA	Short-chain fatty-acids
ss	simple shear
STR	Stirred tank reactor
sybil	Systems Biology Library package
TCD	Thermal conductivity detector
UB	Upper bound
VFA	Volatile fatty acids
VSS	Volatile suspended solids
vvm	volume of gas per volume of liquid per minute
WGS	Water-gas shift
X	Independent factor in Design of Experiments
Y	Response factor in Design of Experiments

List of Figures

CHAPTER 1

CHAPTER 2

CHAPTER 3

CHAPTER 4

List of General Nomenclature

SYMBOLS

a	mass transfer interfacial area (m^2)
A_{proj}	projected area of the bubble (mm^2)
$C_{G,i}$	concentration of the component *i* in the gas phase (mol L^{-1})
$C^*_{L,i}$	concentration of component *i* in the liquid side of the interface in equilibrium with the partial pressure of the component in the gas phase (mol L^{-1})
C_L	dissolved concentration (mg L^{-1})
$C_{L,0}$	initial dissolved concentration (mg L^{-1})
$C_{L,i}$	concentration of the component *i* dissolved in the liquid (mol L^{-1})
C_L^*	concentration of saturation (mg L^{-1})
C^{Liq}_{CO}	CO concentration in the liquid phase (mol L^{-1})
C^{Liq}_{CO}	H_2 concentration in the liquid phase (mol L^{-1})
CO_{LR}	specific CO loading rate (mmol g_{VSS}^{-1} d^{-1})
D	dilution rate of the liquid (s^{-1})
$D_{3,2}$	Sauter mean diameter (mm)
d_c	internal diameter of the column (mm)
$dC_{L,i}/dt$	concentration gradient of component *i* along time (mol L^{-1} s^{-1})
d_e	equivalent spherical diameter of bubble (mm)
d_h	equivalent hydraulic diameter for single-orifice column (mm)
d_o	orifice diameter (mm)
d_{obs}	equivalent diameter of the obstacle (mm)
d_p	diameter of piston (mm)
f	frequency of the oscillation (Hz)
$F_{m,CH4}$	CH_4 specific molar productivity (mmol g_{VSS}^{-1} d^{-1})
h	height of the column (mm)
h_L	liquid height in the column (mm)
K_I	constant of the model in Eq. (3.1) (mol^2 L^{-2})
K_La	overall gas-liquid mass transfer coefficient (h^{-1})

K_P	constant of the probe (h^{-1})
K_S	constant of the model in Eq. (3.1) (mol L^{-1})
K_x	constant of the model in Eq. (5.10) (mmol g_{VSS}^{-1} d^{-1})
L	spacing between baffles (mm)
m_S	mass of CO_2 supplied to the column (g)
m_U	mass of CO_2 uptake (g)
n	number of orifices in the baffle (dimensionless)
p_{CO}	CO partial pressure (atm)
P_T	gas total pressure (atm)
Q_{gas}	gas aeration rate (vvm or L min^{-1})
q_i	specific uptake rate of the component *i* (mol g_{VSS}^{-1} s^{-1})
$Q_{syngas\ (in)}$	inlet syngas flow rate (mL min^{-1})
$Q_{syngas\ (out)}$	outlet syngas flow rate (mL min^{-1})
Q_{syngas}	syngas sparging rate (vvm or mL min^{-1})
Re_o	oscillatory Reynolds number (dimensionless)
Re_o'	modified oscillatory Reynolds number (dimensionless)
r_i	maximum initial reaction rate (mmol L^{-1} d^{-1})
r_i^{max}	maximum reaction rate (mmol L^{-1} d^{-1})
$r_{x,i}$	specific reaction rate for component *i* (mmol g_{VSS}^{-1} d^{-1})
$r_{x,i}^{max}$	maximum specific reaction rate for component *i* (mmol g_{VSS}^{-1} d^{-1})
S	substrate concentration (mmol L^{-1})
St	Strouhal number (dimensionless)
St'	Modified Strouhal number (dimensionless)
t	aeration/fermentation time (s)
t_0	time delay for the measuring of dissolved CO_2 concentration (s)
U_G	mean superficial gas velocity (mm s^{-1})
$V_{G,total}$	total volume of gas in the column (L)
V_{HS}	total volume of headspace (L)
V_L	working liquid volume (L)
V_M	molar volume (L mol^{-1})
V_y	instantaneous axial (vertical) bubble or liquid velocity (mm s^{-1})
X	concentration of biomass as volatile suspended solids (g_{VSS} L^{-1})

x_0	centre-to-peak amplitude of fluid oscillation (mm)
x_{CO2}	CO_2 molar composition inlet gas (mol/mol)
$Y_{CH4/CO}$	instantaneous yield of CH_4 from CO (dimensionless)
Y_D	CO_2 dissolution yield (dimensionless)
$Y^u_{CH4/CO}$	ultimate yield of CH_4 from CO (dimensionless)

GREEK LETTERS

α	fraction of open area of the baffle (dimensionless)
ΔG	Gibbs free energy change (kJ reaction^{-1})
$\Delta G^{o'}$	standard Gibbs free energy change (kJ reaction^{-1})
Δt	time interval (s)
Δy	vertical displacement (mm)
ε_G	gas holdup or gas volume fraction (dimensionless)
μ	kinematic fluid viscosity (kg m^{-1} s^{-1})
ρ	specific mass of fluid (kg m^{-3})
τ_G	gas residence time (h)
$\dot{\gamma}$	shear rate (s^{-1})

List of Tables

CHAPTER 2

CHAPTER 3

CHAPTER 4

CHAPTER 5

CHAPTER 6

CHAPTER 1

Introduction

1.1 RESEARCH MOTIVATION

Energy demand in the world has increased as consequence of industrial development and population growth in many countries. In the last century, a 17-fold increase in worldwide energy consumption has been reported (Demirbas, 2007). In the next decades, the more conventional energy resources, as is the case of fossil fuels, will become scarce and unable to fulfil energy demands, for transportation, heating, and industrial processes (Mojovic *et al.*, 2009). This scenario rises the need for the development of sustainable, efficient, and cost-effective technologies, based on the utilisation of renewable and environmentally friendly resources (Mojovic *et al.*, 2009). The biorefinery concept matches this perspective by generating biofuels, bioenergy and biochemicals from biomass (Cherubini, 2010). Figure 1–1 illustrates this biorefinery concept, coupling energy and mass integration.

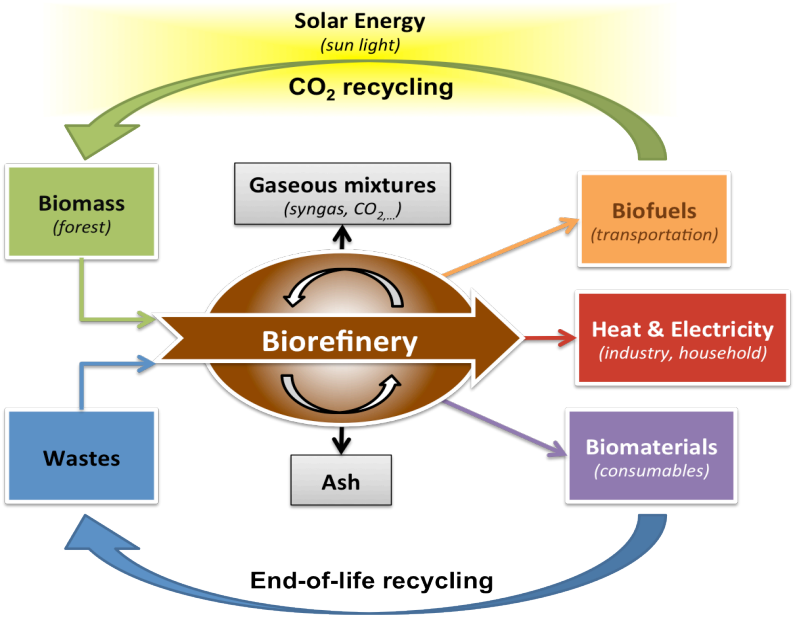

Figure 1-1 Schematics of the general biorefinery concept integrated with energy and mass balance cycle, for sustainable technologies (adapted from Ragauskas *et al.* (2006)).

Biomass is an abundant renewable resource and a major potential feedstock for fuel production in the future (Bridgwater, 1995). Moreover, at least 50 % of the total energy requirement in

Europe could potentially be supplied by biomass sources, including land-grown biomass (not food competing agricultural land), wastes and residues from agriculture, trade and consumers (Grassi & Bridgwater, 1991). Because it is a solid material, biomass utilisation in many processes and applications requires substantial modification (Bridgwater, 1995). Thus, converting biomass to gaseous and liquid energy carriers is the most promising way to effectively increase biomass utilisation. In Canada, biomass gasification and subsequent methanation and upgrading were estimated to yield about 16 to 63 % of Canada's current gas use, generating only 8.2 to 10.0 % of life-cycle greenhouse gas emissions compared to coal-fired power (National Energy Board of Canada, 2006).

In this purpose, biomass can be submitted to gasification producing a gas mixture commonly designated synthesis gas, producer gas or, simply, syngas. This mixture is mainly composed of CO, H_2, and CO_2, which can be used as mass and energy building blocks for biofuels. Syngas utilisation had earlier gained interest since the discovery of the Fischer-Tropsch Synthesis (FTS), in 1922, a catalytic process in which a variety of liquid hydrocarbons can be obtained from syngas (Dalai & Davis, 2008; Fischer & Donath, 1938). More recently, interest in biological syngas conversion has emerged as a promising field that overcomes some of the disadvantages of chemical processes. Advantages of biological over chemical catalysts are mainly the higher specificity, higher yields, lower costs, and possibly higher resistance to poisoning (Klasson *et al.*, 1991). Additionally, the mild processing conditions required (lower pressure and temperature) could help reducing both the capital and operating costs of the conversion process (Heiskanen *et al.*, 2007). Nevertheless, biological processes present an important disadvantage since they are slower compared with chemical reactions. Figure 1-2 shows a representation of a process diagram for biological production of bioethanol from syngas, integrated in the general biorefinery concept.

Interest in biological syngas conversion relies on the fact that some anaerobic microorganisms can effectively use CO and H_2 to produce added-value carbon compounds, such as ethanol, butanol, acetic acid, butyric acid, hydrogen and methane (Fischer *et al.*, 2008). Companies, such as, NEOS Bio, Lanzatech and Coskata, are already exploring ethanol production from cellulosic biomass. These companies are in the market offering hybrid technology combining gasification and biological conversion. The microbiology of syngas bioconversion to biofuels has been recently

reviewed (Henstra *et al.*, 2007; Oelgeschläger & Rother, 2008; Sokolova *et al.*, 2009). Several mesophilic anaerobic microorganisms were shown to produce short-chain fatty-acids (SCFA) and alcohols from CO and H_2. Moreover, such compounds can also be converted to methane by syntrophic mixed cultures (Schink & Stams, 2006).

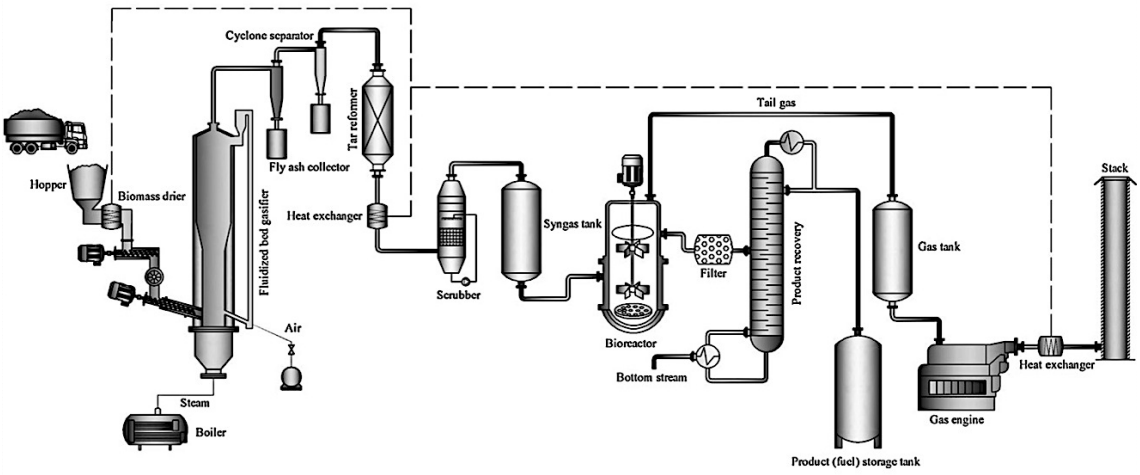

Figure 1-2 Representation of the process setup of biofuel production from syngas conversion, coupled with biomass gasification (Mohammadi *et al.*, 2011).

Mixed culture fermentation systems can be managed by both engineering and microbiological tools in order to achieve competitive bioprocesses (Rodríguez *et al.*, 2008). In such systems operational conditions will determine which catabolic product allows the more efficient growth and will therefore dominate (Claassen *et al.*, 1999). A key characteristic of anaerobic processes is that metabolic reactions occur very close to thermodynamic equilibrium and have small Gibbs free energy variations (Rodríguez *et al.*, 2008). A Gibbs-energy-based methodology for mathematical modelling of energy-limited anaerobic ecosystems provides a basis for the description of microbial activities as a function of environmental factors, which will allow enhanced catalysis of specific reactions of interest for process development (Rodríguez *et al.*, 2008).

Effective syngas utilisation is also dependent on gas-liquid mass-transfer rates. Conventional gas-liquid contacting technologies, such as stirred tank reactors, airlift reactors or bubble columns, show low gas-liquid mass transfer rates, also due to the low solubility of the major syngas components in the aqueous culture medium (Bredwell *et al.*, 1999). Volumetric mass-transfer gas-liquid coefficient (K_La) higher than 360 h^{-1} for O_2 is unlikely to be obtained with any of the conventional gas-liquid contacting technologies (Vasconcelos *et al.*, 2003). However, higher K_La (up to 560 h^{-1}) were obtained using a new gas-liquid contacting technology based on oscillatory flow mixing technology featuring a peculiar combination of flow constrictions and fluid oscillations, which can perform efficiently using minimum power inputs (Reis *et al.*, 2007, 2008). Further important features presented by oscillatory flow reactors are linear scale-up, efficient mixing and particle suspension as well as narrow residence time distributions (Mackley & Ni, 1991).

Insights from mixed culture approach and mass transfer enhancement, applied to syngas bioconversion to biofuels, appear as a prospective approach to motive and develop research. The possibility of recovering the energy potential from biomass and wastes is also a strong motivation for developing processes with the same purpose. Such prospection is the greatest motivation topic for the present work. In the context of syngas conversion for biofuels production, some works have been recently published, reviewing much of the literature on this topic, and presenting and discussing its opportunities and challenges, either from a technological or microbiological perspective (Demirbas, 2009; Henstra *et al.*, 2007; Klasson *et al.*, 1991; Mohammadi *et al.*, 2011; Munasinghe & Khanal, 2010a, 2010b; Ragauskas *et al.*, 2006).

1.2 OBJECTIVES

This study aims to develop a new process for the bioconversion of syngas to biofuels, with principal interest in the production of organic acids, alcohols, and CH_4. The specific objectives targeted were:

(1) to explore the prospect of using defined anaerobic mesophilic mixed cultures for the production of biofuels from artificial syngas mixture, under different operational

conditions (pH, initial syngas total pressure, and CO partial pressure);

(2) to perform flux balance analysis using a defined metabolic network of syngas conversion, constrained with the experimental reaction rates of main process compounds;

(3) to study gas-liquid mass transfer, using CO_2 as a model gas, in a reactor system based on the oscillatory flow mixing;

(4) to optimise the design and scale-up of a multi-orifice oscillatory baffled column capable of enhancing gas-liquid mass transfer rates;

(5) to enhance methane production, by performing biological syngas conversion process in a multi-orifice oscillatory baffled bioreactor, under different operating modes (batch and continuous).

1.3 THESIS OUTLINE

This thesis is organised in seven chapters, three of them describing experimental laboratory work (Chapters 3 to 5) and one based on mathematical modelling of metabolic pathways (Chapter 6). The other three chapters contain information about literature review and main research highlights.

A brief introduction to the subject of this thesis, describing the research motivation and the principal objectives are presented in **Chapter 1**.

In **Chapter 2**, the main literature on syngas conversion topic is reviewed in depth. The current limitations of biological syngas utilisation for the production of biofuels are presented and the perspectives for overcoming those limitations discussed. The main bioreactor designs used so far and the microbiological developments and potentials in syngas conversion processes are also overviewed. Mathematical modelling approaches for exploiting the potential of metabolic process are also presented. The main principles, concepts, and applications of the oscillatory flow mixing technology are also introduced and described in this chapter.

Batch conversion of syngas by anaerobic sludge is studied in **Chapter 3.** The effect of three operating variables (pH, initial syngas total pressure, and CO partial pressure) is evaluated in terms of process performance. The range of possible reaction products is also assessed considering methanogenic-active and methanogenic-ihnibited scenarios.

Chapter 4 presents the main results and discussion of the gas-liquid mass transfer performance of the novel multi-orifice oscillatory baffled column (MOBC). In this mass transfer study CO_2 is used as model gas to evaluate performance of the column.

The potential enhancement on syngas conversion performance by oscillatory flow mixing is then evaluated, in a bench scale system, using the novel multi-orifice oscillatory baffled bioreactor (MOBB), at different operational modes (batch and continuous). Results of this study are presented and discussed in **Chapter 5**.

The experimental data obtained in syngas conversion experiments, shown in Chapters 3 and 5, are then used to perform flux balance analysis, using a defined metabolic network. **Chapter 6** presents the main results and discussion of this analysis and its prospective indications on the main chemical pathways involved in syngas conversion process studied in this thesis.

Finally, **Chapter 7** summarises the main conclusions of this research and draws some future research directions in syngas conversion. Main scientific output of this research work is also presented.

CHAPTER 2

Literature Review

The energy crisis of the 1970s has raised interest and need in new approaches for obtaining renewable, low-cost, effective, and sustainable energy carriers. Such energy can be used as an alternative to fossil fuels, contributing to fulfil energy demands (Datar *et al.*, 2004). Primary energy sources subjected to physical operations, such as hydraulic and wind power, are relatively easy to get and to transform into secondary energy forms. The application of chemical and biological processes to the conversion of other resources, such as biomass or wastes, to usable energy carriers has shown to be more complex. However, a strong economic interest is being directed to such processes, due to the large quantities and availability of those raw materials (Lynd, 1996). Biomass has been considered the most promising source for renewable energy (Ragauskas *et al.*, 2006).

2.1 EMERGING CHEMICALS AND BIOFUELS

Biomass-based sources, such as lignocellulosic raw materials and some types of waste, cannot be directly bio-transformed to fuels, due to its high complexity and low degradability. For those resources, gasification is an option, since different types of materials varying from coal, char, biodegradable or recalcitrant wastes, lignocellulosic biomass or sewage sludge can be transformed into an energy rich gas mixture, called synthesis gas or syngas. The principal components of syngas are carbon monoxide (CO), hydrogen (H_2), and carbon dioxide (CO_2); small amounts of methane (CH_4) and sulphur gases can also be present (Klasson *et al.*, 1990b). Depending on the types of gasifier, the gasification conditions, and the primary source materials, the composition of the producer gas can be different. This difference, measured in terms of H_2/CO ratio, can vary from 0.34 (Datar *et al.*, 2004) to 0.67 (Bridgwater, 1995).

Gasification can be seen as an intermediary process in which syngas is a platform for conversion into chemicals and fuels of added value. In gasification, different processes can be used to produce fuels and chemicals from syngas (Figure 2-1). Among the catalytic processes, Fischer-Tropsch Synthesis (FTS) is the most well-known and applied for syngas utilisation (Dalai & Davis, 2008; Fischer & Donath, 1938). The range of potential advantages presented by the biological processes opens way to raising interest for research and development to make syngas conversion a competitive process for market applications.

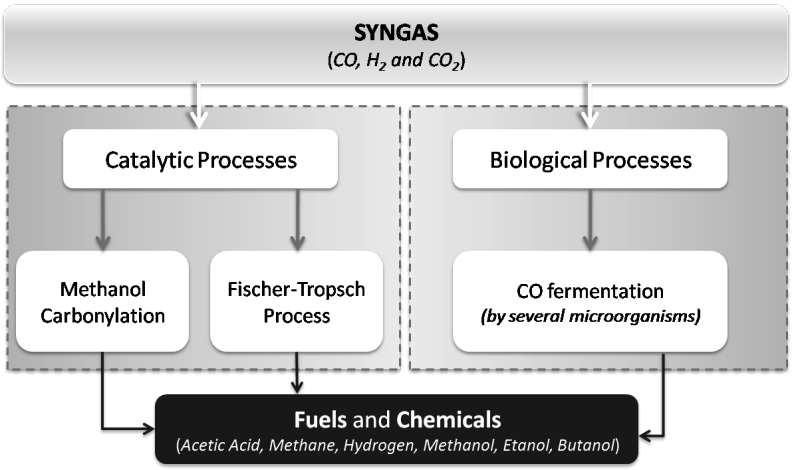

Figure 2-1 Pathways of syngas utilisation to obtain valuable products (adapted from Sim, (2006)).

The principal advantages are the higher substrate specificity and production yield, and the lower energy costs. Main limitations are related with lower reaction rates (inherent to the microbiology of the process), and mass transfer limitations in commonly used reactor systems (Klasson *et al.*, 1991). The overall volumetric gas-liquid mass transfer coefficient, K_La is used to describe mass transfer performance of the systems. As a novel process, many issues of biological syngas conversion are not yet optimised and thus are in need of further exhaustive research.

2.2 PANORAMA OF MICROBIAL SYNGAS CONVERSION

Syngas conversion is performed by several microorganisms, which are capable of utilising syngas components to produce valuable products. Either mass transfer or reactor design optimisation, allows getting substantial product yield improvements (Klasson *et al.*, 1991). Combining such aspects with microbiology fundamental research is a route of interest in pursue of novel intensified bioprocesses.

Production of ethanol from syngas has been widely studied since the discovery of Fischer-Tropsch Synthesis. Biological syngas conversion to ethanol has gained an increased interest since the isolation of *Clostridium ljungdahlii*, which has the ability to convert a mixture of CO and H_2 to ethanol and acetic acid. Presently, syngas conversion to ethanol by *C. ljungdahlii* is object

of commercial processes developed by a few technology leader companies. Bioengineering Resources Inc. commercialise a process (the "BRI Renewable Energy Process") that combines biomass gasification, syngas conversion and ethanol distillation from the reactor effluent. In the same process, syngas cooling before feeding to bioreactor is coupled to heat recovery. Coskata Inc. also commercialise a similar three-step process for fuel-grade ethanol production. The Coskata process with wood biomass uses half the water required to produce a gallon of gasoline and reduces lifecycle greenhouse gas emissions by as much as 96 %. LanzaTech and INEOS Bio are other examples of companies developing processes for biological syngas conversion with residues from industry into fuels and chemicals. LanzaTech process is still at pilot scale presently, though. All these processes have also environmental benefits.

2.2.1 Syngas-converting microorganisms

At present, there is significant development in syngas conversion research and several new species have been discovered and identified that can use syngas components. Several research studies have been carried out in fundamental aspects of syngas conversion to biofuels, especially related with process microbiology (Munasinghe & Khanal, 2010a). Microbiology of syngas bioconversion to biofuels has been reviewed (Henstra *et al.*, 2007; Oelgeschläger & Rother, 2008; Sokolova *et al.*, 2009). Table 2-1 summarises the main microorganisms, both bacteria and archaea, commonly involved in syngas or CO conversion. The optimum temperature depends on the specie, but can vary from 30 to 39 °C, for mesophilic microorganisms, and between 55 and 82 °C, for thermophilic microbes. Some thermophilic bacteria can operate at higher temperatures than those reported though (Henstra *et al.*, 2007). The optimum pH has been reported ranging from 6 to 8.5, depending on the specie. For *C. ljungdahlii* an optimum pH around 6 has been reported (Tanner *et al.*, 1993). However, Klasson *et al.* (1993a) reported ethanol concentration as high as 48 g L^{-1}, using *C. ljungdahlii* culture at pH between 4.0 and 4.5, in a nutrient-limited environment.

Several pure culture studies have shown butanol, H_2 and CH_4 production from syngas components. The conversion of CO or CO/H_2 to ethanol and butanol was demonstrated for

Butyribacterium methylotrophicum and *Clostridium carboxidivorans* (Liou *et al.*, 2005; Shen *et al.*, 1999; Svetlitchnyi *et al.*, 2001).

Table 2-1 Examples of mesophilic and thermophilic microorganisms involved in syngas conversion processes (Henstra *et al.*, 2007; Munasinghe & Khanal, 2010a)

Microbial Species	T_{opt} (°C)	pH_{opt}	Products	Reference
Mesophilic bacteria				
Clostridium ljungdahlii	37	6	Acetate, ethanol	Tanner *et al.* (1993)
Clostridium aceticum	30	8.5	Acetate	Sim *et al.* (2007)
Clostridium carboxidivorans	38	6.2	Acetate, ethanol, butyrate, butanol	Liou *et al.* (2005)
Oxobacter pfennigii	36–38	7.3	Acetate, n-butyrate	Krumholz and Byant (1985)
Blautia producta (former *Peptostreptococcus productus*)	37	7	Acetate	Lorowitz and Bryant (1984)
Acetobacterium woodii	30	6.8	Acetate	Genthner and Bryant (1987)
Eubacterium limosum	38–39	7.0–7.2	Acetate	Genthner and Bryant (1982, 1987)
Butyribacterium methylotrophicum	37	6	Acetate, ethanol, butyrate, butanol	Grethlein *et al.* (1991); Lynd *et al.* (1982); Shen *et al.* (1999)
Rubrivivax gelatinosus	34	6.7–6.9	H_2	Dashekvicz and Uffen (1979); Uffen (1976)
Rhodopseudomonas palustris P4	30	n/a	H_2	Jung *et al.* (1999)
Rhodospirillum rubrum	30	6.8	H_2	Kerby *et al.* (1995)
Mesophilic archaea				
Methanosarcina barkeri	37	7.4	CH_4	O'Brien *et al.* (1984)
Methanosarcina acetivorans strain C2A	37	7	Acetate, formate, CH_4	Rother and Metcalf (2004)
Thermophilic bacteria				
Moorella thermoacetica (former *Clostridium thermoaceticum)*	55	6.5–6.8	Acetate	Daniel *et al.* (1990)
Moorella thermoautotrophica	58	6.1	Acetate	Savage *et al.* (1987)
Carboxydothermus hydrogenoformans	70–72	6.8–7.0	H_2	Svetlitchnyi *et al.* (2001)
Carboxydocella sporoproducens	60	6.8	H_2	Slepova *et al.* (2006)
Carboxydocella thermoautotrophica	58	7	H_2	Sokolova *et al.* (2002)
Moorella stamsii	65	7.5	H_2, acetate	Alves *et al.* (2013)
Desulfotomaculum carboxydivorans	55	7	H_2, H_2S	Parshina *et al.* (2005)
Thermophilic archaea				
Methanothermobacter thermoautotrophicus	65	7.4	CH_4	Daniels *et al.* (1977)
Thermococcus strain AM4	82	6.8	H_2	Sokolova *et al.* (2004)

Notes: (n/a) not available.

Several hydrogenogenic bacteria can perform the water shift reaction in which CO is oxidized with the formation of H_2 (Jung *et al.*, 1999; Kerby *et al.*, 1995). Acetate may be produced by several anaerobic bacteria that utilise CO, including *Blautia producta* (former *Peptostreptococcus productus*), *Acetobacterium woodii*, *Clostridium thermoaceticum* and *Eubacterium limosum* (Henstra *et al.*, 2007). Some of these bacteria are also capable of forming acetate homoacetogenically from H_2/CO_2.

Mesophilic and thermophilic carboxydotrophic hydrogenogenic bacteria, such as *Rubrivivax gelatinosus*, *Rhodopseudomonas palustris*, *Rhodospirillum rubrum*, *Carboxydothermus hydrogenoformans*, *Carboxydocella thermoautotrophica*, *Desulfotomaculum carboxydivorans*, can convert CO and H_2O to H_2 and CO_2 (Henstra *et al.*, 2007). Direct conversion of CO to CH_4 can be achieved by a few methanogenic archaea, namely *Methanosarcina barkeri*, *Methanosarcina acetivorans* and *Methanothermobacter thermoautotrophicus* (Henstra *et al.*, 2007). Production of CH_4 from the H_2 and CO_2 present in the syngas or via acetate is also possible using hydrogenotrophic and acetoclastic archaea. Fatty-acids and alcohols can be converted to CH_4 by syntrophic mixed cultures (Schink & Stams, 2006). *C ljungdahlii*, as has been previously referred, is able to convert CO and H_2, into ethanol and acetic acid.

Syngas is produced during a gasification process and therefore its temperature is rather high (i.e. 700–800 °C). Therefore the utilisation of thermophilic processes could be an advantage for syngas conversion, even considering heat recovery (Munasinghe & Khanal, 2010a).

2.2.2 Physiology of microbial syngas conversion

Conversion of syngas components can be coupled to different processes, such as sulphate reduction, hydrogenogenesis, acetogenesis and methanogenesis (Oelgeschläger & Rother, 2008). The potential for these processes relies in detailed knowledge concerning substrate and product fluxes within the systems, and also the role of the different microorganisms involved.

Syngas-converting microorganisms utilise acetyl-CoA pathway to convert CO into ethanol, acetic acid and other products, such as butanol and butyrate (Ahmed & Lewis, 2007; Henstra *et al.*,

2007). Figure 2-2 shows the pathway in which CO and CO_2 are converted to ethanol, acetic acid and biomass, via acetyl-CoA (Drake, 1994).

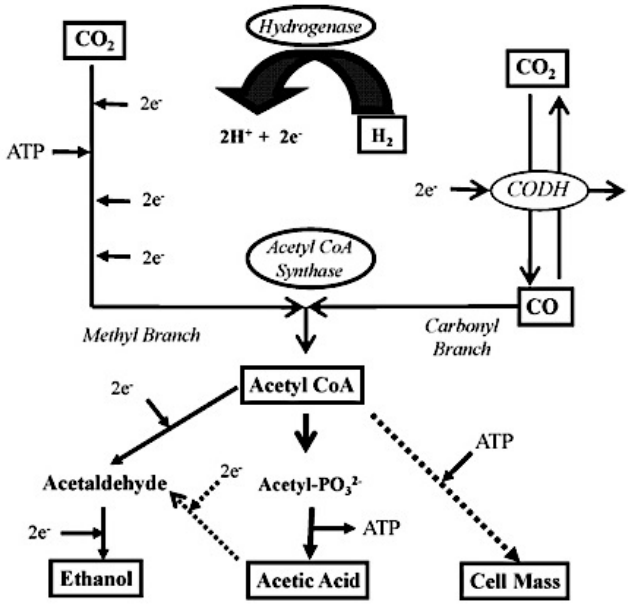

Figure 2-2 Schematic of acetyl-CoA pathway representing CO, CO_2 and H_2 utilisation to produce ethanol, acetic acid and biomass (Drake, 1994; Hurst & Lewis, 2010).

Hydrogenase and carbon monoxide dehydrogenase (CODH) enzymes are involved in the electrons transfer, from H_2 and CO, respectively, required for the conversion. Acetyl-CoA acts as a precursor for cell macromolecules and source of energy, in the form of adenosine triphosphate (ATP). Acetyl-CoA pathway is a reductive, irreversible, and non-cyclic path and takes place under strict anaerobic conditions (Munasinghe & Khanal, 2010a). The production of Acetyl-CoA can occur following two main ways, represented by methyl and carbonyl branches. In the first, a methyl group is formed by reduction of CO or CO_2. In such path, a series of reductive reduction occurs with ATP consumption. In the second, CODH and acetyl-CoA synthase (ACS) complex produce acetyl-CoA, by combining methyl, carbonyl and CoA groups (Henstra *et al.*, 2007).

Since acetyl-CoA production from H_2 and CO_2 has a negative energy balance, a step to recover metabolic energy is necessary. Thus, acetate is formed from acetyl-CoA to recover the energy

that was early invested in such pathway. Ethanol is then formed by acetate reduction. Butyrate and butanol can be further produced, as well. Such products are obtained from acetoacetyl-CoA, which is formed from two acetyl-CoA molecules (Henstra *et al.*, 2007). The products that can be obtained from H_2 and CO_2 are limited to those that allow conservation of sufficient metabolic energy (Henstra *et al.*, 2007). Perhaps, other products could be obtained since an additional energy substrate could be provided.

The ability of hydrogenase (via H_2) and CODH (via CO) enzymes to generate reducing equivalents that are critical for product formation is an important issue for process efficiency (Xu & Lewis, 2012). In syngas conversion, transforming CO and CO_2 into other carbon-containing products with high efficiency would require using all available H_2 to produce reducing equivalents, along with those that could be obtained from CO (Xu & Lewis, 2012). The utilisation of H_2 simultaneously with CO has been reported in some studies (Datar *et al.*, 2004); however, it is possible that process conditions can affect H_2 utilisation (Hu *et al.*, 2011). Thus, whenever H_2 is available for the process, producing maximum possible reducing equivalents from H_2 is crucial in order to leave CO free for product formation. To make this possible, hydrogenase enzyme activity must be maintained at its maximum and potential inhibitory effects from direct hydrogenase inhibitors interaction must be minimised (Xu & Lewis, 2012).

2.2.3 Ethanol and acetic acid production

Ethanol (C_2H_5OH) and acetic acid (CH_3COOH) production from syngas can be described by six general reactions, described in Table 2-2. The Gibbs free energy change, at standard conditions ($\Delta G^{0'}$), is also presented (Liu *et al.*, 2014; Munasinghe & Khanal, 2010a).

Stoichiometric and thermodynamic analysis gives evidence to the important role played by H_2 in such process. Thus, in the absence of H_2, just one-third of the carbon in CO can be converted to ethanol and one-half to acetic acid. Such evidence occurs because CO acts both as carbon source and as reducer of electrons generated by H_2 (Hurst & Lewis, 2010). In the presence of H_2, the reducing equivalents are generated by H_2 and CO can be used as a carbon source (Menon & Ragsdale, 1996).

Table 2-2 Stoichiometry and ΔG changes of reactions involved in the anaerobic production of ethanol and acetic acid from syngas components (Liu *et al.*, 2014; Munasinghe & Khanal, 2010a)

Reaction	$\Delta G^{0'}$ (25 °C) kJ reaction^{-1} (pH 7.00)
From CO	
$6\ CO + 3\ H_2O \rightarrow \mathbf{C_2H_5OH} + 4\ CO_2$	– 222.0
$4\ CO + 2\ H_2O \rightarrow \mathbf{CH_3COOH} + 2\ CO_2$	– 154.6
From H_2/CO	
$2\ CO + 4\ H_2 \rightarrow \mathbf{C_2H_5OH} + H_2O$	– 288.0
$2\ CO + 2\ H_2 \rightarrow \mathbf{CH_3COO^-} + H^+$	– 134.0
From H_2/CO_2	
$2\ CO_2 + 6\ H_2 \rightarrow \mathbf{C_2H_5OH} + 3\ H_2O$	– 97.3
$2\ CO_2 + 4\ H_2 \rightarrow \mathbf{CH_3COOH} + 3\ H_2O$	– 75.3

Since some hydrogenases are inhibited by CO, H_2 could not be used and electrons will not be produced. Consequently, CO has to supply all the electrons required in the conversion and will act as an electron donor rather than carbon source. Syngas composition is, thus, critical for the overall yields of the conversion process (Munasinghe & Khanal, 2010a).

Some syngas components, even when present in residual amounts, could have an inhibitory effect over such metabolic pathway and, therefore, in the overall process productivity. One example of such compounds is nitric oxide (NO), reported by Ahmed and Lewis (2007). Those authors hypothesised that NO present in biomass-derived syngas could be the possible cause of hydrogenase enzyme inhibition. In such study, the specific hydrogenase activity was monitored with different NO concentrations, above 40 ppm. The experiments have shown that NO is a non-competitive inhibitor hydrogenase activity and the enzyme activity loss was reversible. At final, Ahmed and Lewis (2007) referred that NO concentration above 40 ppm can be tolerated by cells without compromising hydrogenase activity, cell growth and product distribution. Sulphur gas (H_2S) tolerance of *C ljungdahlii* has been also examined (Klasson *et al.*, 1993a). However, no significant effect was detected at H_2S concentrations as high as 5.2 % (v/v).

2.2.4 Methane production

Methane can be directly produced from, either CO or CO_2/H_2, or indirectly by formation of intermediates (Klasson *et al.*, 1990a). Table 2-3 summarises the main biological routes involved

in CH_4 production from syngas components. Such reactions are carried out anaerobically and at very low redox potentials (Ljungdahl & Wiegel, 1986, in Klasson *et al.*, 1990b).

Table 2-3 Stoichiometry and ΔG changes of reactions involved in the anaerobic conversion of CO to CH_4 (Klasson *et al.*, 1990a; Sipma *et al.*, 2006a)

Reaction	$\Delta G^{0'}$ (25 ºC) kJ reaction^{-1} (pH 7.00)
From CO	
$4\ CO + 2\ H_2O \rightarrow 3\ CO_2 + \mathbf{CH_4}$	– 210.8
From H_2/CO	
$CO + 3\ H_2 \rightarrow \mathbf{CH_4} + H_2O$	– 150.7
From H_2/CO_2	
$HCO_3^- + 4\ H_2 + H^+ \rightarrow \mathbf{CH_4} + 3\ H_2O$	– 135.4
$CO_2 + 4\ H_2 \rightarrow \mathbf{CH_4} + 2\ H_2O$	-
From acetate:	
$CH_3COO^- + H_2O \rightarrow \mathbf{CH_4} + HCO_3^-$	– 31.2

According to Klasson *et al.* (1990a), indirect CH_4 production seems more viable than the direct routes. Thus, CH_4 production is preceded by acetate formation or CO utilisation to produce CO_2 and H_2, by the water gas shift (WGS) reaction, as indicated in reaction equation (5).

$$CO + H_2O \rightarrow H_2 + CO_2 \qquad \Delta G^{\circ} = -20.1 \text{ kJ reaction}^{-1} \qquad (5)$$

The mixture of H_2 and CO_2 can be directly converted to CH_4 or produce acetate as an intermediate. Photosynthetic bacteria *Rhodospirillum rubrum* can perform the first process but an additional organic carbon source is required for growth. Acetate production from CO is readily accomplished by acetogenic bacteria, such as *Blautia producta* (former *Peptostreptococcus productus*) (Klasson *et al.*, 1990a). Production of H_2/CO_2 as intermediates is preferred though (Klasson *et al.*, 1990b). Thus, *R. rubrum* can be first used to produce H_2 and CO_2 from CO and H_2O, in the WGS reaction. Then, conversion of CO_2/H_2 to CH_4 can be performed by methanogens, such as *Methanobacterium formicicum* and/or *Methanosarcina barkeri* (Klasson *et al.*, 1990a).

Klasson *et al.* (1990b) performed experiments using a mixed culture, composed by *R. rubrum*, *M. formicicum*, and *M. barkeri*. A packed bubble column and a trickle-bed reactor were tested in the study. Klasson *et al.* (1990b) reported the successful conversion of CO, CO_2, and H_2, as a syngas mixture, to CH_4 in both reactors using the mixed culture. Methane yields from H_2 were of about 83 %. CO conversions of 100 and 79 %, and maximum CH_4 productivities of 0.4 and 3.4 mmol L^{-1} h^{-1} were obtained for the trickle-bed reactor and bubble column, respectively. Klasson *et al.* (1990b) also reported that methanogens *M. formicicum* and *M. barkeri* interact synergistically, being the first inhibited by the presence of CO while having high H_2 uptake rate, and the second one being tolerant to CO, but having low H_2 uptake rate.

2.2.5 Other added-value products from syngas conversion

Besides ethanol and methane, other products, such as butanol and methanol, and short chain fatty acids can be obtained from syngas. However, syngas conversion to these products is not well studied, especially in continuous reactors. Table 2-4 summarises the main reactions possible to occur during syngas conversion and that yield several different products. Gibbs energy free changes of each reaction are also presented.

Table 2-4 Stoichiometry of other products that can also be formed from CO or H_2/CO, and ΔG changes associated to reactions (Henstra *et al.*, 2007; Sipma *et al.*, 2006a)

Products	Stoichiometry	$\Delta G^{0'}$ (25 °C) kJ reaction^{-1} (pH 7.00)
From CO		
formate	$CO + H_2O \rightarrow HCOO^- + H^+$	– 16
butyrate	$10\ CO + 4\ H_2O \rightarrow CH_3(CH_2)_2COO^- + H^+ + 6\ CO_2$	– 440
n-butanol	$12\ CO + 5\ H_2O \rightarrow CH_3(CH_2)_3OH + 8\ CO_2$	– 480
hydrogen	$CO + H_2O \rightarrow CO_2 + H_2$	– 20
From H_2/CO		
butyrate	$4\ CO + 6\ H_2 \rightarrow CH_3(CH_2)_2COO^- + H^+ + 2\ H_2O$	– 240
methanol	$CO + 2\ H_2 \rightarrow CH_3OH$	– 39
n-butanol	$4\ CO + 8\ H_2 \rightarrow CH_3(CH_2)_3OH + 3\ H_2O$	– 324
From acetate		
hydrogen	$CH_3COO^- + 4\ H_2O \rightarrow 2\ HCO_3^- + 4\ H_2 + H^+$	104

2.3 METABOLIC MODELLING APPROACHES

Metabolic models have great relevance in pursuing better understanding of biological systems, due to their close connection to growth and production phenotypes (Carinhas *et al.*, 2013). Mathematical models are ideal tools for integrating large numbers of microbial, chemical and physical phenomena taking place within the microbial communities of interest. Moreover, they can be used to test scientific hypotheses, to design experiments or to control an existing process. They also allow describing quantitatively the substrate and product fluxes in mixed-culture communities, when stoichiometry and kinetics of the relevant metabolic reactions are included (Rodríguez *et al.*, 2008).

2.3.1 Flux balance analysis-based metabolic modelling

Flux balance analysis (FBA) is a mathematical modelling approach widely used approach in the study of biochemical networks (Orth *et al.*, 2010). This approach has found particular application on the genome-scale metabolic network reconstructions built during the last decade (Duarte *et al.*, 2007; Feist *et al.*, 2007; Oberhardt *et al.*, 2009). All known metabolic reactions in an organism and genes that encode each enzyme are contained in these network reconstructions (Orth *et al.*, 2010). The metabolites flow through the metabolic network are calculated by FBA, allowing to predict the either growth rate of an organism or production rate of a relevant metabolite (Orth *et al.*, 2010). FBA approach is based on the mass conservation principle within a metabolic network (Carinhas *et al.*, 2013). Thus, intracellular mass fluxes can be estimated under assumed metabolic steady state at defined and determined rates of nutrient consumption and by-product accumulation (Carinhas *et al.*, 2013).

The concept behind FBA is based on lack of detailed kinetic information for a certain system. In order to overcome that lack, a change in the approach to modelling metabolic systems is required (Edwards *et al.*, 2002). In fact, rather than trying to calculate and predict what a metabolic network does exactly, the range of possible phenotypes that a metabolic systems can display must be narrowed, based on successive imposition of governing physicochemical constraints (Edwards *et al.*, 2002). Thus, constraints are crucial for FBA, making this approach

advantageous over theory-based models, strongly dependent on bio-physical equations which require many difficult-to-measure kinetic parameters (Covert *et al.*, 2001; Edwards *et al.*, 2002).

The metabolites flow through the network is then constrained, based on stoichiometries (Orth *et al.*, 2010). Each reaction is further constrained by upper and lower bounds, defining the maximum and minimum reaction fluxes that are allowable in the system (Orth *et al.*, 2010). Thus, constraints of stoichiometry and bounds define the flux distribution space possible for a system: consumption and production rates for each metabolite. (Orth *et al.*, 2010) Figure 2-3 represents a schematic of the typical FBA formulation, as described by Orth *et al.* (2010).

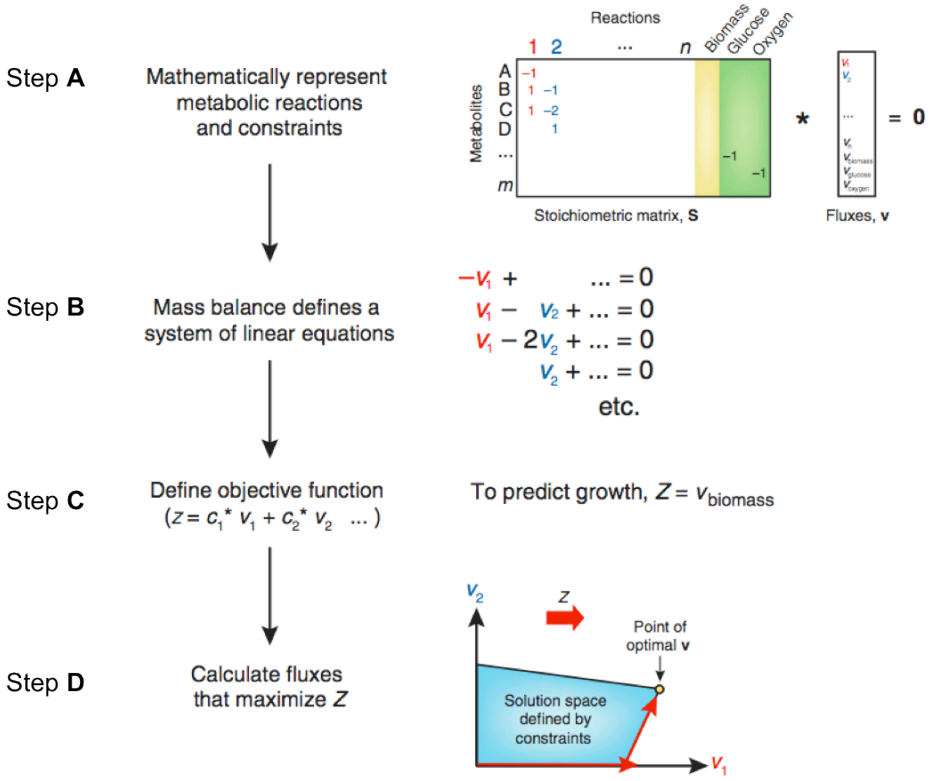

Figure 2-3 Typical FBA problem formulation for a microorganism using a well-defined metabolic network. Example here aim at maximise microbial growth rate (adapted from Orth *et al.* (2010)).

The first step of the analysis consists in the construction of the metabolic network as a matrix of stoichiometric mass balances and exchange reaction, which represent the flow of metabolites

(steps A). Then, the model is constrained with determined reaction rates, at steady state, defining lower and upper bounds and taking into account the reversibility or irreversibility of all the reactions (step B). Finally, the objective function is defined (step C) and a linear programming algorithm is used to calculate the flux distribution in the network (step D) and an optimal solution is achieved.

This approach has been widely used with genome-scale metabolic reconstruction networks for pure cultures and well-defined metabolism (e.g. Carinhas *et al.* (2013), Selvarasu *et al.* (2012)). The utilisation of the FBA in modelling metabolism based on mixed cultures is more recent and only a few number of studies have been reported (Chaganti *et al.*, 2011; Pardelha *et al.*, 2012, 2013). Chaganti *et al.* (2011) predicted the effect of linoleic acid and pH on bio-hydrogen production, modeling fluxes within mixed anaerobic microbial communities. In a similar application, on studying the production of polyhydroxyalkanoates from volatile fatty acids by mixed cultures, Pardelha *et al.* (2012) predicted with accuracy the flux and composition of the product.

FBA approach has shown great benefits on modelling metabolic networks that bring insights for better understanding of the processes, however it does not take into account thermodynamic aspects that always play relevant role in the metabolic pathways.

2.3.2 Energetics framework

Anaerobic microbial ecosystems are usually defined as energy-limited. In this way, anaerobic fermentative reactions usually occur very close to thermodynamic equilibrium and have small Gibbs energy free change (ΔG) values (Jackson & McInerney, 2002). Thus, several anaerobic reactions of interest are only thermodynamically feasible to a narrow range of substrates and products concentrations. A more detailed study of such systems can be achieved by considering both energetics of reactions and transport processes (Rodríguez *et al.*, 2008).

Total amount of Gibbs energy available in a system for microbial growth, is established by the environmental conditions imposed on a given microbial community. Moreover, Gibbs energy calculations allow identifying energy niches required for redox reactions. In energy-limited

ecosystems, such as most anaerobic, thermodynamic calculations can provide a picture of the energetic scenario of the system and help locate threshold that might change the whole microbial ecosystem behaviour (Rodríguez *et al.*, 2008). Although the interdependence between the energetic niches and the microbial activities is not completely understood (Jones, 2005), important information can be obtained from studies of energetic scenarios. An energetic framework can be very useful for developing processes in which specific reactions need to be favoured to obtain the specific desired products. Reactor experiments might be also designed to investigate whether a microbial community might or could be forced to operate in specific energetic regions (Rodríguez *et al.*, 2008).

2.3.3 Energy-based metabolic network modelling

Mathematical modelling has proven to be very useful in describing complex systems. However, most of the existing mathematical models were originally conceived for aerobic systems and are not adequate for these anaerobic ecosystems. Moreover, such models are based just on kinetics. Recently, a new modelling approach based on the integration of bioenergetics and kinetics has been proposed (Rodríguez *et al.*, 2006; 2008). Rodríguez *et al.* (2006) have presented an approach for predicting the product spectrum as a function of the environmental conditions in anaerobic mixed-culture conversion processes. Moreover, they consider that energy limitation entail a selective pressure in such ecosystems. Thus, product formation reactions, which are associated to Gibbs energy yield maximisation, are favoured by those selective pressures. As a result, microorganisms that are capable of catalysing this optimised set of reactions will be selected by the environment (Rodríguez *et al.*, 2008).

The conceptual model proposed by Rodríguez *et al.* (2008) is characterised by assuming the whole anaerobic microbial ecosystem as single microorganism. Such model can be described by a simplified metabolic network of the most common fermentative reactions. The fluxes in the network were defined by optimisation of the net energy yield (Rodríguez *et al.*, 2006). Figure 2-4 illustrates this metabolic network based on energetics. This approach (Figure 2-4) was utilised by Rodríguez *et al.* (2006) to predict the product formation from glucose as a function of H_2 partial pressure (P_{H2}), reactor pH, and substrate concentration, in a mixed culture fermentation system.

Preliminary results showed that the method was able to anticipate system behaviour at variable pH and P_{H2} values. An association between the medium concentrations and their bioenergetic consequences for the microorganisms was established by the model. Therefore, shifts in the net fluxes that led to different products driven by a maximum-energy-yield selective force were also identified by the model (Rodríguez *et al.*, 2008).

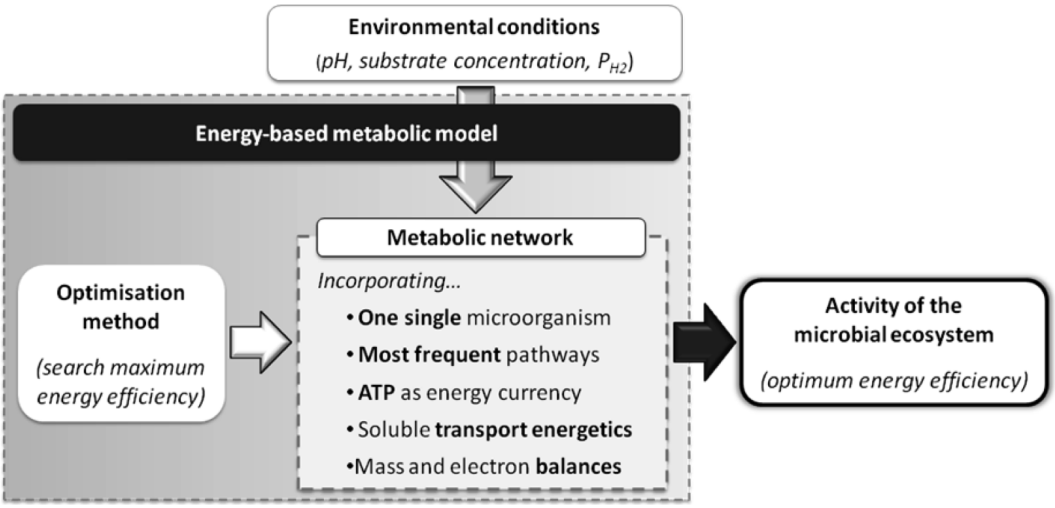

Figure 2-4 Scheme of the energy-based metabolic model to predict the activity of an anaerobic mixed microbial ecosystem (adapted from Rodríguez *et al.*, 2008).

The overall metabolic activity of *Escherichia coli* was recently studied (Almaas *et al.*, 2004). Such study has shown that only a small set of high-flux reactions is dominant in *E. coli* metabolic activity, whereas most of the remaining low-flux reactions were not significant. Thus, a reorganisation of fluxes appeared to occur as response to environmental conditions changes (Almaas *et al.*, 2004). Hitherto, this phenomenon has only been demonstrated for *E. coli*, but it could be a more widespread attribute in the metabolic activity of microorganisms (Rodríguez *et al.*, 2008).

The modelling approach proposed by Rodríguez *et al.* (2008) has shown applicability in the prediction of product formation in anaerobic mixed-culture fermentations as a function of the environmental conditions imposed in a reactor. The applicability of this approach has not been

reported for syngas conversion and the microbial mixed communities that can be involved in the process. However, such dependence between product formation and environmental conditions imposed in a process could hereafter be an advantage in the development of robust processes for producing biofuels or other valuable chemicals (Rodríguez *et al.*, 2008), such as the ones that can be produced from syngas conversion.

2.4 BIOREACTOR DESIGN WITH POTENTIAL FOR UTILISATION IN MICROBIAL SYNGAS CONVERSION

Microbial syngas conversion has been studied using different reactor types, both in batch or continuous operation systems. The choice of a suitable bioreactor is a matter of matching reaction kinetics with the capabilities of the various bioreactors (Klasson *et al.*, 1991). Gas-liquid mass transfer limitations effectively control the process (Munasinghe & Khanal, 2010a). Thus, reactor properties must be managed in order to allow high mass transfer rates balanced with high cell densities (Klasson *et al.*, 1991). The stirred tank reactor (STR) has been the most applied in syngas conversion (Klasson *et al.*, 1991; Klasson *et al.*, 1993a). Bubble column reactors (Datar *et al.*, 2004), monolithic biofilm reactors (Ebrahimi *et al.*, 2005; Kreutzer *et al.*, 2005), trickling bed reactors (Bredwell *et al.*, 1999; Cowger *et al.*, 1992), have also been studied with the same purpose. Membrane-based reactors (Lee & Rittmann, 2002) have been presented as alternative systems, as well. Main characteristics and applications of each one of those reactor types are following reviewed.

Stirred tank reactors

The utilisation of continuous stirred tank reactors (CSTR) for syngas conversion has been used for sparging the gaseous substrates in the liquid phase and making them available for microbial consumption (Klasson *et al.*, 1991). In those systems, generally high gas flow rate and high cell concentrations are necessary to allow near complete substrate conversion. Usually, gas retention time required to achieve desired substrate conversion defines the reactor volume (Klasson *et al.*, 1991). Moreover, high agitation rate is necessary to break gas bubbles into small ones, making gaseous substrate more accessible to microorganisms (Munasinghe & Khanal, 2010a).

Bubble column reactors

Industrial processes, in which large working volumes are required, typically make use of bubble column (BC) reactors. Such systems offer some advantages, such as higher mass transfer rates and low operational and maintenance costs. The possibility to occur back-mixing and coalescence phenomena is considered the major demerit of these systems (Munasinghe & Khanal, 2010a). Datar *et al.* (2004) have used a bubble column reactor to study syngas conversion to ethanol.

Monolithic biofilm reactors

Monolithic biofilm reactors consist in a bed of carrier media, in which microorganisms are attached in a biofilm form. Gaseous substrate is allowed to pass through the bed carrier media, being consumed by microorganisms in the biofilm. Operation under atmospheric pressures, make these systems economically more viable (Munasinghe & Khanal, 2010a). Kreutzer *et al.* (2005) have used a monolytic biofilm reactor to study intensification of biocatalytic processes, showing gas-liquid-solid mass transfer improvements with decreasing of energy input. This configuration has never been used in biological syngas conversion though.

Trickling bed reactors

In columnar reactors, such as trickling bed reactors, mechanical agitation is not required. Thus, their potential for lower power costs is an advantage over stirred tanks. Usually, it consists in a packed-bed reactor gas-continuous. Liquid phase trickles downward over the packing and gas phase flows in either co-current or counter-current. Gas and liquid flow rates are typically low, resulting in relatively low pressure drops. Microorganisms can be either immobilized on the packing or suspended in liquid medium. In some cases, high $K_L a$ values can be achieved using columnar reactors (Bredwell *et al.*, 1999).

Membrane-based reactors

Membrane-based reactors, such as composite hollow fibre membranes (HFM) have been recently used in biological syngas conversion. Luo *et al.* (2013) used a HFM system, for the anaerobic digestion of sewage sludge supplemented with CO. The pressure generated inside the

HFM (up to 1.5 atm), allowed achieving low dissolved CO concentration in the liquid, which avoid CO inhibition. In non-related syngas studies, this kind of system has shown potential for improving H_2 and O_2 mass transfer, allowing biofilm formation in the membrane exterior wall, so that microorganisms can attach and capture the gaseous substrate (Lee & Rittmann, 2002). The system has also allows the gas passing through the membrane without bubbles formation, potentially leading to higher yield and reaction rates. Moreover, operation under high pressure makes possible to obtain higher mass transfer rates and reduced reactor volumes when HFM technology is used (Munasinghe & Khanal, 2010a).

Table 2-5 summarises some studies in which these reactor configurations have been used, either in biological syngas conversion or syngas-related studies.

Table 2-5 Different reactor configurations used in biological syngas conversion or in syngas-related studies

Reactor	Substrate	Culture	Operating conditions	Observations	Reference
Serum bottles	Syngas	*Clostridium ljungdahlii*	Batch	Study of the growth and production rates associated with CO and H_2 consumption	Phillips *et al.* (1994)
Serum bottles	Syngas	*Clostridium aceticum*	Batch	Optimisation of acetic acid production by varying CO partial pressure and fermentation time	Sim *et al.* (2007)
Stirred tank reactor	Syngas	*Rhodospirillum rubrum and Methanobacterium formicicum*	Continuous	Study of the methane production from syngas	Klasson *et al.* (1991)
Stirred tank reactor	Syngas	*Clostridium ljungduhlii*	Continuous	Study of the ethanol production by varying the nutrients assimilation with CO consumption	Klasson *et al.* (1991)
Stirred tank reactor	Syngas	*Peptostreptococcus productus*	Continuous	Study of the CO consumption for various pseudo retention time and total syngas pressure	Klasson *et al.* (1991)
Bubble column reactor	Syngas	*Clostridium ragsdalei*	Continuous	Study of the production of ethanol using artificial or produced syngas mixture	Datar *et al.* (2004)
Trickle-bed reactor	Syngas	*Butyribacterium methylotrophicum*	Continuous (varying)	Study of the cell growth in different packing materials for immobilization matrices, for syngas utilisation purposes	Chatterjee *et al.* (1996)
Trickle-bed reactor	Syngas	*Rhodospirillum rubrum*	Continuous	Study of the CO uptake rate and associated mass transfer performance	Cowger *et al.* (1992)
Membrane-based reactor	CO	Mixed anaerobic biomass (sewage sludge)	Continuous	Study of the CH_4 production from CO utilisation coupled with sewage sludge digestion	Luo *et al.* (2013)

2.5 GAS-LIQUID MASS TRANSFER

Syngas mixture is composed by sparingly soluble gases, especially H_2 and CO. Since these components are the main substrates for biofuels production, mass transfer could limit the process, in the liquid phase. Achieve high reaction yield is imperative, thus the mass transfer process and its limitations must be considered and investigated, attempting to maximise the gas-liquid contact (Klasson *et al.*, 1990b).

Hitherto, numerous studies have been reported on gas-liquid mass transfer of some gases extensively used in most industrial fermentation processes, such as oxygen (O_2). Regarding the main syngas components, CO and H_2, a few work studies have been carried out in which its gas-liquid mass transfer rates are determined (Munasinghe & Khanal, 2010b, 2012). Even experiments using water as liquid medium and being performed under mild process conditions, low temperature and pressure, the amount of reported information is little. In addition, such conditions are critical to promote microbial growth.

2.5.1 Conventional gas-liquid contacting systems

Thus far, conventional reactor systems, such as stirred tank reactors (STRs), bubble columns (BCs) and air-lift reactors (ALRs), are the main systems subjected to mass transfer studies. Most of the gas-liquid mass transfer studies reported refers to the transfer of gases different than the ones present in syngas, though. There are, however, some studies that report CO mass transfer rates in water using stirred tank reactor (Kapic *et al.*, 2006; Klasson *et al.*, 1993b; Riggs & Heindel, 2006). More recent studies carried out in the same conditions have been performed with functionalized MCM41 nanoparticles and electrolytes as well (Zhu *et al.*, 2008, 2009).

Riggs and Heindel (2006) research was focused on CO-liquid mass transfer rates improvement. Their research questions were based on which actual dissolved CO concentrations are present in water and which mass transfer rates for CO are obtained, in such conditions. A water-filled stirred tank reactor was used and dissolved CO concentrations were measured, as function of time. Liquid samples (10 μL) containing dissolved CO were measured following the myoglobin-protein

method proposed by Kundu *et al.* (2003). Different volumetric flow rates (varying from 1 to 6 L min^{-1}) and stirrer speeds (between 200 and 600 rpm) were applied and the previous collected data was employed to determine CO-water mass transfer rates. To determine the K_La values the authors followed the unsteady-state method proposed by Shuler and Kargi (2002, in Riggs & Heindel, 2006). Such method is one of the four common approaches used to determine oxygen mass transfer constants in liquid systems. CO concentration in the gas liquid-interface was assumed to be in equilibrium with the bubble, in the absence of any microorganism.

The results obtained by Riggs and Heindel (2006) showed K_La values ranging from 0.003 to 0.043 s^{-1}, higher than those obtained by Klasson *et al.* (1993b). Moreover, a correlation to predict CO mass transfer in stirred tank reactors was proposed, which showed positive good correlation between experimental data of K_La and reactor characteristics (power gas and superficial gas velocity). Additionally, the usefulness of myoglobin assay to determine CO dissolved concentrations was emphasised. Further research in the topic of syngas conversion scale-up was pointed out by the authors.

Klasson *et al.* (1993b) reported a study similar to that of Riggs and Heindel (2006). However, in the former, a biological system was used and thus, the effect of mass transfer in CO uptake was also studied. The purpose of Klasson *et al.* (1993b) study was evaluate the ability of a photosynthetic bacterium (*Rhodospirillum rubrum*) to produce H_2 from CO and water in a continuous stirred tank reactor. To determine CO conversion kinetics by *R. rubrum* and to show the potential for using such culture as a model system for mass-transfer purposes were the main goals. Experiments were carried out under an operation mode that allowed studying mass-transfer and kinetic aspects of the process, separately. Non-steady state mass CO balance was considered to the determination of K_La values, measured in terms of CO conversion in gas phase.

Regarding the mass transfer aspects of Klasson *et al.* (1993b) study, the results showed an increasing in maximum CO conversion by rising agitation rates. The maximum levels were attained at 58 % of CO conversion and 700 rpm. These values matched CO mass-transfer-limiting conditions in the reactor system. Thus, Klasson *et al.* (1993b) system allowed obtaining K_La values ranging from 0.004 to 0.010 s^{-1}, at different agitation rates.

2.6 OSCILLATORY FLOW MIXING FOR ENHANCED GAS-LIQUID CONTACTING

Efficient transport of mass and energy are the key aspect in many processes. Therefore, a good fluid mixing is necessary to achieve in order to maximise such transport. In a batch process, good mixing can be achieved by using an external agitation, enhancing both heat and mass transfer, while maintaining homogeneous conditions. In a continuous mode, the promotion of turbulent flow conditions is often achieved by adding static packing or baffles. The oscillatory or pulsed flow can be highly effective, and appears as an alternative mean of external agitation for both batch and continuous processes, providing a range of specific process enhancements (Ni *et al.*, 2003).

2.6.1 Historical development

The first use of pulsating systems has occurred in the 1940s and 1950s, in the nuclear industry, as a way to enhance solvent extraction either in plate or packed columns (Ni *et al.*, 2003). These pulsating regimes allowed improvement in dispersed phase mixing and better mass transfer performance in a column of smaller dimensions than conventional, steady-flow counter-current columns Ni *et al.*, 2003).

The first reciprocating plate column (RPC) was developed, in 1950s, by Dr Andrew Karr at Hoffman La Roche Inc., with the purpose of penicillin intermediates extraction from fermentation broths, and is usually known as the 'Karr' column (Ni *et al.*, 2003). Its design consists of one or more vertical shafts of plates, moved from the top by an electro-mechanical oscillator. In each plate, a large number of spaced holes, of about 14 mm in diameter, are designed. The fractional open area is in the range of 0.5–0.6 and gives a much lower flow constriction than that of pulsed plate or packed columns, which is an advantage if the systems are prone to generate fouling. Afterwards, the RPC has been used in many extraction applications and manufactured in sizes up to 1.7 m diameter, using higher frequencies and amplitudes, up to 3 Hz and 2.5 cm, respectively (Ni *et al.*, 2003). Until the early 1980s, the RPC and pulsed packed column (PPC) were the only significant unit operations to exploit the benefits of oscillatory flow mixing. Since

then, the interest of oscillatory flows has been investigated in a wider range of processes.

More recently, several studies have been conducted using tubes containing periodically-spaced orifice baffles (Brunold *et al.*, 1989; Howes *et al.*, 1991; Mackley & Ni, 1991, 1993; Reis *et al.*, 2004, 2007; Stonestreet & van der Veeken, 1999). Whenever, in such a system, the net flow is subjected to a reversing oscillatory flow efficient fluid mixing and a narrow residence time distribution is achieved. Independently of the tube diameter, these phenomena have been found remaining the same. This issue is particularly important in scale-up purposes, indicating that the fluid mechanical conditions in such a system can be linearly scaled-up (Brunold *et al.*, 1989; Ni *et al.*, 1995a; Smith, 1999). The fluid mechanics of oscillatory flow systems at millimetre scales have also been recently studied (Reis *et al.*, 2004, 2007).

The application of oscillatory motion has been applied to different fields of research producing important process enhancements. The use of numerical simulations of oscillatory flow has brought increased knowledge in the understanding of the mixing generated in these systems (Chew *et al.*, 2004; Ni *et al.*, 2002b; Reis *et al.*, 2008). In the following sections the main aspects concerning the fundamentals of oscillatory flow mixing are described. Some of the main applications of the oscillatory system and its potential for process enhancing are also presented.

2.6.2 Oscillatory baffled column

The basic configuration of an oscillatory baffled column (OBC) can be represented by two different designs, differing in the oscillation mechanism, as schematised in Figure 2-5. Figure 2-5(a) represents the configuration in which the baffles are fixed inside the column and the fluid is forced to oscillate by mean of a piston. The reverse mechanism occurs in the configuration represented in Figure 2-5(b), where the shaft of baffles oscillating inside the fluid imposes the motion. The design of the baffles is usually based on a compromise for minimising frictional losses and maximising the mixing effect. Based on that, baffles are characterised for being a low-constriction orifice plates, where the fractional open cross-sectional area is commonly in the range between 20 and 30 %. The distance between each baffle is uniformly defined, in a typical range of 1–2 times the column diameter (Ni *et al.*, 2003).

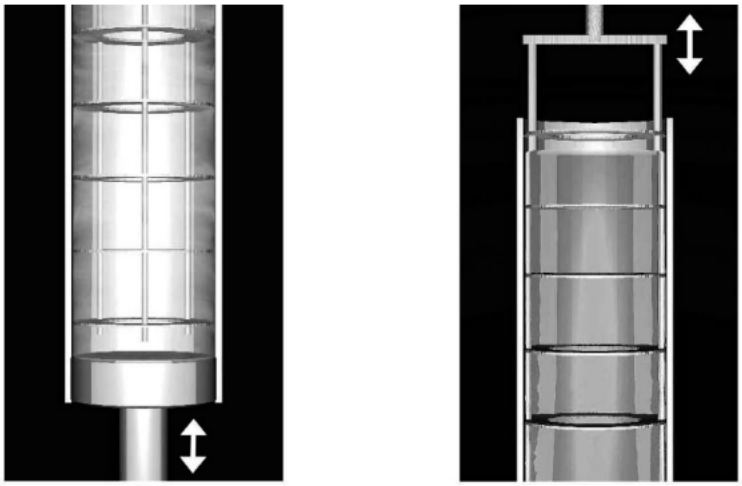

Figure 2-5 Schematic representations of the oscillatory baffled column (OBC) where the oscillatory flow is imposed by (a) the fluid motion and (b) the shaft of baffles motion (Ni *et al.*, 2003).

The oscillatory flow in the OBC generates flow patterns with unique features. In Figure 2-6 different visualisations of the flow pattern in the presence of oscillatory movement of the fluid are represented.

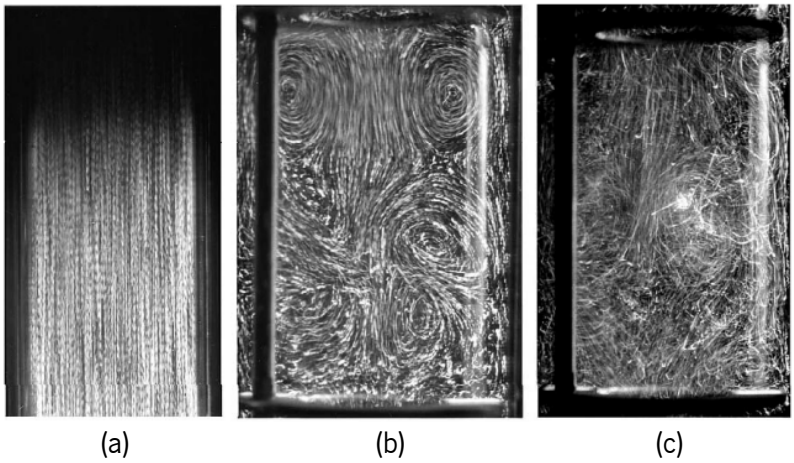

Figure 2-6 Flow visualisations in (a) smooth walled column, and (b)-(c) oscillatory baffled column (Ni *et al.*, 2003).

In the absence of constrictions or baffles (Figure 2-6(a)), imposing fluid oscillations has no effect in the mixing, and the column is a simple tube with fluid moving axially up and down, in laminar

flow. The presence of constrictions either in moderate (Figure 2-6(b)) or high (Figure 2-6(c)) oscillatory conditions, promote well-defined vortices inside the interbaffle cavities (area between two baffles). The level of mixing can be controlled to a very high precision, by adjusting a wide range of conditions, from 'soft' mixing, exhibiting plug flow conditions, to most intense mixing, approaching mixed flow conditions (Ni *et al.*, 2003). Each baffle cavity operates as a continuously stirred tank, in which the radial velocity components are comparable to the axial ones. Moreover, the mixing that takes place near the walls is similar to that in the centre of the column (Reis, 2006).

The baffles that have been used so far have different configuration and shapes, each one affecting significantly the level of mixing that can be obtained. In Figure 2-7, three different configurations of baffles tested to enhance mass transfer in a gas-liquid system are represented.

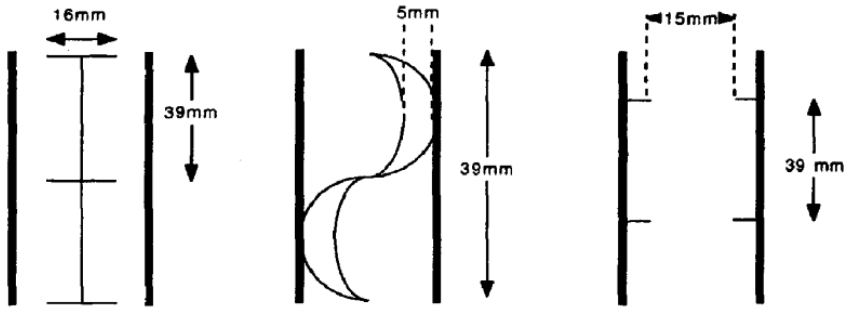

Figure 2-7 Different configurations of baffles inside an oscillatory flow system: (a) central baffle; (b) helical baffle; (c) wall (orifice) baffle (Hewgill *et al.*, 1993).

The wall or orifice baffle type can also assume a different configuration, when several orifices with same diameter are distributed in a plate, as represented in Figure 2-8. In this case, baffles are designated as single-orifice or multi-orifice baffles.

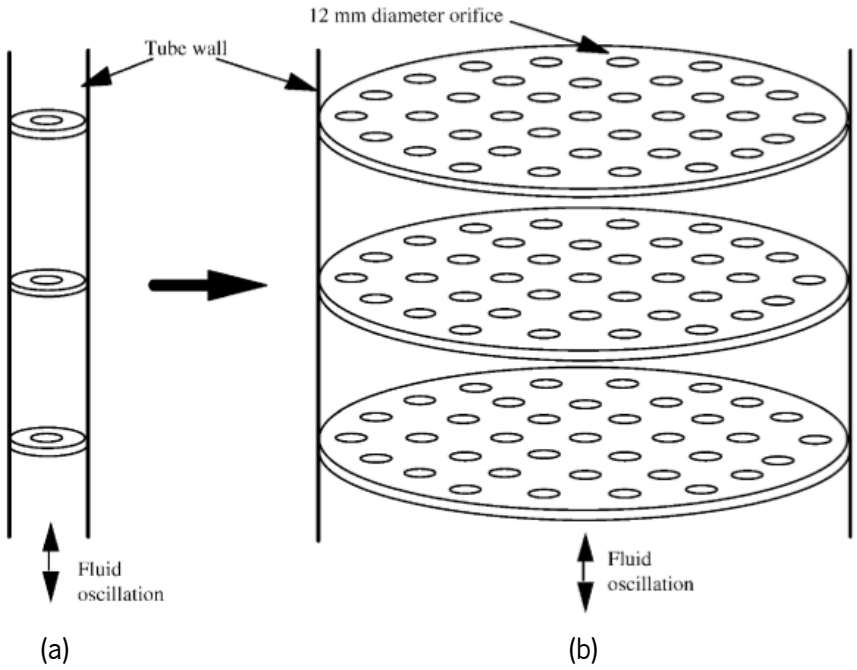

Figure 2-8 Different orifice baffle configurations inside an oscillatory flow system: (a) single-orifice and (b) multi-orifice baffles, with same orifice diameter (Smith & Mackley, 2006).

The technology employing such type of mixing is usually referred as pulsed flow reactor (PFR) or oscillatory flow reactor (OFR), when a reaction occurs, or even oscillatory baffled column when only mechanic fluids operations are involved (Ni *et al.*, 2003).

2.6.3 Oscillatory flow mixing mechanism

The mechanism of oscillatory flow mixing (OFM) is characterised by formation of sharp edges perpendicularly to the periodic and fully reversing flow (Reis, 2006). In Figure 2-9 are represented the main flow patterns during the oscillation cycle.

The mixing pattern in oscillatory reactors shows a complex eddy formation as a result of the presence of wall baffles. During one cycle, with up stroke and down stroke, acceleration and deceleration phases take place as a result of the sinusoidal function along time. On the acceleration phase, vortex rings are shaped downstream of the baffles, until peak velocity is

achieved. Then, the deceleration phase takes place and the vortex rings move into the bulk. In the down stroke acceleration phase those vortices are undone by the bulk flow in the opposite direction. Vortices are formed due to the interactions between baffles and fluid, during periodical reversing direction of the fluid. This interaction generates radial velocities (transversal to the flow direction) in the same order of magnitude of the axial velocities (same direction of flow). These two velocity components create an uniform mixing achieved in each inter-baffle cavity and cumulatively along the length of the column (Brunold *et al.*, 1989; Mackley & Ni, 1991, 1993).

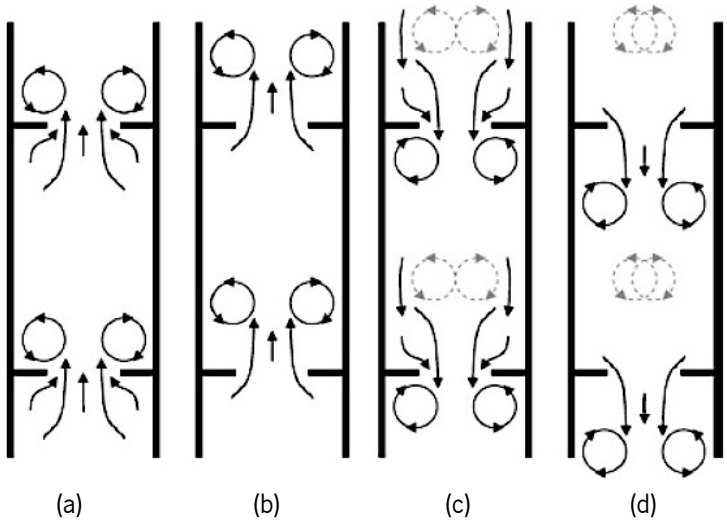

Figure 2-9 Scheme of the OFM mechanism in an OBC at: (a) start of the up stroke; (b) maximum velocity in the up stroke; (c) start of down stroke; (d) maximum velocity in down stroke (Fitch *et al.*, 2005).

2.6.4 Main parameters controlling oscillatory flow mixing

The oscillatory fluid dynamics is characterised by some dimensionless groups, mainly: the classical (net flow) Reynolds number, Re_n, the oscillatory Reynolds number, Re_o, and the Strouhal number, *St*. To better describe the fluid mechanics, two dimensionless geometrical parameters should also be taken into account: the baffle spacing and the baffle free area (Ni & Pereira, 2000). Each of these variables is following briefly described.

Net-flow Reynolds number (Re_n)

The Reynolds number is the dimensionless number most used to specify the type of flow that is circulating in a simple tube. The net flow Reynolds number is defined by Eq. (2.1).

$$\mathrm{Re}_n = \frac{uD\rho}{\mu} \tag{2.1}$$

In this equation, D is the tube diameter (m), μ the viscosity of fluid (kg m^{-1} s^{-1}), ρ the fluid density (kg m^{-3}), and u is the mean superficial flow velocity (m s^{-1}), also known as net flow velocity. In such a simple tube the fluid mechanics are developed predominantly in the axial direction.

Oscillatory Reynolds number (Re_o)

When an oscillatory motion is applied on the net flow, an additional dimensionless group is needed to define the whole flow motion, the oscillatory Reynolds number. Since the beginning of the oscillatory flow characterisation studies, in the 1940s, several equations have been proposed to define an indicator of flow mechanics in pure oscillatory flow (Reis, 2006; Sinada & Karim, 1984a, 1984b). For the situation where baffles are present, the oscillatory motion is more complex, and Re_o takes the form as is shown in Eq. (2.2).

$$\mathrm{Re}_o = \frac{2\pi x_0 f d_o \rho}{\mu} \tag{2.2}$$

The variables in this equation represent: x_0, the oscillation amplitude from centre to peak (m); f, the oscillation frequency (Hz); and d_o, the orifice diameter (m). Moreover, the product $2\pi x_0 f$ represents the maximum oscillatory velocity (m s^{-1}). When multi-orifice baffles are used, the number of orifices (n) must be taken into account, and the tube diameter should be replaced by the effective diameter, d_{ef}, according to Smith (1999), described by Eq. (2.3).

$$d_{ef} = \sqrt{\frac{D^2}{n}} \tag{2.3}$$

The Re_o definition is similar to that of the Re_n, but describing the different flow state since the oscillatory conditions are imposed by a sinusoidal behaviour of the oscillator. Furthermore, the

fluid mechanics in this case will be developed by similar magnitudes for both axial and radial velocity components (Reis, 2006).

The mixing nature in oscillatory systems is nowadays better understood. At low Re_o numbers (100–300), it is known the system exhibits plug flow behaviour and the vortices are axisymmetrically generated within each baffled cavity. For higher Re_o numbers, the symmetry is broken and flow becomes intensely mixed and chaotic and the flow achieves the mixing mode (Ni *et al.*, 1999, 2002a).

Strouhal number (St)

The characterisation of oscillatory flow systems in the presence of tube inserts or varying tube shapes requires the utilisation of another dimensionless number: the Strouhal number (St). This number is defined by the ratio between column or tube diameter and stroke length, as shown in Eq. (2.4). The St number represents numerically the effective eddy propagation in the column (Ni *et al.*, 2003).

$$St = \frac{D}{4\pi x_0} \tag{2.4}$$

2.6.5 Effect of geometrical parameters

The orifice diameter in the baffle (d_o) and the baffle spacing (L) are two variables that play an important role in the performance of oscillatory systems (Ni & Gough, 1997). However, both variables do not contribute for any of the dimensionless numbers previously presented. Moreover, it has been shown that L has influence in the shape of the generated eddies whilst d_o controls the width of the vortices within each baffled cavity (Ni & Gough, 1997). Since both variables affect the fluid mixing in a baffled column, they must be optimised to allow the desired mixing performance.

Effect of free baffle area (α)

The effect of free baffle area (α) in mixing time and axial dispersion has been studied by several authors (e.g. Gough *et al.* (1997), Ni *et al.* (1998), and Zhang *et al.* (1996)). This parameter is defined by relating orifice diameter and column diameter as described by Eq. (2.5).

$$\alpha = \frac{d_o^{\,2}}{d^2} \tag{2.5}$$

For a range of α values from 11 to 55 %, Ni *et al.* (1998) have reported the lowest value as the best to achieve good mixing level, resulting in shorter mixing times. Nevertheless, Gough *et al.* (1997) have found out a higher value for α (0.63) as the best to achieve efficient mixing of a polymerization suspension. In the same study, small symmetrical eddies were formed at the baffles' edges and the vortex rings did not encompass the entire inter-baffle cavity, for the correspondent α value of 0.26. The study conducted by Zhang *et al.* (1996), in liquid-liquid dispersions, has shown a minimum value of α tested (0.19) to achieve the best dispersion of liquid-liquid solutions. In an oil-water system, the increase of dispersion with the oscillatory velocity has superior rate using lower values of d_0 instead of higher ones (Ni *et al.*, 2000b).

Effect of baffles spacing (L)

The baffle spacing is an important parameter in the design of OFR once it influences the shape and extension of eddies within each baffle cavity, for a given x_0 (Brunold *et al.*, 1989; Knott & Mackley, 1980). Despite not included in the dimensionless groups for oscillatory regime, Mackley *et al.* (1993, in Reis, 2006) defined a new dimensionless group, the Stroke ratio, to characterise the flow by relating x_0 and L. The optimal L is the one ensuring that the generated vortex rings fully expand behind baffles and vortices spread effectively throughout the entire inter-baffle cavity (Reis, 2006). Optimal L values have been reported in the range of 1.5–1.8 times the column diameter (Brunold *et al.*, 1989; Ni & Gao, 1996). Small values of L suppress the formation of vortices and reduce the radial dispersion in each cavity, while the opposite effect occurs when baffles are enough spaced (Reis, 2006). Thus, vortex rings formation depends on the L value.

Effect of baffle thickness (δ)

The generation of vortices, due to the presence of a baffle, is comparable to that occurring in a fluid that flows around an object (Reis, 2006). Since there is an optimal time that an eddy needs to be processed, the thickness of the baffle is also important in the vortex formation (Ni & Gough, 1997). Thus, thinner baffles, with small δ values, have been reported as the optimal ones to favour the vortices generation (Ni *et al.*, 1998). Moreover, if vortices attach to baffle edges for too long prior to shedding, using a high δ value, their shape can distort somewhat, and affect mixing time (Reis, 2006). High values of δ can result in high mixing times, in the order of five-fold greater than those of the small thickness (Ni *et al.*, 1998).

2.6.6 Effect of oscillation controlling parameters

The main parameters controlling an oscillatory system are the oscillation frequency (f) and amplitude (x_0). For a constant L and d_0, by varying the combination of f and x_0 is possible to control eddies formation and promote a range of fluid mechanical conditions (Gough *et al.*, 1997). In liquid-liquid extraction processes, x_0 and f have an important effect on the minimum frequency for complete dispersion of oil-water system, as reported by (Zhang *et al.*, 1996). An increase in x_0 from 6 to 12 mm can cause a 50 % reduction in dispersion of phases. For columns with a L value from 1 to 2.5 times the column diameter, mixing time can decrease with the increase of both f and x_0 (Ni *et al.*, 1998). In fact, in oil-water dispersion, mixing can be much more affected by f and x_0 than design parameters, such as d_o and L (Ni *et al.*, 2000b). The degree of dispersion increase linearly with the oscillatory velocity until a complete dispersion is achieved (Reis, 2006).

In mass transfer studies, f and x_0 appear to affect the mass transfer measurements, as has been found by Ni *et al.* (1995a), using a yeast cell suspension. The oxygen mass transfer coefficient, K_La, has been reported to increase with the increasing of f (from 3 to 12 Hz) for different x_0 (from 4 to 14 mm), using a 25 mm internal diameter OFR. Moreover, K_La is more affected by changes in x_0 than in f. This fact means that x_0 is responsible for the length of eddies generated in the column (Ni *et al.*, 1995a).

2.6.7 OFM applications diversity

The OBC has been used to improve the performance of a variety of operations and processes in chemical and biological engineering. Among these operations and processes the following are included: heat transfer (Mackley & Stonestreet, 1995; Mackley *et al.*, 1990), mass transfer (Hewgill *et al.*, 1993; Ni *et al.*, 1995a; Ni & Gao, 1996; Oliveira & Ni, 2004; Reis *et al.*, 2008), particle mixing and separation (Mackley *et al.*, 1993, in Reis, 2006), plug flow operation in continuous reactors, filtration, bio-reaction, and fermentation (Ni *et al.*, 2003). Some examples of the main typical enhancements that can be achieved, in some of these processes and operations, due to oscillatory flow utilisation, are following described.

Heat transfer enhancement

The application of oscillatory flow in a baffled column can significantly enhance heat transfer, either in batch or continuous operation. The tube-side heat transfer coefficient, given by Nusselt number (*Nu*), in laminar regime for the mean flow, can be improved by a factor of 10 to 30. Therefore, it is possible to achieve heat transfer coefficients of the same order as in smooth column working on a turbulent regime, with high Reynolds numbers. This evidence was found by Mackley and Stonestreet (1995) and is illustrated in Figure 2-10.

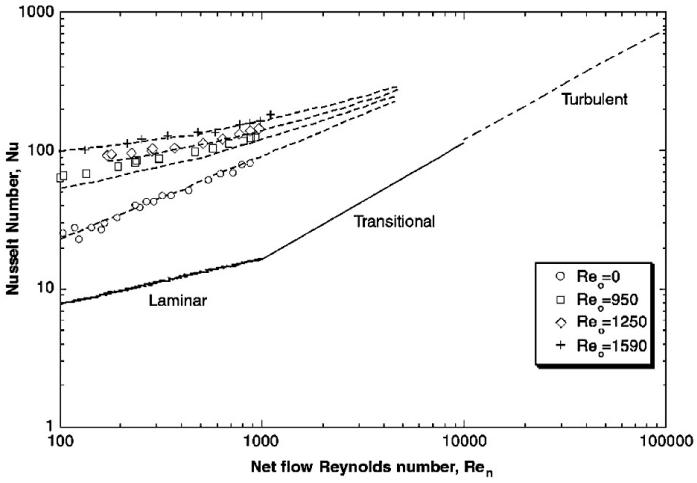

Figure 2-10 Heat transfer enhancement in oscillatory baffled tubes (Ni *et al.*, 2003).

The authors also claim that the presence of oscillations in the flow has a good effect on the heat transfer beyond the effect of the mean flow velocity. Furthermore, this effect is most significant at low net flow rates (less than 1000), which corresponds to laminar flow, in steady flow conditions. Then, the enhancement of heat transfer by using oscillatory flow resides in the fact that high heat transfer coefficients can be obtained in continuous mode, at considerably lower Re_n than in conventional tubular reactors (Ni *et al.*, 2003).

Plug flow reactors

An important advantage of OBC in continuous operation is related with the residence time distribution (RTD) performance, which can be improved independently of net flow conditions (Ni *et al.*, 2003). Several studies have been conducted for this phenomenon, using single-phase systems (Mackley & Ni, 1991, 1993; Ni & Pereira, 2000; Stonestreet & van der Veeken, 1999). The main aspects that have been found reveal the possibility to achieve plug flow by working in laminar regime (low bulk flow Re_n), and the control of RTD can be done by controlling the oscillation conditions, independently of the bulk flow. Therefore, OBC are found as an ideal system when plug flow conditions and long residence time are required.

Effective solids suspension

The advantages of the OBC for particles suspension in a vertical column either uniform or stratified according to size and density has been presented by Mackley *et al.* (1993, in Reis, 2006). An empirical correlation has also been reported describing this behaviour. Either uniform or stratified suspension can be obtained in the column, depending on the relation between the maximum oscillation velocity and the settling velocity of the particles. This makes the OFM application advantageous, whenever separation of particles by different size and/or density is desired, during operation. This separation technique is known as 'wet sieving' (Ni *et al.*, 2003).

Effective low shear mixing capability

The volume averaged shear rate in OBC normally achieves values as low as 10–20 s^{-1}, compared to those obtained in stirred tank reactors, typically on the order of 100 s^{-1} or greater (Ni *et al.*, 2003). The very low and uniform shear rate along with good bulk mixing is an advantageous characteristic of the OBC in the areas of bio-applications, such as chemical, medical and

pharmaceutical (Ni *et al.*, 2000a; Ni *et al.*, 1995b). On a large industrial scale, the mixing of liquids and suspensions that can be achieved by one single oscillating baffle is more efficient than the corresponding impeller agitators. This phenomenon occurs because vortex mixing in large tanks is much more affected by bulk transport than shear (Ni *et al.*, 2003).

Process intensification of batch reactors

In processes at which continuous mode is not viable to perform a particular reaction, batch process is an alternative solution. Nevertheless, there are some important aspects in batch systems that limit the degree of optimisation that can be achieved and large amounts of substrate are required. Thus, batch process intensification appears as an optimal solution to overcome this problem and optimise reactor performances. In chemical industry, the batch production of sterols by the saponification of steryl esters is an example of optimisation by process intensification (Ni *et al.*, 2003). The large volume of solvent (50 m^3 of ethanol), above its ambient pressure boiling point required to perform the reaction raises important safety concerns. Furthermore, the long reaction time (2 h) make the process impractical to be performed in conventional tubular reactors, since high length-to-diameter ratio would be required, to achieve high enough Reynolds numbers for good mixing and plug flow (Ni *et al.*, 2003). Since, in OBR the mixing is controlled by oscillations rather than by the net flow, a much smaller length-to-diameter ratio would be needed to perform the same reaction, making the process practicable and feasible. Thus, by converting long residence time batch processes in continuous processing, OBR application is an example of process intensification (Ni *et al.*, 2003). Figure 2-11 shows the reduction of reactor volume that is possible to achieve (by two order of magnitude) in a pilot-scale study for this reaction, by converting the conventional batch system into a continuous OBR (Harvey *et al.*, 2001). Since there are no mixing limitations in the OBR, the residence time can be largely reduced, resulting in a reduction in the size of the reactor. Furthermore, the total reaction time can be reduced to one-twelfth of the batch cycle time (Ni *et al.*, 2003).

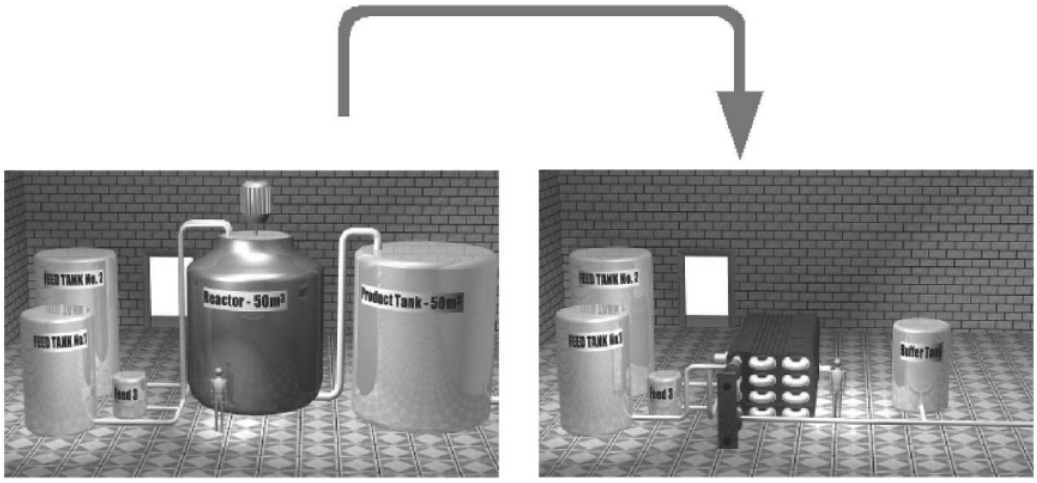

Figure 2-11 Representation of the size scale reduction achieved in process intensification using an oscillatory baffled reactor (Ni *et al.*, 2003).

Scale-up and design of OBR

The OBR can be scaled-up by a simple linear geometric scaling, assuring that dynamic similarity via the oscillatory and net flow Reynolds numbers are maintained (Ni *et al.*, 2003). This method has been used as the basis for industrial-scale OBR design, studied by Stonestreet and Harvey (2002). In fact, the predictability of scale-up for an OBR is an advantage over STR, in which changing from lab-scale to full-scale needs to be tested at increasing reactor size. Several studies have proven this linearity of OBR scale-up (Lee *et al.*, 2001; Ni & Gao, 1996; Smith & Mackley, 2006; Smith, 1999).

Experiments conducted by Smith (1999) have shown that the results obtained for a column in a small laboratory scale (less than 1 L of fluid) can with confidence be used to predict mixing behaviour in a much larger scale (hundreds of litters). A lab-scale OFR, used as protein-refolding reactor, has analogous performance and mixing properties to a conventional batch reactor, as described by Lee *et al.* (2001). The mass transfer coefficients in an OBR increase with the increase of scale, for a given power density, confirming the linearity of scale-up, as has been shown by Ni and Gao (1996). Similarly, the power consumption of an OBR in a large scale can be estimated by adding the individual power consumptions of the net flow (with an oscillatory enhancement factor) and the oscillatory flow (Baird & Stonestreet, 1995 in Ni *et al.*, 2003).

An important aspect to be considered is whether the oscillatory technology can be scaled-up. In the case of PPC and RPC, which are technologies extensively used in industry since the 1950s with a range of equipment sizes documented and commercialised, makes the oscillatory technology robust (Ni *et al.*, 2003). On the other hand, scale-up and design of OBR and large-scale industrial reactors are still being developed (Ni *et al.*, 2003).

Gas-liquid mass transfer enhancement

Effective enhancement can be achieved in the mass transfer coefficient, for gas-liquid systems, when oscillatory flows are used instead of conventional mixing. Herein, some more details on the application of OFM for mass transfer purposes are described. Typical K_La in air–water systems, as a function of power density, are compared for an OBC and a conventional stirred tank, and exemplarily represented in Figure 2-12 (Ni & Gao, 1996).

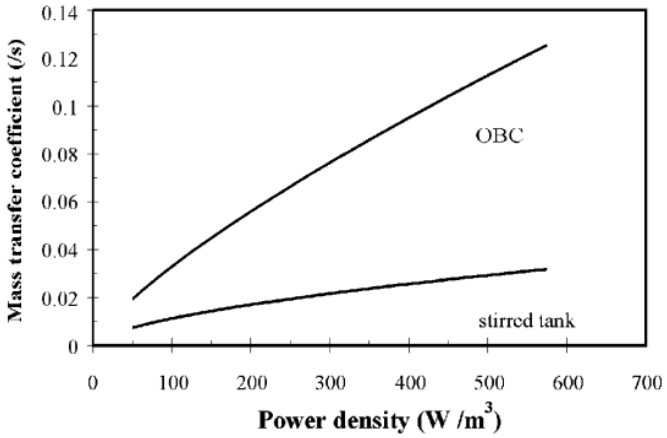

Figure 2-12 Air-water mass transfer enhancement, for OBC and stirred tank systems (Ni *et al.*, 2003).

The same comparison can be seen for a system with yeast culture, as shown in Figure 2-13, resulting in an increase in the mass transfer rates due to flow oscillations (Ni *et al.*, 1995a). This enhancement occurs due to combination of continuous breakage and coalescence of bubbles and the larger gas holdup that results from the oscillatory motion (Oliveira & Ni, 2001).

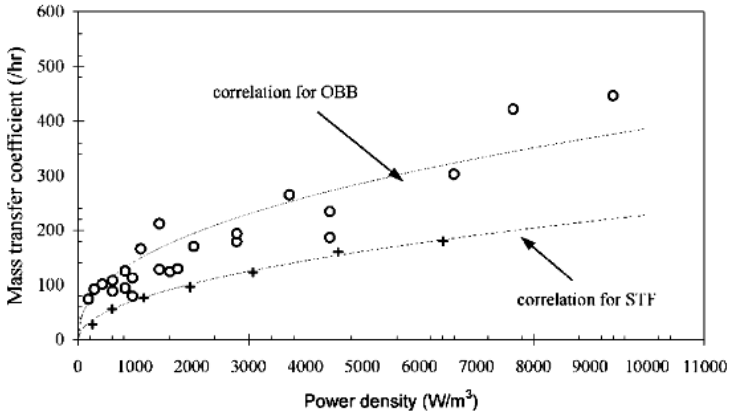

Figure 2-13 Air-yeast mass transfer enhancement in an oscillatory baffled bioreactor (OBB) and a stirred tank fermentor (STF) (Ni *et al.*, 2003).

Technology based on oscillatory flow mixing (Mackley & Ni, 1991) has shown great results compared with the more conventional technology, regarding to residence times and mixing, and intensification of gas-liquid flows (Reis *et al.*, 2004; 2007). The application of this technology to enhance gas-liquid mass transfer has been recently reported in some studies (Reis *et al.*, 2008; Taslim & Takriff, 2004).

Research carried out by Reis *et al.* (2008) was focused on the study of the effect of the fluid oscillations on the K_La values for O_2, imposing variations in the oscillations amplitude (centre-to-peak) and frequency. They monitored the dissolved oxygen saturation levels, in continuous mode by using a micro-optrode instead of an electrode, because of the more suitability it presents to bioengineering applications. To calculate the K_La values, they used a mathematical model of O_2 mass transport at different combinations of oscillations frequency (ranging from 0 to 20 s^{-1}) and amplitude (in the range of 0–3 mm), such a model is described elsewhere (Reis *et al.*, 2008). Their results showed a good improvement in the K_La values (up to 0.16 s^{-1}) for O_2 using this kind of technology, especially by involving very low mean superficial gas velocity (0.37 mm s^{-1}), when comparing with other conventional technologies. This enhancement occurred due to the increase gas holdup by reducing the rise velocity of bubbles, caused by the presence of narrower constrictions along the reactor. Reis *et al.* (2008) classified this work as an important step toward the design of scale-down platforms based on the oscillatory flow, with particular interest in

applications where gas-liquid mass transfer of a solute, such as O_2, is often the rate-controlling step. The technology used by Reis *et al.* (2008) consists on a mesotube with smooth periodic constrictions, in which the maximum internal diameter is equal to 4.4 mm.

Ni and Gao (1996) technology consisted in a two baffled columns with 50 and 100 mm of internal diameter. Such reactors were used to study the mass transfer issues in order to determine scale-up correlations. Their results showed that mass transfer performance was better for the larger reactor. Ni and Gao (1996) also realized that scale-up correlation of mass transfer is linear for this kind of system, which provide essential information to enable reactor design and scale-up.

In another study, Taslim and Takriff (2004) used an oscillatory baffled column with 50 mm of internal diameter to evaluate the mass transfer performance of pure CO_2 in water. The authors reported significant increase in mass transfer compared to that obtained in bubble columns. The continuous liquid flow rate used in the process showed no effect on K_La values for CO_2.

Also, Hewgill *et al.* (1993) studied the effect of oscillations on the mass transfer performance of O_2, whose results are in agreement with the previous ones described. Moreover, they reported power density calculations showing that the oscillatory flow system is more energy efficient than the conventional gas-sparged systems.

Oscillatory flow mixing, either in baffled column or in constricted mesotube, appears as a promising technology to enhance mass-transfer rates of O_2. The application of such technology for sparingly soluble gases, such as H_2 and CO, is viewed as a promissory research direction to syngas conversion purposes.

CHAPTER 3

Anaerobic syngas conversion using granular sludge: effect of pH and pressure

3.1 INTRODUCTION

Biomass and recalcitrant residues are suitable and available feedstocks for the production of biofuels (Bridgwater, 1995). These materials can be converted to syngas – a gaseous mixture mainly composed by carbon monoxide (CO), hydrogen (H_2), and carbon dioxide (CO_2) –, which can be further converted to biofuels using thermochemical or biotechnological processes. Anaerobic digestion (AD) of syngas can be used for the production of *e.g.* hydrogen, methane, ethanol, butanol, acetic and butyric acid (Henstra *et al.*, 2007). Coupling syngas AD processes to waste treatment facilities can substantially improve energy recovery – for example, it is estimated that the production of biogas from municipal solid wastes can be improved by over 80 % if the nonreadily organic fraction is gasified to syngas and further anaerobically converted (Guiot *et al.*, 2011).

In syngas conversion, the reaction pathways that can derive from combinations of the main components, CO, H_2, and CO_2 is vast and unpredictable, when a complex microbial consortium, as anaerobic sludge is used as catalyst. Figure 3-1 schematise a complex possible network of reactions resultant from three combinations of syngas components: CO with water from the liquid phase, CO and H_2, and H_2 and CO_2. The simple CO reaction with water (1 mol each) producing H_2 and CO_2, is also known as Water-Gas Shift (WGS) reaction, can be performed by hydrogenogenic CO-oxidizing microorganisms, such as *Carboxydothermus hydrogenoformans* (Svetlitchnyi *et al.*, 2001). Other microorganisms that may be present in an anaerobic mixed culture are able to perform other specific reactions. Moreover, some reactions are thermodynamically more favourable than others, depending on the conditions of the process (Guiot *et al.*, 2011). Different lines of products can be formed, which are mainly gases compounds (H_2, CO_2 and CH_4), and liquid compounds (organic acids and alcohols). Some of these products formed can act as intermediates to be further converted to methane, whose reactions are performed by methanogenic microorganisms, such as, some *Methanosarcina* and *Clostridium* species (Demirel & Scherer, 2008).

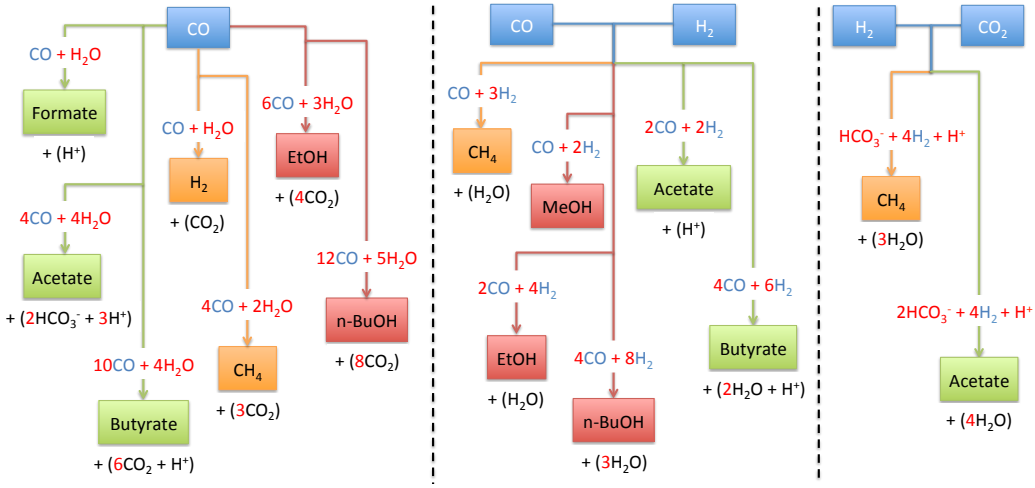

Figure 3-1 Schematic representation of the possible reactions network for syngas conversion. The three sections represent pathways form different combinations of syngas components (blue boxes). In each section different lines of products are represented: gases (orange), organic acids (green), and alcohols (red).

Figure 3-2 represents a schematic of the possible reactions that can be performed to produce CH_4 from intermediates, organic acids and alcohols, during syngas conversion, in the presence of a mixed culture.

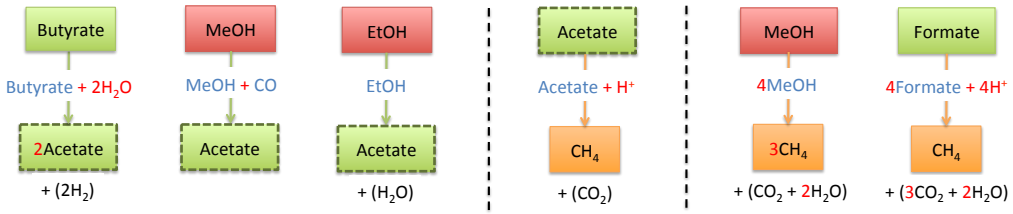

Figure 3-2 Possible reactions for methane production from intermediates of syngas conversion.

The potential of using mixed cultures based on natural inocula, is a promising approach to produce a wide range of bulk chemicals compounds, using the same reaction vessel and process conditions (Temudo *et al.*, 2008). Unlike pure culture-based systems, mixed cultures utilisation presents no high risk of contamination or strain degeneration and does require high cost for

process operation or culture maintenance. Moreover, a mixed culture is able to perform conversions from a diversity of substrates, such as syngas conversion. Products formed during the AD of syngas are dependent on the environmental conditions of the process. The big challenge nowadays is to direct biochemical pathways towards the formation of a specific compound of interest, which can be done by exploiting energy niches within mixed cultures (Rodríguez *et al.*, 2008). It is important to study the effect of environmental parameters, such as media composition, pH, temperature, pressure, mixing properties, and substrate or/and product concentrations in the conversion pathways of syngas (Gaddy, 2000).

In this study, syngas conversion by a mesophilic anaerobic granular mixed culture was studied in batch assays. The effect of the some environmental parameters, initial medium pH, initial total syngas pressure, and CO partial pressure, in syngas conversion were assessed. The range of products that can be formed in such conditions, were also evaluated. In parallel, methanogenic-inhibited sludges were also used to study the potential of mixed cultures for the production of specific compounds, such as short-chain fatty acids and alcohols.

3.2 EXPERIMENTAL METHODS AND PROCEDURES

3.2.1 Experimental Design

Two different factorial experimental designs were implemented in this study. The first design was initially implemented to evaluate the effect of both pH and initial syngas pressure, P_T on substrate conversion by anaerobic mixed cultures at 37 °C. Two scenarios were evaluated using methanogenic-active and methanogenic-inhibited inocula. Thus, this assay consisted in a factorial experiment with 36 runs ($2 \cdot 3^n$, with $n = 2$ variables, in duplicate).

The second design was planned to evaluate the combined interaction effect between total syngas pressure and CO partial pressure, p_{CO} on substrate conversion, using the same type of inocula at 37 °C. All the tested variable combinations in factorial design 2 are summarised in Table 3-1.

Table 3-1 Combination of the independent variables tested in the factorial experimental design 2, with respective minimum, average, and maximum values

	Initial total syngas pressure, P_T (atm)		
CO Partial Pressure	Minimum	Average	Maximum
p_{CO} (atm)	1.00	1.75	2.50
0.0	✓	✓	✓
0.2	✓	✓	✓
0.4	✓	✓	✓
0.6	✓	✓	✓
0.8	–	✓	✓
1.0	–	✓	✓
1.2	–	–	✓
1.5	–	–	✓

Notes: (✓) combination tested; (–) combination not tested; (shaded area) set of points used in the factorial experimental design.

This second design consisted in a total of 51 runs, from which only 27 runs (points on the shaded area of the Table 3-1) were used as part of the factorial experimental design (3^n, with n = 2 variables, in triplicate). The remaining 18 runs were used to evaluate patterns for each P_T value. Table 3-2 shows the design matrix of the two factorial designs studied.

Table 3-2 Design matrix of the 3^2 factorial experimental design 1 and 2

	Design 1		Design 2	
	X_1	X_2	X_1	X_2
Test	pH	P_T	P_T	p_{CO}
	[-]	atm	atm	atm
1	+1	-1	+1	-1
2	0	0	0	0
3	-1	+1	-1	+1
4	-1	-1	-1	-1
5	-1	0	-1	0
6	+1	0	+1	0
7	0	-1	0	-1
8	0	+1	0	+1
9	+1	+1	+1	+1

Notes: (+1) maximum value; (-1) minimum value; (0) average value

Experiments were carried out in 160 mL vials (Figure 3-3), prepared with 80 mL of liquid medium and equal volume of headspace. The liquid medium was composed by 20 mM of buffer solution (MES, 2-(N-morpholino)ethanesulfonic acid, or HEPES, 4-(2-hydroxyethyl)-1-piperazineethane-sulfonic acid, depending on the required pH), 5 g L^{-1} of granular sludge (sourced from the brewing industry), 0.1 M of reducing agent (Na_2S) and 1 mL L^{-1} of vitamin solution (Stams *et al.*, 1993). Besides, in assays where methanogens were inhibited (design 1), 50 mM of BES (2-bromoethanesulphonate) was also added. Vials were sealed with rubber stoppers and aluminum caps and the headspace was filled with syngas mixture at the initial total syngas pressures studied (1.0, 1.75, and 2.5 atm).

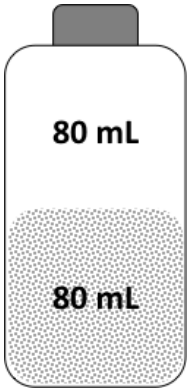

Figure 3-3 Representation of the 160 mL-vials used in this study (white area: headspace; grey area: liquid medium).

The composition of the syngas mixture used was constant and equal to 60 % CO, 30 % H_2, and 10 % CO_2, for the factorial experimental design 1 (corresponding to initial CO partial pressures of 0.6, 1.0 and 1.5 atm, respectively). Medium pH was an independent variable tested in the factorial experimental design 1, in which three values were set: 5.8 (using MES buffer), 6.9 and 7.6 (using HEPES solution).

In the factorial experimental design 2, medium pH of 5.8 was chosen for all conditions, based on the results of design 1. For each total syngas pressure tested (1.0, 1.75, and 2.5 atm) a range of eight different CO partial pressure values were examined (see Table 3-1), ensuring that CO did

not exceed 60 % of initial gas composition. Moreover, CO/H_2 and CO_2/H_2 ratios were kept constant at 2 and 0.25, respectively. In order to keep total pressure constant, while varying partial pressures of gas components, N_2 gas was used for dilutions.

3.2.2 Analytical Methods

Gaseous compounds (H_2, N_2, CO_2, CH_4, and CO) were analysed by Gas Chromatography (Chrompack 9001B) equipped with a TCD detector and two columns: Porapak Q and Molsieve 5 Å (2 m × 1/8'' × 2 mm SS, 80-100 mesh, Varian). In this method, all gaseous compounds are separated in the Molsieve, except CO_2 that is only separated in the Porapak. Argon was the carrier gas at a flow rate of 10 mL min^{-1}. The column, injector, and detector temperatures were 35, 110, and 110 °C, respectively.

Volatile fatty acids (VFA) were determined by HPLC (Jasco, Japan) equipped with a UV detector set at a wavelength of 210 nm and a Chrompack column (6.5 × 30 mm^2) at 60°C. Sulphuric acid (0.01 N) was used as mobile phase at a flow rate of 0.6 mL min^{-1}.

Alcohols were determined by Gas Chromatography (Varian 4000) equipped with a FID detector and a TRB-WAX column (30 m × 0.25 mm × 0.25 μm, Teknokroma). Helium was the carrier gas (1 mL min^{-1}). The injector and detector temperatures were 250 °C, and column was run with temperature ramps from 50 to 60 °C, at a rate of 0.5 °C min^{-1}, and from 60 to 200 °C, at a rate of 40 °C min^{-1}, followed by a stabilization period (1.5 min) at 200 °C. A split ratio of 1:10 was set in the injector.

3.3 RESULTS AND DISCUSSION

3.3.1 Effect of pH and total pressure on syngas conversion by anaerobic sludge

Methane can be directly produced from syngas components, according to the reaction equations (1) to (3).

(1) $4\ CO + 2\ H_2O \rightarrow CH_4 + 3\ CO_2$

(2) $CO + 3\ H_2 \rightarrow CH_4 + H_2O$

(3) $CO_2 + 4\ H_2 \rightarrow CH_4 + 3\ H_2O$

Acetate can also be produced directly from CO or CO/CO_2 plus H_2, as described by reaction equations (4) to (6).

(4) $4\ CO + 4\ H_2O \rightarrow Acetate + 3\ CO_2$

(5) $2\ CO + 2\ H_2 \rightarrow Acetate$

(6) $2\ CO_2 + 4\ H_2 \rightarrow Acetate + 4\ H_2O$

In methanogenic systems, acetate can be further converted to biogas (CH_4 and CO_2 mixture). In this work, and for the sake of comparison between the different conditions tested, product formation was reported to the initial pressure of syngas, whose results will be expressed as mM of product per atm of syngas in the beginning of the assay. Whenever concentrations are shown the amount of components is always referred do to volume of the liquid medium.

3.3.1.1 Syngas conversion by methanogenic sludge

Methanogenic mixed cultures were able to completely consume CO and H_2 present in syngas, with the production of mainly CH_4. Carbon monoxide conversion by these cultures, when incubated with 1.0 atm syngas, was achieved in less than 72 h. A longer incubation time, up to 240 h, was necessary for converting CO in assays at higher syngas pressures. Methane production, in assays conducted at different combinations of pH and initial syngas total pressure, P_T is shown in Figure 3-4. Variation of both P_T and pH had a stringent effect in methane production. Nevertheless, no trend with these two variables is concluded from the production profiles. The highest methane production, i.e. 31.4 mM CH_4/atm, was achieved with pH 5.8 and 1.0 atm syngas. On the other hand, the lowest methane production, 9.0 mM CH_4/atm, was obtained at the same pH and 2.5 atm of syngas.

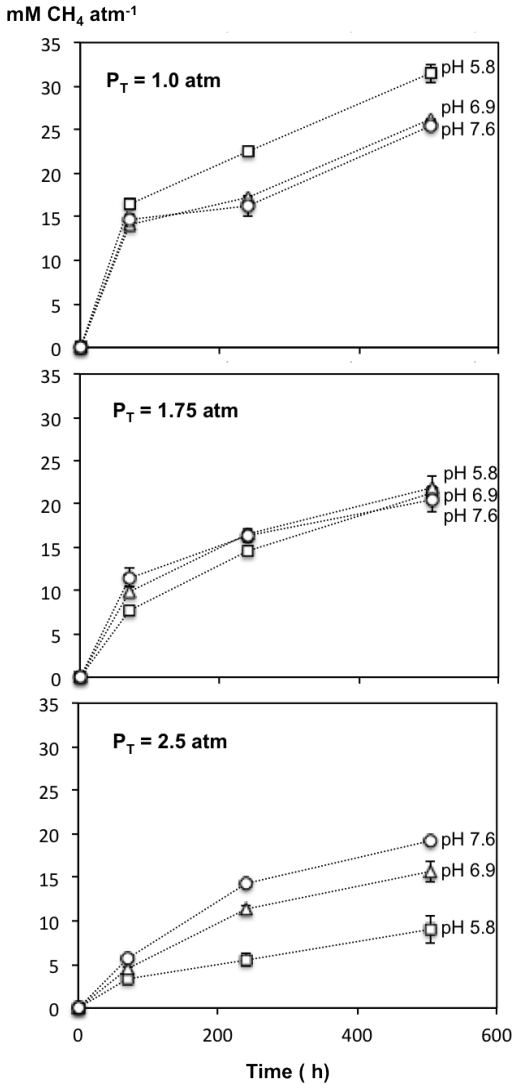

Figure 3-4 Methane production profiles (as mol of CH_4 produced per atm of initial syngas) over time, for the factorial experimental design 1, at different initial pH and total syngas pressure (P_T): (a) P_T = 1.0 atm, (b) P_T = 1.75 atm, and (c) P_T = 2.5 atm. Vertical bars represent standard deviation.

A negative trend between methane production and pH was observed in assays with 1.0 atm syngas, that is, methane production increased with decreasing the pH. The opposite was observed for the highest syngas pressure – in these assays methane production increased with increasing the pH. Thus, a combined effect of both pH and P_T seems to occur in the conditions tested. Using the methane production values achieved at the end of the experiment for each set of conditions, a 2D surface graphic was generated and is represented in Figure 3-5.

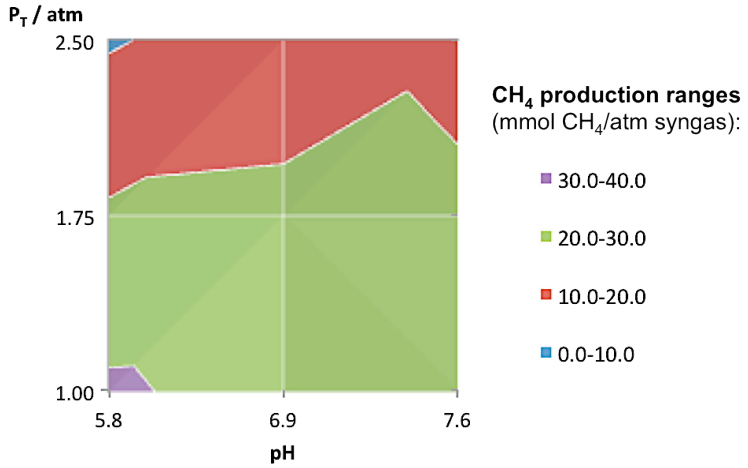

Figure 3-5 2D surface representation of final methane production (as mol of CH_4 produced per atm of initial syngas) obtained at the different combinations of pH and initial syngas total pressure (P_T), for factorial experimental design 1.

The graph clearly shows that the combination of lower levels of the variables tested (pH = 5.8 and P_T = 1.0 atm) was responsible for the maximum methane production obtained. Residual concentrations of VFA were detected in almost all the conditions tested, corresponding to a production of VFA below 0.34 mM VFA/atm by the end of the assays performed under 1.0 atm syngas. Nevertheless, a VFA production as high as 5.41 mM VFA/atm was obtained for the assay at pH 5.8 and 2.5 atm syngas, the same assay where methane production was the lowest. This seems to indicate that, under these conditions, methanogens activity tends to be inhibited. No alcohols were detected during the experiment time.

The effect of CO partial pressure in methane production has been reported in literature, using either pure or mixed cultures, during syngas conversion. *Methanosarcina barkeri* could use H_2 to produce methane, but consumption time doubled with an increase in CO partial pressure from 0 to 0.6 atm. This shows that some hydrogen-utilizing organisms require low dissolved CO concentrations (Klasson *et al.*, 1991). In fact, the decrease in syngas conversion with increasing syngas pressure, observed in the present study, might have been caused by the inhibition of methanogenic microorganisms for higher CO partial pressures. Mixed cultures might be more robust than pure cultures, but methanogenic activity from anaerobic sludges seems also to be affected by CO. Guiot *et al.* (2011) tested different CO partial pressures ranging from 0.42 to

0.96 atm, in a continuous gas-lift reactor with a mixed culture. Maximal CO conversion efficiency of 75 % was obtained at 0.6 atm of CO partial pressure combined with gas recirculation (Guiot *et al.*, 2011).

3.3.1.2 Syngas conversion by methanogenic-inhibited sludge

The main products from syngas conversion by methanogenic-inhibited sludge were VFA. Alcohols were detected in small concentrations (maximum, 1.1 mM ethanol and 0.5 mM butanol). Lower syngas pressure lead to the accumulation of higher amounts of VFA. Production of VFA, under the different conditions tested, is shown in Figure 3-6.

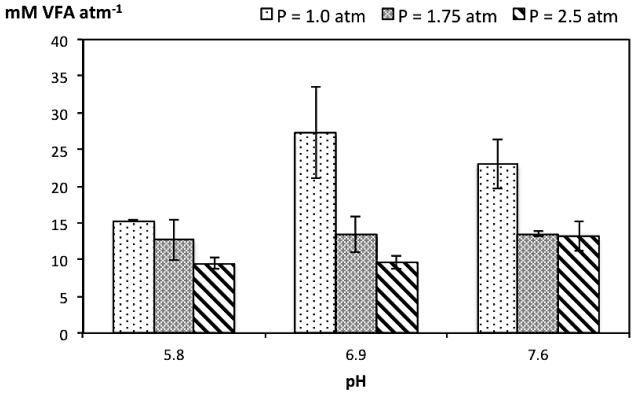

Figure 3-6 VFA production (expressed as sum of the total mM of VFA per atm of initial syngas) with pH, for the factorial experimental design 1, using methanogenic-inhibited sludge. Vertical bars represent standard deviation.

Acetate and propionate were the VFA detected in higher concentrations, varying in the range of 7.8–18.2 mM and 2.4–7.4 mM, respectively; lower amounts of butyrate were also detected (maximum 4.0 mM). The best VFA production occurred at pH 6.9 and 1.0 atm (27.3 mM VFA/atm). Furthermore, the lowest VFA production (9.6 mM VFA/atm) was obtained at the same pH and the 2.5 atm. According to data, no trend is possible to attribute to pH variation with gas pressure, for VFA production using methanogenic-inhibited sludge. In the present study the final concentrations of VFA have shown to be independent of the pH tested.

The effect of pH and gas pressure in VFA and alcohols production has been reported in literature, using pure cultures, during syngas or only CO conversion. Enhancement in the production of butyrate over acetate by *Butyribacterium methylotrophicum*, or ethanol over acetate by *Clostridium ljungdahlii*, has been achieved by reducing pH during the process (Gaddy & Clausen, 1992; Worden *et al.*, 1989). The same effect has been reported for ethanol production from CO by *Clostridium autoethanogenum*, in which up to 200 % enhanced has been achieved by lowering initial pH of experiments from 5.75 to 4.75 (Abubackar *et al.*, 2012). In that study, statistically significant interactions have been found with other factors, as cysteine–HCl·H_2O (0.5–1.2 g/L) and yeast extract concentration (0.6–1.6 g/L), and initial total pressure (0.8–1.6 atm).

In a metabolic perspective, the effect of pH in the electron production along the acetyl-CoA (Wood-Ljungdahl) metabolic pathway was studied by Hu *et al.* (2011). This pathway in which CO and CO_2 are used as carbon sources, and electrons produced from H_2 and/or from CO, electron production from CO is always more thermodynamically favourable over electron production from H_2 and not affected by pH.

Regarding the syngas pressure effect, no inhibition was observed in ethanol and acetate production by *Clostridium carboxidivorans* P7T, up to 2.0 atm of CO partial pressure (Hurst & Lewis, 2010). *Peptostreptococcus productus* was able to convert CO to acetate, with gradual increase of the CO partial pressure up to 10 atm. However, this high level of resistance to CO was only possible after promoting cell growth in the absence of CO in order to get very high cell densities (Klasson *et al.*, 1991).

3.3.2 Effect of syngas total pressure and CO partial pressure on bioconversion

The effect of total syngas pressure and/or CO partial pressure over production formation remained unclear from the results previously stated in experimental factorial design 1. Therefore, this fact has raised a question: is methane and VFA production affected by initial CO partial pressure, p_{CO} rather than syngas total pressure, P_T? In order to find an answer to this question, the effect of both p_{CO} and P_T was studied in a second set of experiments whose results are following presented. As lower pH has shown to enhance methane production, as well as other

products, in the experimental design 1, pH = 5.8 was chosen for the second experimental design. Measurement of pH at the end of the assay, have shown no significant variation, in the range of 6.0–6.3.

3.3.2.1 Hydrogen and carbon monoxide consumption

The mixed culture used in this experiment was able to completely consume CO and H_2, during the conversion process. The time required for full consumption, varied for the different conditions used and increased with increase in both P_T and p_{CO}. Hydrogen was the first compound to be consumed and consumption time ranges were 13–25 h (P_T = 1.0 atm), 15–35 h (P_T = 1.75 atm), and 20–110 h (P_T = 2.5 atm). This fastest consumption may be related to the hydrogenotrophic methanogenic microorganisms present in the mixed culture that are able to rapidly use H_2 and CO_2 to produce methane (Sipma *et al.*, 2003). Regarding the time of CO consumption, the ranges obtained were 35–60 h (P_T = 1.0 atm), 55–130 h (P_T = 1.75 atm), and 40–150 h (P_T = 2.5 atm). It is known that during syngas conversion, hydrogen reactions produce electrons that are directed to CO conversion process. When hydrogenase enzyme activity is inhibited, electrons may be generated from CO using CODH enzymes, which reduce the amount of carbon available for production formation (Abubackar *et al.*, 2011). In this case it is noted that consumption of CO is slower particularly when higher amount of CO is present in the headspace.

The variation of the amount of CO and H_2 present in the headspace of each vial was monitored along time. Figure 3-7 shows the consumption profile for CO and H_2, for each experiment. Using the initial points of consumption profile curves, the maximum initial consumption rates, r_i was calculated for each assay. These data was then plotted as a function of the initial dissolved CO concentration in the liquid (in equilibrium with the partial pressure of the gas in the headspace, according to Henry's Law).

Figure 3-8 shows the variation of these consumption rates for both CO and H_2. It should be noted that despite consumption rate variation for H_2 is plotted against CO dissolved concentration, the same patterns would be obtained if plotted against H_2 dissolved concentration, as the CO/H_2 ratio was kept constant (equal to 2).

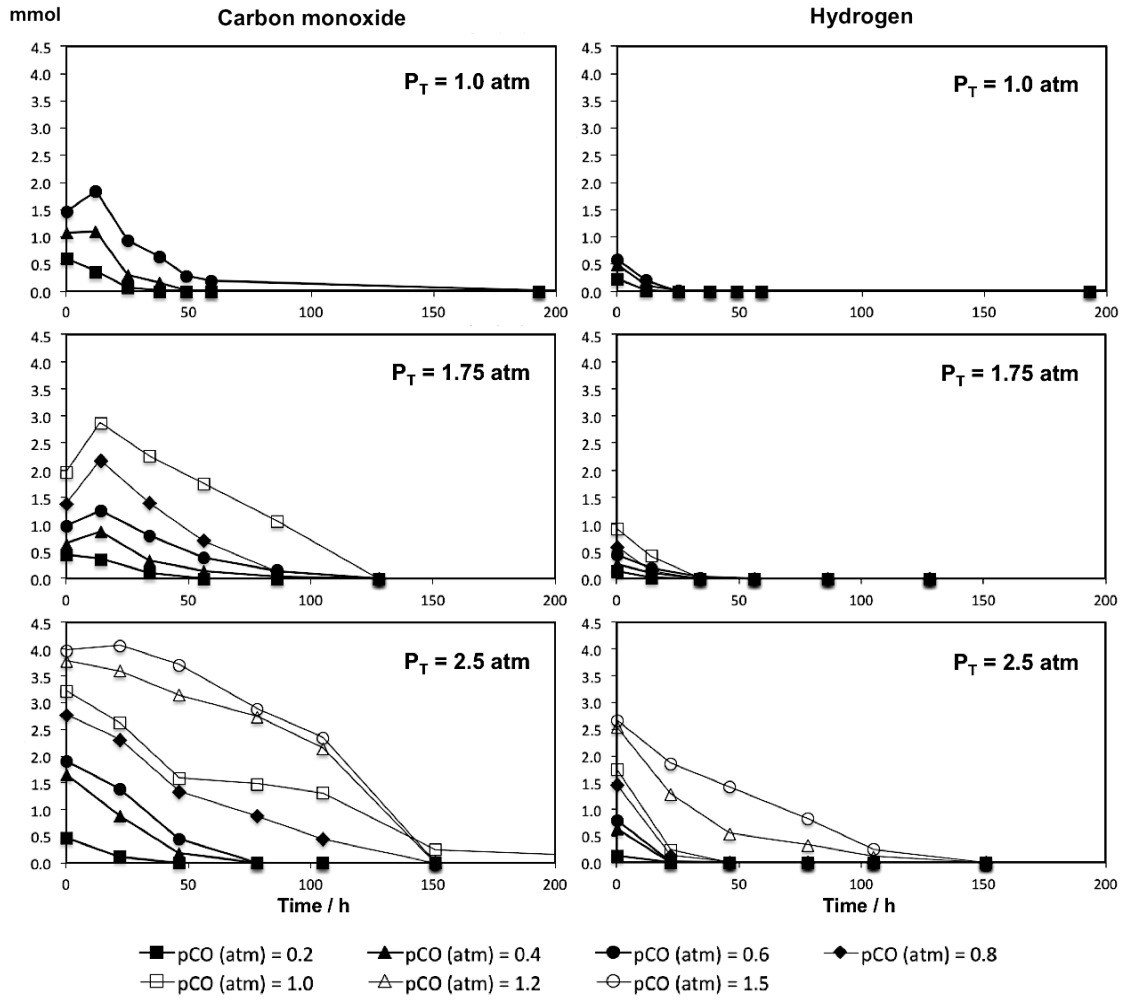

Figure 3-7 Carbon monoxide and hydrogen consumption profiles, expressed as the amount (mmol) of gas component present in the headspace as a function of time, for different initial CO partial pressure, at constant initial syngas total pressure of 1.0, 1.75, and 2.5 atm, for experimental design 2.

As shown in the graphs of Figure 3-8, generally consumption rates increase with increments in CO dissolved concentration for each P_T applied. Although, for assays at P_T = 2.5 atm, this increasing trend was inverted above dissolved concentration of 0.31–0.46 and 0.77 mM, for CO and H_2 consumption rate curves, respectively. Moreover, H_2 consumption rates at P_T = 2.5 atm is twice of as the ones for CO, while for the assays at lower P_T almost similar rates were obtained. This makes evidence that microbial mixed culture tend to significantly prefer to perform H_2 uptake by reaction with CO_2 present in the syngas rather than CO uptake. Consumption rates as high as 0.77 mmol CO d^{-1} and 1.64 mmol H_2 d^{-1} were obtained at P_T of 2.5 atm.

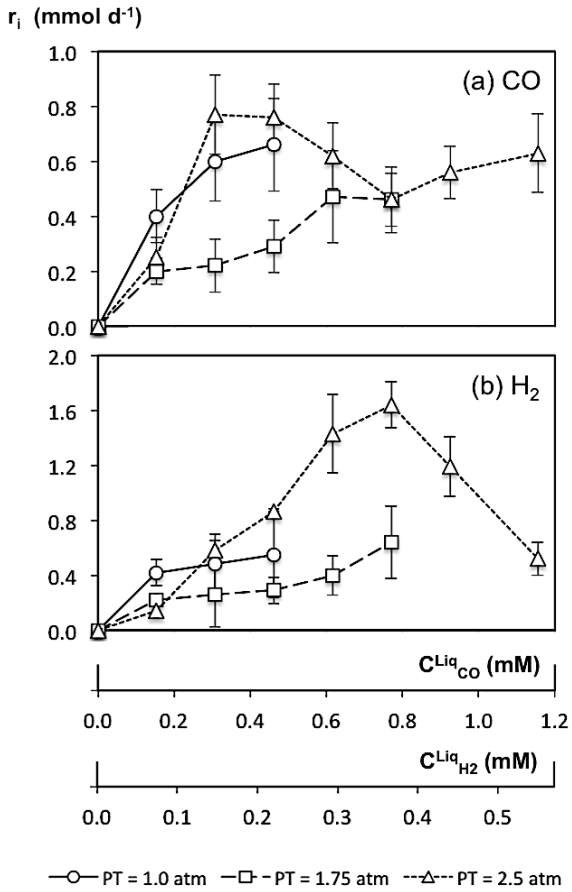

Figure 3-8 Maximum initial consumption rate, r_i variation with dissolved CO concentration in the liquid medium, C^{Liq}_{CO} for (a) CO and (b) H_2, at each initial syngas total pressure studied, in experimental design 2. An axis with dissolved H_2 concentration in the liquid medium, C^{Liq}_{H2} is also represented.

3.3.2.2 Methane production rate and yield

Methane is the one of the most important products resulting from syngas conversion under anaerobic conditions, using a mixed culture. The amount of methane present in the headspace of the vials was monitored along time. The methane production profiles in the first 60 hours of the experiment, for each conditions tested, are represented in Figure 3-9.

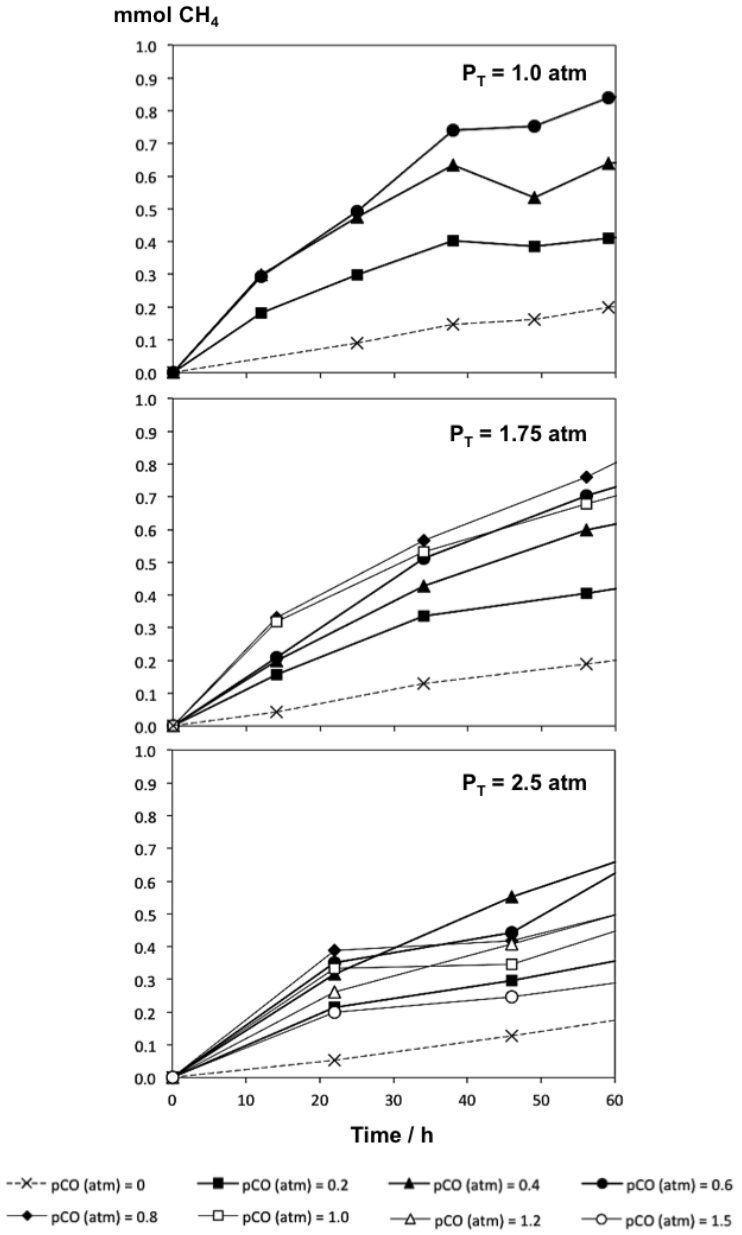

Figure 3-9 Methane production profile, expressed as the amount (mmol) of CH_4 present in the headspace as a function of time, for different initial CO partial pressure, at constant initial syngas total pressure of 1.0, 1.75, and 2.5 atm, for experimental design 2.

Using these concentration profiles, maximum initial methane production rates, $r_{i,CH4}$ were determined, following the same procedure as for consumption rates of CO and H_2, and plotted against dissolved CO concentration, C^{Liq}_{CO}, represented in Figure 3-10(a). Methane production rates seem to be significantly dependent on both P_T and p_{CO}.

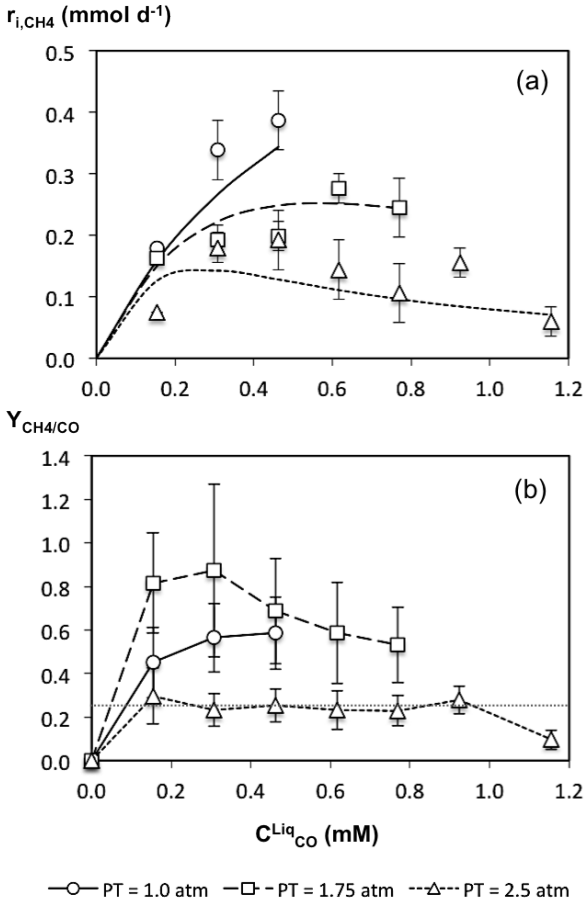

Figure 3-10 Initial methane production rate, $r_{i,CH4}$ (a) and yield from CO, $Y_{CH4/CO}$ (b) variation, as a function of CO dissolved concentration, C^{liq}_{CO} for all the conditions applied in the experimental design 2. Lines in graph (a) represent the fitting of data to the adapted Monod's kinetic modelling (Eq. (3.1). Dashed line in graph (b) represents the minimum threshold for theoretical CH_4 yield from CO.

Data of $r_{i,CH4}$ variation with C^{Liq}_{CO} was then fitted to an adapted typical Monod equation for kinetic behaviour (Sivakumar *et al.*, 1994), considering substrate inhibition, described in Eq. (3.1).

$$r_i = r_i^{max} \cdot \frac{S}{K_S + S + \frac{S^2}{K_I}} \qquad (3.1)$$

In this adaptation, the microorganism growth rate is replaced by production rate of a compound. Thus, in this Eq. (3.1), r_i is the production rate (mol d^{-1}), r_i^{max} is the maximum production rate (mol d^{-1}), S is the substrate concentration (mol L^{-1}), K_S and K_I are constant of the model. K_S

represent the concentration of substrate at which production rate is half of the maximum (mol L^{-1}), while K_I represent a measure of the inhibition effect of the substrate (mol^2 L^{-2}).

Data of $r_{i,CH4}$ variation with C^{Liq}_{CO} have shown relatively good fitting to Eq. (3.1), which helps to explain the kinetic behaviour of this microbial systems, during syngas conversion, under the tested conditions. According to Monod's kinetics, this change of shape in the curves (Figure 3-10(a)) is explained by the inhibitory effect of the substrate over the biocatalyst. In this case, it represents the effect of dissolved CO concentration over the microbial consortium as a whole system, and the change of shape should not be described as pure inhibition by substrate, but rather a slow down in the production rate affected by the interaction with substrate. The inexistence of inhibitory effect could be explained with the fact that main substrates were completely consumed in all tested conditions, as shown before. Thus, the highest maximum CH_4 production rate achieved was 0.39 mmol CH_4 d^{-1}, at P_T = 1.0 atm and p_{CO} = 0.6 atm. Interestingly, the conditions in this assay correspond to syngas mixture composition (60 % CO) as commonly generated by coal-based gasification processes (Alves, 2013; Sipma *et al.*, 2006a; Tirado-Acevedo *et al.*, 2010), at atmospheric pressure. This fact seems to reveal a set of optimal conditions in which considerably high methane production rate is achieved and feasible to apply in continuous conversion process at relatively low process costs.

Methane yield variation, expressed as the ratio of initial rates of CH_4 production over CO consumption, $Y_{CH4/CO}$ with dissolved CO concentration, C^{Liq}_{CO} was also studied and is shown in Figure 3-10(b). It is important to highlight the fact that methane yield is here reported only to CO consumption. Although product formation can also be generated by CO_2 and H_2, due to the complexity of the network of reactions involved in the whole process, CO was defined as the main carbon source of the syngas conversion process. This approach allows estimating normalised methane conversion yields for comparison purposes. As a matter of interest, the shape of the curves for methane yields reported to CO plus H_2 consumption rate instead of only CO consumption, is very similar the ones represented in Figure 3-10(b), although all values are half of the ones in here (data not shown). As can be observed in Figure 3-10(b), $Y_{CH4/CO}$ seems to be affected by P_T, although no trend is observed, since the highest values were achieved for P_T = 1.75 atm. Besides, at constant P_T, methane yield seems to be slightly affected by p_{CO}, since

methane yield start to decrease for C^{Liq}_{CO} higher than a certain value, except for the curve at P_T = 1.0 atm.

Total syngas pressure as high as 2.5 atm has clearly shown poor methane yield varying in the range of 0.1–0.3. A theoretical range of CH_4 yields from CO, can be estimated as between 0.25 and 1, corresponding to the simple direct reactions where to produce 1 mol of CH_4, 4 and 1 mol of CO, respectively, are required. These minimum and maximum limits are represented by the chemical reactions (1) and (2) previously presented in section 3.3.1. The straight dashed line represented in the graph of Figure 3-10(b), correspond to the lowest theoretical $Y_{CH4/CO}$ of 0.25. It can also be observed in the same graph that most the curve for P_T = 2.5 atm, is equal or under this lower threshold. This fact seems to indicate that some specific metabolic pathways are preferred in these conditions, specially the ones that form organic acids as intermediates.

Assays at lower P_T values tested in this experiment, resulted in higher CH_4 from CO yield, in the range of 0.45–0.59 and 0.53–0.87 for 1.0 and 1.75 atm of P_T, respectively. In fact, the highest CH_4 yields (above 0.81) were obtained at P_T = 1.75 atm and $p_{CO} \leq 0.4$ atm, while relatively similar yields (in the range of 0.5–0.7) were obtained for the other conditions at 1.0 and 1.75 atm.

3.3.2.3 Volatile fatty acids production and accumulation

Volatile fatty acids (VFA) and alcohols can be directly formed from syngas components. Several studies have reported the optimal conditions to efficiently produce either VFA (acetate and butyrate) and alcohols from syngas (e.g. Sim *et al.*, 2007; Worden *et al.*, 1989; Younesi *et al.*, 2005). Subsequently, VFA can also be reduced into alcohols, mainly ethanol using molecular hydrogen (Steinbusch *et al.*, 2008).

In this study, methane was the main final product resulting from the whole process of syngas conversion. The liquid composition in each vial, along time, was assessed in terms of VFA and alcohols content. No alcohols were detected in the vials though, and thus, it can be stated that if any amount of alcohols were produced during the process it was converted to acetate and its accumulation did not occurred.

Regarding VFA content, different performance was observed. Although, for the analysed samples, no VFA was detected in the assays at P_T = 1.0 atm, for the other assays at higher P_T (1.75 and 2.5 atm) some VFA accumulation was detected. Table 3-3 summarises the VFA concentrations detected in the vials at three different stages of the process, for the assays at P_T = 1.75 and 2.5 atm. Acetate, propionate and n-butyrate were the VFA detected in the liquid medium, in this experimental design 2. Four stages of the process were selected to evaluate the VFA content: (1) beginning of the assay; (2) end of H_2 consumption; (3) end of CO consumption; and 4 – end of the assay.

Table 3-3 Volatile fatty acids (VFA) accumulation during syngas conversion, at the initial syngas total pressures, P_T of 1.75 and 2.5 atm, for the factorial experimental design 2

	VFA concentration / mM					
	P_T / atm					
	1.75			2.5		
p_{CO} / atm	Acetate	Propionate	n-Butyrate	Acetate	Propionate	n-Butyrate
0.2	×	×	×	×	×	×
0.4	×	×	×	×	×	×
0.6	×	×	×	0.40 [(a)]	×	×
0.8	0.93 [(a)]	0.59 [(a)]	0.32 [(a)]	×	0.41 [(b)]	0.81 [(b)]
1.0	2.44 [(b)]	0.87 [(b)]	0.81 [(b)]	4.57 [(b)]	0.79 [(b)]	1.56 [(b)]
1.2	–	–	–	7.87 [(b)]	0.95 [(b)]	1.34 [(b)]
1.5	–	–	–	19.64 [(c)]	0.97 [(c)]	2.37 [(c)]

(–) Not tested; (×) Not detected; (a) detected at the end of H_2 consumption with CO not totally consumed; (b) detected at the end of CO consumption; (c) detected at the end of the experiment.

In the beginning of the assay, no VFA was detected. In general, it can be observed that VFA accumulation increased after H_2 complete consumption. Since, H_2 is necessary to reduce VFA to alcohols, this may explain why no alcohols accumulation was detected (Kleerebezem & van Loosdrecht, 2007). Nevertheless, concentration of VFA in the assays at P_T = 1.75 atm were not significantly high, only acetate achieved nearly 2.5 mM, and no VFA was detected at the end of the experiment. However, in the assays at P_T = 1.75 atm, significantly high concentrations of VFA were detected even at the end of the assay, up to 20 mM of acetate, and 1.0 and 2.4 mM of propionate and n-butyrate, respectively. These assays where VFA accumulation was detected are the same where both methane production rate and yield were significantly lower. This fact seems

to make evidence of the susceptibility of the acetoclastic methanogenic organisms to convert VFA intermediates into CH_4 and CO_2, under higher pressures and in the absence of H_2.

According to literature, VFA reduction using the hydrogen present in the syngas mixture, has received little attention regarding the whole syngas conversion process balance (Kleerebezem & van Loosdrecht, 2007). An alternative approach to enhance methane production rate, as a result of VFA reduction, in processes performed at higher pressure, could be the increment of hydrogen partial pressure in the main inlet gas. An additional punctual injection of hydrogen could be considered in the process, in order to prevent VFA accumulation, especially at higher total syngas pressures.

3.3.2.4 Factorial design statistical analysis

Data from syngas conversion carried out in 27 test vials from 9 different conditions, in experimental design 2, were selected to perform factorial experimental design, using design of experiments (DoE) approach (see Table 3-1). A 3^2-design matrix (including 9 independent runs in triplicate) was defined, with P_T and p_{CO} as the two independent factors tested. Maximum initial methane production rates were the response factor. Statistical analysis was performed in order to optimise these methane production rates, using *Design Expert®* software.

A model weighting the effect of each single factor and interactions between them was generated. Statistical analysis was also performed in order to optimize methane production rate. Equation (3.2) describes the model obtained, in which the effect of each individual factor is measured, along with the interactions between them.

$$r_{i,CH_4} = 2.93 - 3.68 \cdot P_T + 16.39 \cdot p_{CO} - 1.85 \cdot P_T \cdot p_{CO} + 0.90 \cdot P_T^{\,2} - 11.75 \cdot p_{CO}^{\,2} \qquad \textbf{(3.2)}$$

The model was then used to calculate predicted methane production rates, and compare with the real values determined in the experiments, according to the design matrix, as presented in Table 3-4.

Table 3-4 Design matrix of factorial experimental design 2 and observed response factor, Y (methane production rate, $r_{i,CH4}$ observed and predicted) for the two independent factors tested, X_1 and X_2 (initial syngas total pressure, P_T and CO partial pressure, p_{CO},)

	Independent variables matrix		Maximum CH_4 production rate ($r_{i,CH4}$)	
	X_1	X_2	Y (Real)	Y (Predicted)
Test	P_T / atm	p_{CO} / atm	mmol CH_4 L^{-1} d^{-1}	
1	+1	-1	0.93	1.24
2	0	0	2.40	2.63
3	-1	+1	4.83	4.64
4	-1	-1	2.25	2.59
5	-1	0	4.23	4.09
6	+1	0	2.25	2.18
7	0	-1	2.04	1.41
8	0	+1	2.49	2.91
9	+1	+1	2.40	2.18

It is worth to highlight the higher positive and negative factors obtained for the p_{CO} parameter in the model, which tends to denote the importance of its effect on the methane production rate. The R^2 coefficient obtained for the adjusted model was 0.7725, however the prediction R^2 was below 0.01. This indicates that the model generated is not suitable to be used as a tool to accurately predict the response for different values of the factors tested. Thus, the model will be not considered for further analysis. Nevertheless, a 2D surface response graph was generated and is shown in Figure 3-11. The graph of Figure 3-11 makes clearly evidence of the effect that both P_T and p_{CO} have over determined maximum initial methane production rate, $r_{i,CH4}$. In fact, in the range of the conditions tested, it might be expected that in a bioprocess highly limited by gas-liquid mass transfer, high pressure would be favourable for reactions.

From a physical point of view impose higher total gas pressure and partial pressures of main gaseous substrates would generally improve production rates in the process, by increasing solubility of the compounds. Interestingly, the opposite was here observed: lower total pressure (1.0 atm) and CO partial pressure up to 0.6 atm, covered the set of conditions that led to achieving the highest methane production rates, with lower cost input. Although the result generated by the statistical analysis of the DoE, it suggests evidences that are in agreement with the discussion previously so far.

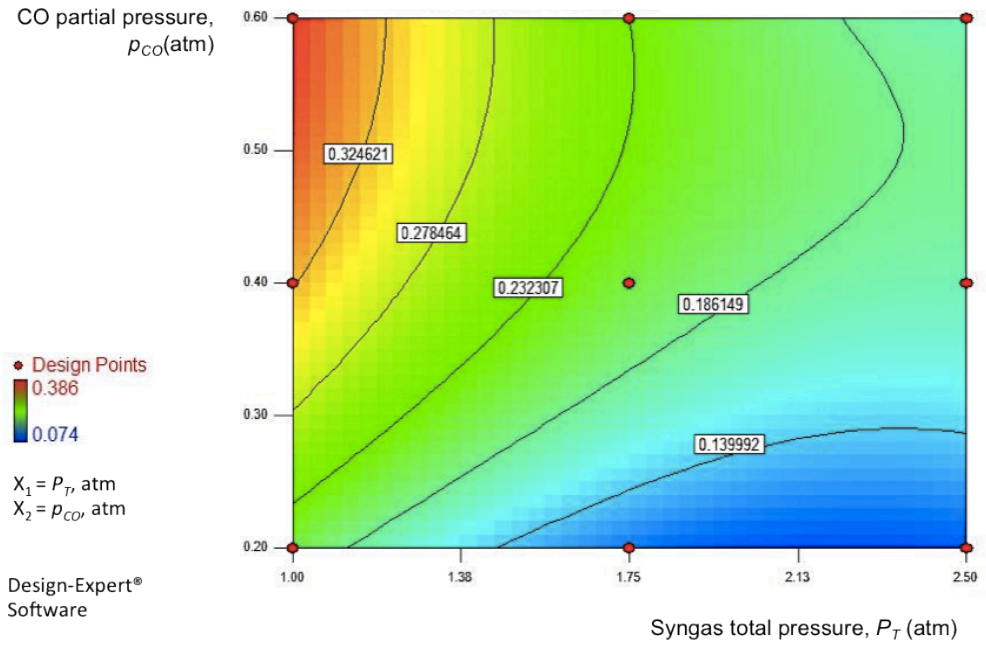

Figure 3-11 2D Surface representation of the maximum initial methane production rate, $r_{i,CH4}$ expressed in mmol CH_4 d^{-1}, as a function of initial CO partial pressure, p_{CO} and initial syngas total pressure, P_T obtained from *Design-Expert®* Software, for the factorial experimental design 2. Colour distribution corresponds to different levels of $r_{i,CH4}$ from the lowest (blue zone) to the highest (red zone). Lines represent sequence of p_{CO}, P_T combination conditions with the same $r_{i,CH4}$ level (equal to the value represented in the white box).

This study has contributed with novel results regarding the performance of syngas conversion using an anaerobic mixed culture, in a batch system. The results also unlock future research perspectives based on the challenge: how to improve overall productivity by improving both gas-liquid mass transfer and metabolic reactions.

CHAPTER 4

CO_2 dissolution and design aspects of a multi-orifice oscillatory baffled column

4.1 INTRODUCTION

The sequestration of carbon dioxide, CO_2 is a topic of major industrial interest motivated by the recent increased need for reducing the greenhouse gas emissions. New biotechnological processes are being developed where microalgae, anaerobic bacteria or cyanobacteria use CO_2 to produce bulk chemicals and green fuels (Jansson & Northen, 2010; Phillips *et al.*, 1994; Ugwu *et al.*, 2008). The intensification of dissolution of CO_2 and other gases requires generating fine bubbles and reducing the mass transfer resistances around the bubbles surface by means of strong mechanical mixing using e.g. a mechanical impeller, which is not always possible in biological processes involving living cells as the external energy input has also to ensure cell integrity (Klasson *at al.*, 1993a; Worden *et al.*, 1991).

Conventional gas-liquid contacting technology based e.g. on bubble columns (BCs), stirred tank reactors (STRs) and air-lift reactors (ALRs) are somewhat inefficient and present very modest performances in respect to the dissolution of gases with large gas aeration rates (Q_{gas}) of 1 vvm (volume of gas per volume of liquid per minute) or above; in the particular case of BCs and ALRs this is due to the intensity of mixing being directly linked to the gas flow rates, therefore the contacting times being extremely short.

The overall volumetric mass transfer coefficient (K_La) for CO_2 has been experimentally measured only in a small number of studies (Boogerd *et al.*, 1990; Calderbank & Lochiel, 1964; Hill, 2006; Taslim & Takriff, 2004). Calderbank and Lochiel (1964) investigated K_La, bubble's velocity and shape for CO_2 freely rising in distilled water, and showed that K_La remained constant along the height of the column for bubbles with an equivalent spherical diameter, d_e in the range 4–31 mm. Boogerd and co-authors (1990) showed that K_La for CO_2 can be predicted from the known K_La values measured for O_2, using the following relation: $K_La_{,CO2} = 0.893 \cdot K_La_{,O2}$, which has been derived from a diffusion coefficient correction factor. Based on the same relationship these authors have predicted a maximum possible K_La value for CO_2 in the order of 140 h^{-1}, based on K_La values measured for O_2 at a Q_{gas} = 1 vvm in a lab scale fermenter operating at pH = 2, which has yet to be demonstrated experimentally. Hill (2006) determined the dependence of K_La for CO_2 with the temperature, stirring speed and Q_{gas} = 0.08–0.8 vvm in a 2.45 L STR using distilled water, and obtained K_La values of 20–120 h^{-1} using 10 % v/v CO_2, so well below the typical K_La

values measured for O_2-water mass transfer in well-mixed vessels. It is however unclear from that study what were the specific conditions that allowed Hill (2006) achieving the highest K_La values reported, as a maximum K_La in the range of 41.4 h^{-1} can be inferred from supplied data. Nevertheless, this stresses the difficulty in predicting or comparing performance of different gas contacting systems in respect to CO_2 dissolution.

The oscillatory baffled column (OBCs) (Mackley & Ni, 1991) is a new mixing technology that has been successfully applied to the intensification of a wide range of chemical and biological processes, including gas-liquid and multiphase systems. The eddy mixing in the periodic baffles or constrictions delivers a good degree of radial mixing and secondary flow that is very effective for controlling the bubble/drop size distribution in the column enhancing the contact between immiscible phases. Few studies have previously used OBCs for O_2 and CO_2 dissolution in water (Baird *et al.*, 1996; Hewgill *et al.*, 1993; Mackley *et al.*, 1998; Ni & Gao, 1996; Oliveira *et al.*, 2003a, 2003b; Oliveira & Ni, 2001; Taslim & Takriff, 2004), as overviewed in Table 4-1.

Table 4-1 Gas-liquid mass transfer studies in oscillatory baffled columns (OBCs)

OBC	Gas-liquid system	i.d. [mm]	Q_{gas} [vvm]	U_G [mm s^{-1}]	d_o [mm]	α [%]	K_La [h^{-1}]	Reference
Batch single-orifice OBC	Air-fermentation media	50	0.5	3.2	20[1]	16	~90–450	Ni *et al.* (1995a)
	Air-water	50	0.05–0.2	1.1–4.3	24	23	~0–144	Oliveira and Ni (2004a, 2004b)
	Air-water	26	n/d	0.4–2.4	15	33	~0–133	Hewgill *et al.* (1993)
	Ozone-water	25	n/d	3–68	12.5	25	36–252	Al-Abduly *et al.* (2014)
Batch reciprocating plate baffled column	Air-water (self-aerating)	190	n/a	n/a	10–50	7–31	~0–23	Mackley *et al.* (1998)
	Air-water	150	n/d	0.32–1.14	70–90	22–36	n/a	Baird *et al.* (1996)
	Air-water	16.6	n/d	5–15	7.8	46.6	180–2880	Vasic *et al.* (2007)
	Air-water	228	n/d	1.2–11.8	6.4–19.1	31.2–35.7	~20–720	Gagnon *et al.* (1998)
Continuous dual-reciprocating plate baffled column	Air-water	100	n/d	0–1700	1.6–3.2	38	~72–432	Gomaa *et al.* (2012)
Continuous reciprocating plate baffled column	Air-water	150	n/d	6.3–17.7	6.4–90	23.5–54	~7–54	Rama Rao & Baird (2003)
Continuous single-orifice OBC	Pure CO_2-water	94	1.3–3.6	26–72	50	28	~8–100	Taslim & Trakriff (2004)
Continuous, single-orifice meso-OBC	Air-water	4.4	0.064	0.37	1.6	14	~0–576	Reis *et al.* (2007)

[1]Authors reported a baffles width/diameter of 30 mm, so it was assumed an open diameter orifice of 20mm in the calculations; (n/d) not disclosed by the authors; (n/a) not applicable/available.

Reis *et al.* (2008) reported values of K_La up to 576 h^{-1} for O_2 dissolution in a meso-OBC using a very low value for superficial gas velocity (U_G) of 0.37 mm s^{-1} (equivalent to Q_{gas} = 0.064 vvm). The superior gas-liquid performance of the meso-OBC resulted mainly from the enhanced gas hold-ups associated with the trapping of microbubbles in the periodic eddies generated in the space between the constrictions, as well as the enhanced shear and velocity fluctuations in the gas-liquid interface. Only in one occasion the dissolution of CO_2 has been experimentally studied in OBCs, but in this instance using pure CO_2 in a continuous 94 mm i.d. column by Taslim and Takriff (2004); K_La values up to ~ 100 h^{-1} were reported for Q_{gas} = 1.3–3.6 vvm. Overall, OBCs are very efficient in respect to gas-liquid mass transport, and the large values of K_La reported were obtained with a 5 to 10-fold reduction in Q_{gas} when compared to the gas aeration rates typically used for BCs, ALRs or STRs. An additional feature perhaps unique to OBCs is its linear scale-up (Brunold *et al.*, 1989; Ni *et al.*, 1995a; Ni & Gao, 1996; Smith & Mackley, 2006), however no rules have yet been established in respect to scale-up of gas-liquid mixing in OBCs.

In this work, the dissolution of CO_2 on a vertical 150 mm i.d. batch multi-orifice baffled column (MOBC) was experimentally studied and three baffle configurations with different α and orifice diameter (d_o) were developed and tested, and the impact of baffle design and Q_{gas} on K_La quantitatively evaluated. Optical flow visualisation and image analysis was applied for quantifying the impact of oscillatory flow mixing on the Sauter mean diameter ($D_{3,2}$) and BSDs. For the first time the connection between microbubbles trapping and the toroidal vortices in OBCs is quantitatively illustrated. In addition, the main governing oscillatory flow dimensionless numbers were revisited for scale-up of OBCs from single-orifice to multi-orifice OBCs.

4.2 EXPERIMENTAL METHODS AND PROCEDURES

4.2.1 Multi-Orifice Oscillatory Baffled Column (MOBC)

The 150 mm internal diameter MOBC used in this work was presented in Figure 4-1. The total volume of the column was 10.6 L, with a working volume (V_L) of 9.6 L, and a total column height (h) of 540 mm. All experiments have been carried out at atmospheric pressure and room temperature (20 °C).

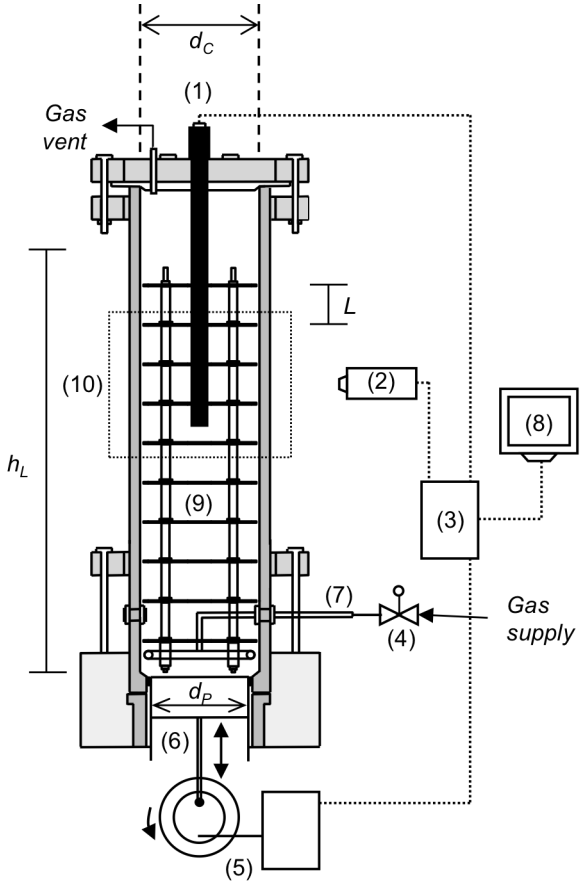

Figure 4-1 Configuration of the multi-orifice oscillatory baffled column (MOBC) used on CO_2 mass transfer studies. 1 – Dissolved CO_2 probe; 2 – CCD camera; 3 – CPU; 4 – Gas flow controller (rotameter); 5 – Servo-hydraulic unit; 6 – Piston; 7 – Gas sparger; 8 – Display; 9 – Interbaffle cavity; 10 – Optical box (filled with glycerol). Dimensions were: liquid height in column, h_L = 450 mm; inter-baffle spacing, L = variable (specific of the baffle design tested – see Table 4–2 for more details); diameter of piston, d_P = 125 mm; maximum internal diameter of column, d_c = 150 mm.

The gas phase consisted of 5 % v/v of CO_2 in air sparged from the bottom of the MOBC. The composition of the gas phase was chosen to prevent changes in the bubbles size due to CO_2 absorption and to minimise the effect of response time of the dissolved CO_2 probe. The sparger consisted of a circular plastic tube perforated with a 0.6 mm diameter needle to deliver an even bubble formation within the column. Q_{gas} was controlled by a needle valve and measured with a calibrated in-line gas flow meter. The range of Q_{gas} herein tested was 0.01–0.1 vvm, corresponding to a range of mean superficial gas velocity, U_G = 0.12–0.81 mm s^{-1}.

The liquid phase (distilled water) in the MOBC was kept at a constant volume, with the free liquid surface always kept well above the top baffle in order to avoid air entrapment from the headspace. Sinusoidal fluid oscillations were imposed on the fluid using a servo-hydraulic system that controlled a 125 mm o.d. piston attached to the bottom of the column. This moving base piston was capable of delivering fluid oscillation frequency (f) and centre-to-peak amplitude (x_0) in the ranges of 0–10 Hz and 0–10 mm, respectively. Due to the nature of design of the servo-hydraulic system, a maximum value of f = 8 Hz could be used with x_0 = 3 mm.

The batch oscillatory column was equipped with equally spaced multi-orifice baffles with unique designs. Three stainless steel rods (6 mm diameter) were placed inside the column to support the set of baffles. Baffles were designed to fit closely to the column wall. Three different baffles configurations were used in this study (described as designs 1, 2, and 3), with significant differences in d_o and α as detailed in Table 4-2.

Table 4-2 Configuration of the 3 internal baffle designs used in the MOBC

	Baffles design 1	Baffles design 2	Baffles design 3
	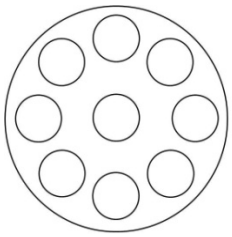	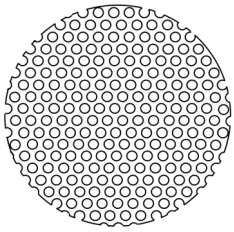	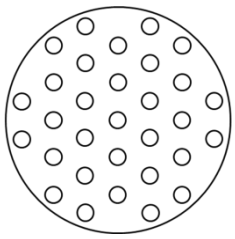
Number of baffles in the column	10	9	9
Average number of orifices per baffle	9	210	31
Orifice diameter d_h, mm	30.0	6.4	10.5
Equivalent diameter of obstacle d_{obst}, mm (Eq. 4–7)	40.0	7.9	24.8
Equivalent hydraulic diameter for single-orifice column d_h, mm (Eq. 4–10)	50.0	10.4	26.9
Baffle spacing L, mm	50	50	40
Baffle thickness, mm	2.0	3.4	3.0
Open area α, %	36	42	15
Construction material for baffle	Stainless steel	Polypropylene sandwiched between 2 thin stainless steel layers	Acrylic

Design 1 was initially tested as it had been successfully applied to liquid-liquid systems and photochemical oxidation in recent times in the same column (unpublished data). The baffle design with d_o = 30 mm and α = 36 % mimicked that of single-orifice OBCs used in similar studies (Baird *et al.*, 1996; Hewgill *et al.*, 1993). Baffle designs 2 and 3 were developed using smaller values for d_o and α which were observed to be beneficial for enhancing gas-liquid contacting. In all experimental sets, baffles were stacked inside the column at an equal baffle spacing (L) of 50 mm (design 1 and 2) or 40 mm (design 3). Design 3 aimed at replicating a set of single orifice baffled tubes working at same peak oscillatory liquid flow velocity, where a stack of baffles is fixed and the liquid moved by the action of a piston, following the OBC scale-up rule established by Smith and Mackley (2006).

4.2.2 Flow visualisation and BSDs

For optical imaging of gas bubbles and particle tracing experiments in the MOBC, a Perspex-optical box was fitted at mid-height of the MOBC and filled with glycerol as shown in Figure 4-1. The gap between the external and internal walls of the jacketed glass column was also filled with glycerol in order to reduce optical distortion (Reis *et al.*, 2005).

A fluorescent lamp attached to a light diffusor provided the necessary illumination for tracking of bubble size using low speed (60 fps, frames per second) or high-speed (1,000 fps) CCD cameras. For liquid flow visualisation, polyamide particles having mean size of 20 μm were dispersed in the liquid phase and illuminated at 90 degrees to the camera by a mercury vapour lamp to give a bright illuminated field. A high-speed CCD camera (Photron FastCam) with a faster shutter speed was used to continuously acquire 512×512 pixels images. Images were saved to a PC in TIF format at a frequency of 1,000 fps. A sequence of at least 600 image snapshots was taken at different combinations of x_0 and f, which provided more than 2,000 bubbles for image analysis at each condition. This number of bubbles was concluded to be sufficient for the BSDs to be independent of the number of bubbles analysed (results not shown).

Bubble image analysis was carried out using *ImageJ* software (NHI Image, USA). A set of 600 images for each experimental condition was converted to 8-bit binary images by applying a

threshold. The binary images were then treated through a number of image processing steps in order to obtain a clear edge and area for each individual bubble, which included filling holes, erosion and dilation. Finally, bubbles with minimum size higher than 0.02 mm^2 and circularity in the range of 0.7–1.0 were measured on the entire image sequence. Two important bubble diameters are usually relevant for gas-liquid mass transfer studies: the equivalent spherical bubble diameter (d_e) and the Sauter mean diameter ($D_{3,2}$). The size of each individual bubble was quantified from d_e which was calculated from the projected area (A_{proj}) according to Eq. (4.1):

$$d_e = \sqrt{\frac{4 \cdot A_{proj}}{\pi}} \tag{4.1}$$

In this equation it is assumed that all bubbles have spherical shape. This might had resulted in underestimated equivalent bubble size for the larger bubbles, which are less spherical and more likely to be oblate ellipsoids. Nevertheless, for the purpose of comparing baffle performances, the use of $D_{3,2}$ provides a good approximation resulting and reduced error propagation from Eq. (4.1).

Given the restrictions in the flow visualisation and post-processing of imaged bubbles, the minimum value of d_e that could be resolved was 0.16 mm. As CO_2 dissolution involved mass transfer through an interfacial area, $D_{3,2}$ was used and calculated using Eq. (4.2).

$$D_{3,2} = \frac{\sum_i {d_{e_i}}^3}{\sum_i {d_{e_i}}^2} \tag{4.2}$$

4.2.3 Measurement of K_La for CO_2 dissolution

The dissolved CO_2 concentration in water was continuously monitored for each set of experiments using a dissolved CO_2 probe (InPro5000, Mettler Toledo), installed at a fixed position at the centre of the MOBC column, with the tip located at half column height. Because of the large oscillatory Reynolds numbers used in the study, the estimate mixing times were in the range of few seconds (Mackley *et al.*, 1989) which is insignificant compared to the response time

of the probe (150–180 s) and the long aeration times with 5 % v/v CO_2 gas mixture. For that reason, the batch column was assumed to be well mixed.

The dynamic gassing-out method with instantaneous gas interchange, from pure nitrogen, N_2 to 5 % CO_2 mixture was used to estimate K_La values for CO_2 in the batch MOBC. Before each set of experiments the column was filled with fresh distilled water. Nitrogen was then sparged for at least 60 minutes to promote degassing of the liquid and set the reference 0 % CO_2 saturation whilst starting data acquisition. The gas phase was then switched to 5 % v/v CO_2 mixture and the gas flow rate adjusted using a calibrated rotameter. The percentage of dissolved CO_2 was then monitored until it reached a perfect plateau (i.e. 100 % saturation). The pH electrode of the probe was calibrated in buffer at pH 7.00 and pH 9.21 as recommended by the manufacturer.

A time-lag on the dissolved CO_2 probe response was detected which has been associated by other authors (Hill, 2006) with the time required for replacement of the gas in the connection tubing (connecting gas valves in the cylinder to the sparger), in the bubbles, in the liquid phase, and in the headspace. Consequently, a floating coordinate system ($t - t_0$), set as constant for each gas flow rate used, was defined during data analysis, in which the time delay (t_0) was an arbitrary parameter determined by best-fitting the experimental data with the model using as objective function the minimum square of the difference. The value of t_0 determined for each Q_{gas} was within ± 10 % of the gas residence time that can be calculated based on the gas flow rate, headspace volume and gas holdups in the column.

In order to compensate for the effect of gas and liquid dynamics in the probe response, only values corresponding to 10–95 % of the saturation dissolved CO_2 concentration (C_L^*) were considered during the best-fitting procedure. According to Oliveira and Ni (2004b) a first order model and a step change in concentration technique can be used to evaluate probe dynamics. Hence, the constant of the probe (K_P) was determined using a first order model in the column in a step change in CO_2 concentration, which could be determined from a mass balance to CO_2 in the batch column, according to Eq. (4.3).

$$\frac{C_L^* - C_L(t)}{C_L^* - C_{L,0}} = exp(-K_p \cdot t) \tag{4.3}$$

The probe constants (K_P) determined were 18 ± 2 h^{-1} for the set of experiments using baffle designs 1 and 2, and 23 ± 1 h^{-1}, for the set of experiments shown with baffle design 3. These constants were different as these set of experiments have been performed in different instances, and therefore some alteration to the membrane of the probe could have occurred.

Once the K_P value was determined, it was then used to determine the volumetric CO_2-water mass transfer coefficient, K_La from the CO_2 dissolution plots, assuming a steady-state behaviour for the gas dynamics (i.e. no significant decrease in partial pressure of CO_2 in the gas phase) and perfectly mixed liquid phase. A mass balance to the gas phase combined with the first order model for probe dynamics defined in Eq. (4.4) yields:

$$C_L(t) = C_L{}^* - \frac{C_L{}^* - C_{L,0}}{K_p - K_L a} \cdot \left\{ K_p \cdot exp\left[-K_L a \cdot \left(t - t_0 \right) \right] - K_L a \cdot exp\left[-K_p \cdot \left(t - t_0 \right) \right] \right\} \tag{4.4}$$

Equation (4.4) was then used to determine the K_La values for each experiment by best-fitting the experimental CO_2 dissolution profiles data to the model using *Excel Solver*, being the objective function the minimum root-square difference between the two curves in the range of CO_2 saturation levels of 10–95 % of $C_L{}^*$.

4.2.4 Modified oscillatory flow dimensionless numbers

In OBCs the oscillatory motion is complex (Ni & Mackley, 1993) and traditionally the mixing intensity and mass transfer rates in the inter-baffle regions of small diameter single-orifice OBCs is assumed as governed by two dimensionless numbers, the oscillatory Reynolds number (Re_o) and the Strouhal number (St):

$$Re_o = \frac{2\pi f x_0 \rho d_c}{\mu} \tag{4.5}$$

$$St = \frac{d_c}{4\pi x_0} \tag{4.6}$$

where d_c is the internal diameter of the column (m), f the fluid oscillation frequency (s^{-1}), μ is kinematic fluid viscosity (kg m^{-1} s^{-1}), ρ is the specific mass of the fluid (kg m^{-3}) and x_0 is the centre-to-peak fluid oscillation amplitude (m).

The Re_o in Eq. (4.5) was described in analogy to net flow Reynolds number where the product ($2\pi \cdot x_0 \cdot f$) represents the peak fluid velocity (m s^{-1}) during an oscillation cycle which occurs halfway the piston full stroke. The St and Re_o dimensionless numbers in Eqs. (4.5) and (4.6) are routinely used in studies involving single-orifice OBCs where there is a direct link between the internal diameter of the column, d_c and the open diameter of the orifice, d_o however they were found unsuitable for scaled-up OBCs and MOBCs for a number of reasons as follows.

A possible strategy for scale-up of OBCs from single-orifice columns is based on increasing d_c by keeping both Re_o and St constant. Following from Eq. (4.6) this would require x_0 to be increased in proportion to d_c, therefore f being reduced by 1–2 orders of magnitude in order to keep Re_o constant according to Eq. (4.5). This happens because currently Re_o on its current form is only based on d_c and not in d_o or the equivalent diameter of the obstacle, d_{obs} as anticipated from a detailed understanding of the fluid mechanics behind flow separation around obstacles. An alternative and more elegant approach for scale-up of OBCs uses multi-orifice baffles. With that approach, d_c is increased but both d_o and d_{obs} are kept constant. This is equivalent to consider multiple OBCs working effectively in parallel in the same column.

A number of variants to Eq. (4.5) has been proposed by several authors for multi-orifice baffles, see for example Ni and Gough (1997), Smith and Mackley (2006), yet the effect of α in the performance of MOBCs has not yet been considered. As this current study used baffles with a range of d_o and α both Re_o and St were modified to accurately represent the state of mixing in the MOBC and support scale-up from single-orifice to multi-orifice OBCs.

Eddy formation in the free flow problem around obstacles is controlled by the diameter of the obstacle, the properties of the fluid and the free mean liquid velocity. In that respect, the most important characteristics length in respect to vortices formation is d_{obs}, and in analogy it can be described for the MOBC as the "equivalent" diameter of the baffle area that surround each open orifice:

$$d_{obs} = d_c \sqrt{\frac{1-\alpha}{n}} \tag{4.7}$$

where, d_c is the internal diameter of the column; α is the fraction of open area of the baffle, and n is the number of orifices in the baffle. For multi-orifice baffles d_{obs} (not d_o or d_c as it happens for single-orifice OBCs) should be the main geometrical parameter governing flow separation and eddy formation in the column.

From the perspective of mass conservation, the flow of an uncompressible fluid through a multi-orifice baffle differs from free-boundary flow problem for the fact that the fluid has to accelerate when passing through the orifices. Neglecting the effect of the column walls (because of large d_c value the pseudo-steady flow is turbulent in the inter-baffle spaces), the mean free stream velocity relevant for vortices formation from the surface of the obstacles is not just controlled by the imposed mean fluid velocity (or peak fluid velocity $2\pi \cdot x_0 \cdot f$ in case of unsteady flow) but also by α. Taking these simple concepts into account, a modified Re_o' for multi-orifice baffles could be written as follows:

$$\mathrm{Re}_o' = \left(\frac{2\pi f x_0 \rho}{\mu}\right) \cdot d_{obs} \cdot \left(\frac{1}{\alpha}\right) \tag{4.8}$$

Combining Eq. (4.8) and Eq. (4.7) yields:

$$Re_o' = \left(\frac{2\pi f x_0 \rho}{\mu}\right) \cdot \left(\frac{d_c}{\sqrt{n}}\right) \cdot \sqrt{\frac{1-\alpha}{\alpha^2}} \tag{4.9}$$

Mathematically Eq. (4.9) differs from the equation presented by Smith and Mackley (2006) for a multi-orifice OBC on the term $[(1-\alpha)/\alpha^2)^{1/2}]$ which measures the effect of the open area of the baffle. This yields significant differences in Re_o' values as can be seen in Table 4–3. For example, Re_o' calculated from Eq. (4.9) for baffle design 2 is about 8-fold lower than value of Re_o based on Eq. (4.5) because of the small value of d_o used.

Table 4-3 Averaged bubble Sauter mean diameter ($D_{3,2}$) and overall CO_2 mass transfer coefficient (K_la) values obtained in the different baffle designs

Baffle	Q_{gas} [vvm]	U_G [mm s^{-1}]	f [Hz]	x_0 [mm]	Re_o [-]	Re_o' [-]	St [-]	St' [-]	$D_{3,2}$ [mm]	k_la [h^{-1}]
Design 1	0.05	0.43	0	0	0	0	*	*	5.51	9 (± 1)
	0.05	0.43	0.2	2.5	460	340	4.8	1.6	-	12 (± 1)
	0.05	0.43	3	1	2740	2030	11.9	4.0	5.28	-
	0.05	0.43	3	2.5	6850	5070	4.8	1.6	5.41	-
	0.05	0.43	3	5	13700	10140	2.4	0.8	-	9 (± 2)
	0.10	0.81	0	0	0	0	*	*	6.07	-
	0.10	0.81	3	1	2740	2030	11.9	4.0	5.28	-
	0.10	0.81	3	2.5	6850	5070	4.8	1.6	5.41	-
	0.10	0.81	5	5	22830	16900	2.4	0.8	-	21
	0.01	0.12	0	0	0	0	*	*	5.65	-
	0.01	0.12	3	1	2740	2030	11.9	4.0	5.00	-
	0.01	0.12	3	2.5	6850	5070	4.8	1.6	5.07	-
Design 2	0.10	0.81	0	0	0	0	*	*	3.23	48 (± 7)
	0.10	0.81	1	10	9130	1160	1.2	0.1	3.25	35 (± 14)
	0.10	0.81	2	10	18270	2310	1.2	0.1	2.33	-
	0.10	0.81	4	5	18270	2310	2.4	0.2	2.59	20 (± 10)
	0.07	0.58	2	10	18270	2310	1.2	0.1	2.46	23 (± 13)
	0.04	0.35	2	10	18270	2310	1.2	0.1	2.43	4 (± 1)
Design 3	0.10	0.81	0	0	0	0	*	*	+	20 (± 1)
	0.10	0.81	2	2	3650	4040	6.0	1.1	+	22
	0.10	0.81	2	5	9130	10110	2.4	0.4	+	30
	0.10	0.81	5	2	9130	10110	6.0	1.1	+	33 (± 8)
	0.10	0.81	4	3	10960	12130	4.0	0.7	+	37
	0.10	0.81	5	3	13700	15160	4.0	0.7	+	43
	0.10	0.81	2	8	14610	16170	1.5	0.3	+	45
	0.10	0.81	8	2	14610	16170	6.0	1.1	+	57 (± 9)
	0.10	0.81	2	10	18270	20220	1.2	0.2	+	94
	0.10	0.81	10	2	18270	20220	6.0	1.1	+	65 (± 12)
	0.10	0.81	7	3	19180	21230	4.0	0.7	+	48 (± 1)
	0.08	0.66	8	2	14610	16170	6.0	1.1	+	31 (± 2)
	0.06	0.50	8	2	14610	16170	6.0	1.1	+	27 (± 3)
	0.04	0.35	8	2	14610	16170	6.0	1.1	+	20
	0.01	0.12	8	2	14610	16170	6.0	1.1	1.70	14
	0.01	0.12	8	3	21920	24260	4.0	0.7	-	-
Un-baffled column	0.10	0.81	No fluid oscillations						5.27	24 (± 3)

(-) not measured; (*) Strouhal number not applicable for steady flow; (+) insufficient number of individual bubbles available for image analysis.

Similarly, the Strouhal number *St* in Eq. (4.6) was modified to represent the actual ratio of diameter of column to fluid amplitude in the region around each individual orifice on the baffles in a MOBC. That required determining the equivalent hydraulic diameter of a single-orifice column, d_h.

$$d_h = \frac{d_c}{\sqrt{n}} \tag{4.10}$$

Replacing d_c in Eq. (4.6) by d_h from Eq. (4.10) a modified Strouhal number, *St'* was obtained, as shown in Eq. (4.11).

$$St' = \frac{d_c}{4\pi x_0}\frac{1}{\sqrt{n}} \tag{4.11}$$

4.3 RESULTS AND DISCUSSION

4.3.1 The impact of Q_{gas} and fluid oscillations on bubble size and comparison with a bubble column

The $D_{3,2}$ and BSD are recognised to play a major role in controlling K_La in gas-liquid and multiphase systems in single-orifice OBCs and other gas-liquid contacting systems, therefore the first part of this study aimed testing the effect of Q_{gas} and fluid oscillations on the mean bubble size in the MOBC for selected multi-orifice baffle designs. This was done using very low values of U_G of 0.12–0.81 mm s^{-1}, which is desirable to attain very high efficiencies of dissolution. Figure 4-2 shows the optical visualisation of bubbles rising in the MOBC equipped with different sets of multi-orifice baffles in the absence and presence of fluid oscillations.

The mean bubble size was found strongly dependent on the baffle design, in particular the small orifice diameter in design 2 (d_o = 6.4 mm, α = 42 %) resulted in nearly 50 % reduction in bubble size when compared to design 1 (d_o = 30 mm and α = 36 %). Nevertheless, no trend could be observed in respect to the effect of intensity of fluid oscillations on the mean bubble size, as increasing Re_o' and *St'* for a given baffle design returned similar values for $D_{3,2}$ of ~5 or ~3mm for baffle designs 1 and 2, respectively.

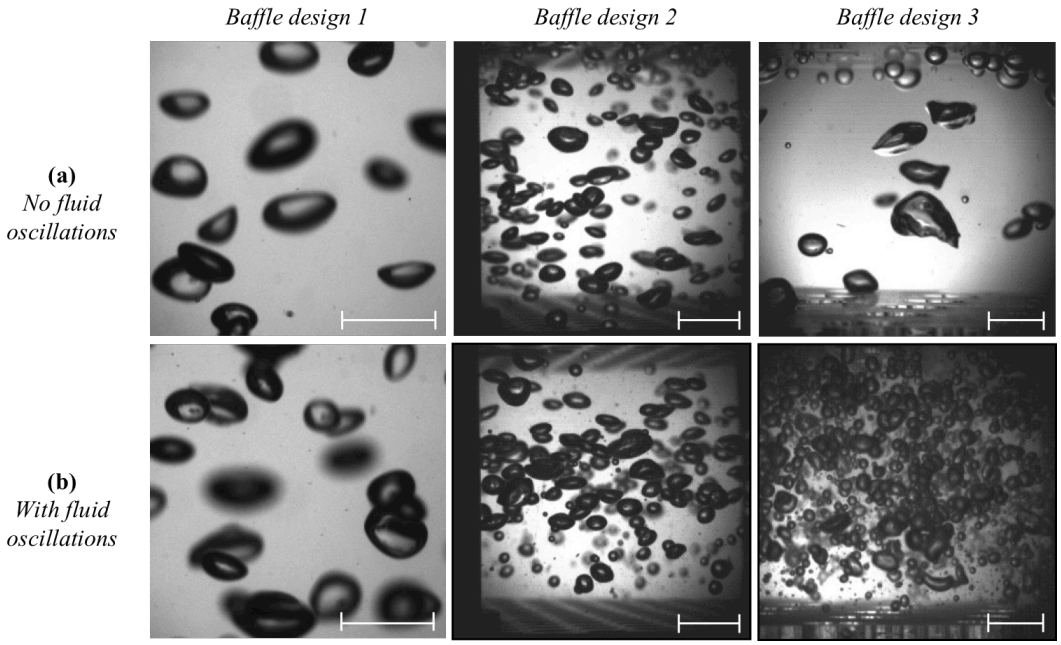

Figure 4-2 Optical observation of air bubbles rising in an interbaffle cavity in the vertical MOBC. (a) Stagnant fluid; (b) Oscillated fluid. The gas flow rates, Q_{gas} and fluid oscillation conditions used were: baffle design 1 - f = 3 Hz, x_0 = 2.5 mm, Re_o' = 5070, St' = 1.6, and Q_{gas} = 0.1 L min^{-1} (0.01 vvm); baffle design 2 - f = 2 Hz, x_0 = 10 mm, Re_o'= 2310, St' = 0.1 and Q_{gas} = 0.4 L min^{-1} (0.04 vvm); baffle design 3 - f = 2 Hz, x_0 = 10 mm, Re_o'= 20220, St' = 0.2 and Q_{gas} = 0.1 L min^{-1} (0.01 vvm). Scale bar corresponds to 10 mm.

With baffle designs 1 and 2 it was generally observed that the presence of the baffles *per si* had a stronger impact on bubble size than the intensity of the fluid oscillations on its own, as can be concluded by comparing the $D_{3,2}$ for each data set with the steady column baffled MOBC conditions (i.e. f = 0 Hz and x_0 = 0 mm) in Table 3. Baffle design 3 (d_o = 10.5 mm, α = 15 %) with the smaller value of α produced an extremely large fraction of microbubbles, which is desirable for enhancement of gas-liquid mass transfer process. Nevertheless, this presented a barrier for optical visualisation of individual bubbles in the MOBC, which is essential for calculating mean bubble sizes and BSDs even at such low values of U_G. The three baffle geometries developed in this study aimed at covering the spectrum of orifice diameters and open areas previously used in single-orifice OBCs and its impact on BSD is presented in more detail in Figure 4-3 and Figure 4-4 for varying Q_{gas} in a realist number of experiments.

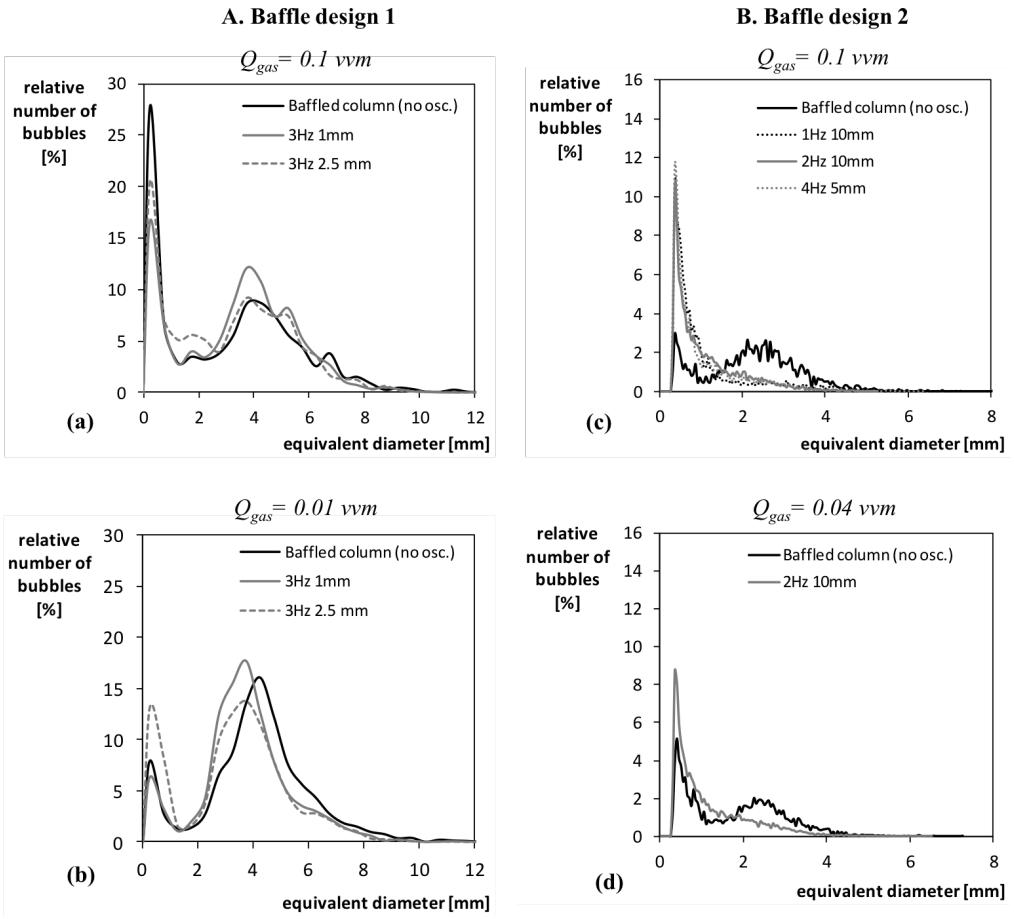

Figure 4-3 Bubble size distributions in the MOBC fitted with (a-b) baffle design 1, or (c-d) baffle design 2.

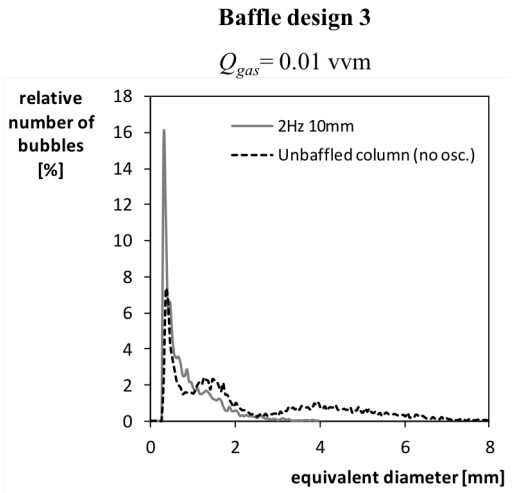

Figure 4-4 Bubble size distribution in the MOBC fitted with baffle design 3; comparison with un-baffled column.

The operation of the MOBC with baffle design 1 revealed a bimodal bubble population in the column (Figure 4-3(a-b)), with the first population having d_e < 1 mm, and the second bubble population an average d_e around 4 mm. This bimodal population is typical in gas-liquid systems and results from the simultaneous bubbles coalescence and breakage phenomena occurring in the column. At the higher Q_{gas} of 0.1 vvm (Figure 4-3(a)) a number of fine bubbles in the range of few hundreds of micrometres could be detected in the column, however there was no significant difference between the MOBC and sparging the baffled column in the absence of fluid oscillations. This is illustrated in Figure 4-3(a) for two different combinations of fluid oscillations (f = 3 Hz, x_0 = 1 mm, St' = 4.0; and f = 3 Hz, x_0 = 2.5 mm, St' = 1.6). At a lower Q_{gas} = 0.01 vvm (Figure 4-3(b)), the effect of fluid oscillations remained unnoticed. The large d_o value used in baffle design 1 (i.e. 30 mm) was clearly ineffective in promoting radial mixing and bubble breakage in gas-liquid flow, consequently Q_{gas} was the main effect in respect to control of overall BSDs. This result was to some extent unexpected, as several studies using oscillatory flow mixing have previously shown enhanced bubble breakage for experiments performed with similar Q_{gas} but different single orifice OBC designs (Oliveira & Ni, 2004a; Reis *et al.*, 2007). This suggested that a correct length of d_o and d_{obs} combined with an even distribution of the orifices across the baffle are essential to promote effective eddy formation and achieve a desirable reduction in bubble sizes.

The BSDs obtained using baffle design 2 with d_o = 6.4 mm is shown in Figure 4-3(c-d). Again, a bimodal distribution was observed for all experiments in the baffled vertical column in the absence of fluid oscillations at the gas flow rates tested, with a main population of larger bubbles with d_e in the range of 1.5–3 mm, and a second population composed of small bubbles having d_e < 1 mm. In the presence of fluid oscillations unimodal BSDs were produced for all values of Q_{gas} tested. In fact, in the presence of fluid oscillations mainly sub-millimetre size bubbles were observed in the MOBC. A detailed optical observation of the CO_2 bubbles using high-speed image recording showed that in certain phases of the oscillation cycle the fine bubbles moved in the opposite direction of the liquid flow, revealing strong secondary mixing and consequently bubble being trapped within each inter-baffle cavity for a fraction of the period of oscillation. This is expected to enhance contacting times and its overall impact in respect to K_La is discussed in detail in section 3.3.3.

In the presence of baffle design 3 (with d_o slightly larger but smaller α than baffle design 2) an unimodal BSDs was observed in the presence of fluid oscillations, with virtually no bubbles larger than 1 mm to be observed in the column (Figure 4-4). For the range of Re_o' and St' tested it was not possible to accurately determine $D_{3,2}$ because virtually at all combinations of f and x_0 tested with this baffle design an extremely large number of microbubbles was generated even at the lowest value of Q_{gas}. At the highest values of Re_o' the liquid in the column turned opaque as a result of the extremely high number of microbubbles in the gas-liquid solution, which suggests enhanced gas-liquid contacting.

Figure 4-5 shows photographic images of bubbles at increasing Re_o' and a constant gas flow rate of Q_{gas} = 0.01 vvm when the MOBC was equipped with baffle design 3.

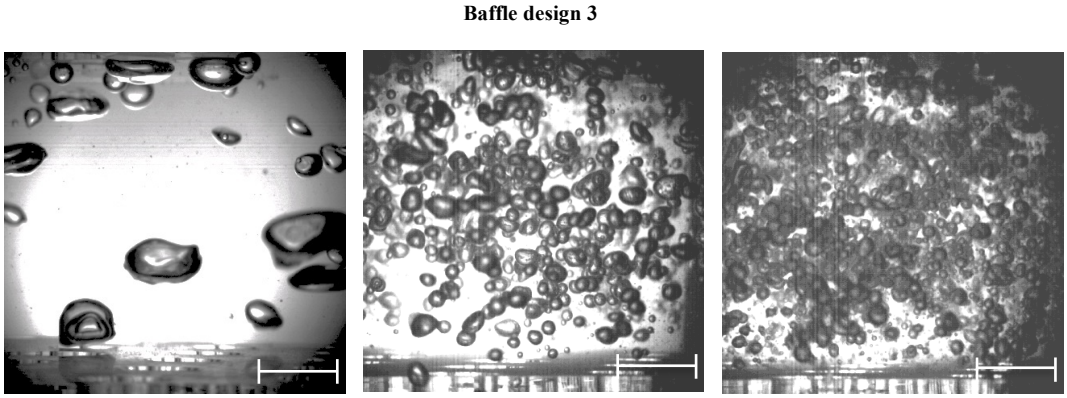

Figure 4-5 Impact of fluid oscillation conditions on bubble sizes in the MOBC configured with baffle design 3. (a) Re_o' = 0 (no fluid oscillations); (b) Re_o' = 16170, St' = 1.1, f = 8 Hz and x_0 = 2 mm; (c) Re_o' = 24260, St' = 0.7, f = 8 Hz and x_0 = 3 mm. Q_{gas} was kept constant at 0.1 L min^{-1} (0.01 vvm). The scale bar corresponds to 10 mm.

A 68 % reduction in $D_{3,2}$ was observed with fluid oscillations, at Re_o' = 16170 and St' = 1.1 (Figure 4-5(b)) and Re_o' = 24260 and St' = 0.7 (Figure 4-5(c)), compared with the un-baffled steady column. This significant reduction in $D_{3,2}$ at high values of Re_o' resulted in increased interfacial area for mass transfer, which is an effective means of increasing the gas hold-ups and enhancing mass transfer rates in gas-liquid systems. The combination of a small d_o (as used by

Reis *et al.* (2007)) with high Re_o values (as used by Oliveira and Ni (2004a)) was apparently the central point for achieving reduced mean size of bubbles in the MOBC. This can be briefly explained by recalling the physics behind drop generation in constricted flows as follows in section 4.3.2.

4.3.2 The effect of open orifice diameter and simple shear on bubble breakage

The breakup of liquid drops or gas bubbles can occur in constricted flows by the action of interfacial forces or inertial forces. Resulting from the very low viscosity of the liquid phase, the maximum capillary number calculated from the peak fluid velocity through the orifices in the three baffle designs tested was Ca = 0.012 (calculated for f = 7 Hz and x_0 = 3 mm), which usually indicates the interfacial forces should dominate the shear stresses. Nevertheless, the high Reynolds numbers of the fluid being forced through the orifices means the dynamics of fluid flow should be actually dominated by inertial effects. As mentioned in section 4.3.1, the presence of baffles *per si* was sufficient for reducing the mean size of bubbles, which suggested the bubble breakup mechanism is mediated by inertial effects as the liquid and bubbles were pushed through the orifices. On such conditions, the bubble breakup can be connected to the simple shear, $\dot{\gamma}_{SS}$ through an orifice with diameter d_o, which can be estimated from:

$$\dot{\gamma}_{SS} = \frac{V_{mean}}{d_o} \tag{4.12a}$$

where V_{mean} is the peak fluid velocity through the orifice during the fluid oscillation, which can directly calculated from the input f and x_0:

$$V_{mean} = 2\pi f x_0 \cdot \frac{1}{\alpha} \tag{4.12b}$$

Combining Eqs. (4.12a) and (4.12b) yields:

$$\dot{\gamma}_{SS} = \frac{a}{\alpha\, d_o} \tag{4.13}$$

where $a = 2\pi \cdot f \cdot x_0$ and depends only the fluid oscillation conditions selected. Equation (4.13) returned $\dot{\gamma}_{SS} = 93 \cdot a$, $\dot{\gamma}_{SS} = 372 \cdot a$, and $\dot{\gamma}_{SS} = 634 \cdot a$, for the baffle design 1, 2 and 3, respectively. Comparatively, this represents a 4-fold increase in simple shear by replacing the baffle design 1 with baffle design 2 (with smaller orifice size) and a 6.9-fold increase in $\dot{\gamma}_{SS}$ by replacing baffle design 1 with baffle design 3 which highlights the relevance of α and d_o on BSD. This also showed that $D_{3,2}$ is inversely proportional to the $\dot{\gamma}_{SS}$ agreeing with the traditional models for energy dissipation. Similar conclusions were also reported in other studies available in literature (Gagnon *et al.*, 1998; Rama Rao & Baird, 2003).

4.3.3 Flow visualisation of liquid and spatial tracking of bubbles in the MOBC

A further set of experiments used a high-speed camera for tracking the liquid flow and CO_2 bubbles in the MOBC equipped with baffle designs 2 or 3; design 1 was discarded as it underperformed in respect to BSD control as mentioned in section 4.3.1. Firstly, the liquid phase was traced with polyamide particles, and an image sequence recorded at 1000 fps. Figure 4-6 shows photographic sequences taken in the MOBC equipped with baffled design 2 in three different positions of the oscillation cycle using $f = 4$ Hz and $x_0 = 5$ mm.

The area viewed corresponded to an entire inter-baffle cavity (the position of the two baffles can be seen in the top and bottom of the figures). Although a range of values of Re_o' and St' was tested, baffle design 2 showed little evidence of strong eddy formation. The very large ratio $L/d_h = 4.8$ and the large number of orifices used in that particular baffle design presumably means the eddies were unable to reach the centre of cavity and the energy dissipation was limited to the edges of the orifices. The particle tracing experiments (Figure 4-6) showed poor evidence of secondary eddy mixing through the oscillation cycle as fluid appeared to move only in straight lines in the direction of the piston stroke. Although this baffle configuration delivered smaller bubbles sizes than design 1 it was also found inappropriate for the intensification of gas-liquid flows for presenting limited gas-liquid contacting (K_La values presented in section 4.3.4 were in the basis of this final conclusion).

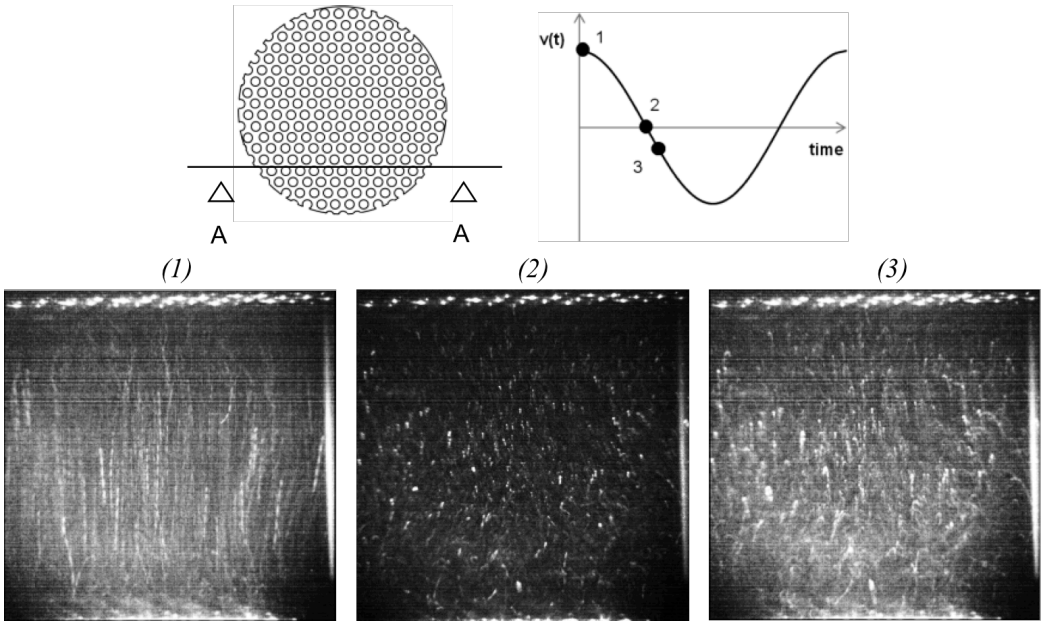

Figure 4-6 Flow visualisations of liquid mixing in the MOBC configured with baffle design 2 using tracing polyamide particles (f = 4 Hz, x_0 = 5 mm, Re_o' = 2310, St' = 0.2). Images are shown for 3 stroke positions throughout an oscillation cycle.

Optical flow visualisation in the MOBC equipped with baffle design 3 showed a very distinct liquid flow patterns, when compared to the other baffle designs. Figure 4-7 shows a photographic sequence of the liquid flow patterns in the inter-baffle region (baffles position can be seen on the top and bottom of the figures) with increasing Re_o' but approximately constant St'. Strong eddies were observed at different phases of the oscillation cycle and the intensity and size of eddies increased with increasing Re_o' as expected. At the highest value of Re_o' tested (Re_o' = 24260, f = 8 Hz, x_0 = 3 mm), the flow patterns revealed a mix of chaotic flow with well-defined toroidal vortices resulting in strong radial fluid motion, desirable for enhancing gas-liquid contacting and ultimately extend the contacting times in the column.

A second set of optical observations consisted in real-time tracking of bubbles in the MOBC. This was carried out only for baffle designs 2 and 3, and aimed establishing a qualitative link between gas-phase movement and the mass transfer performance.

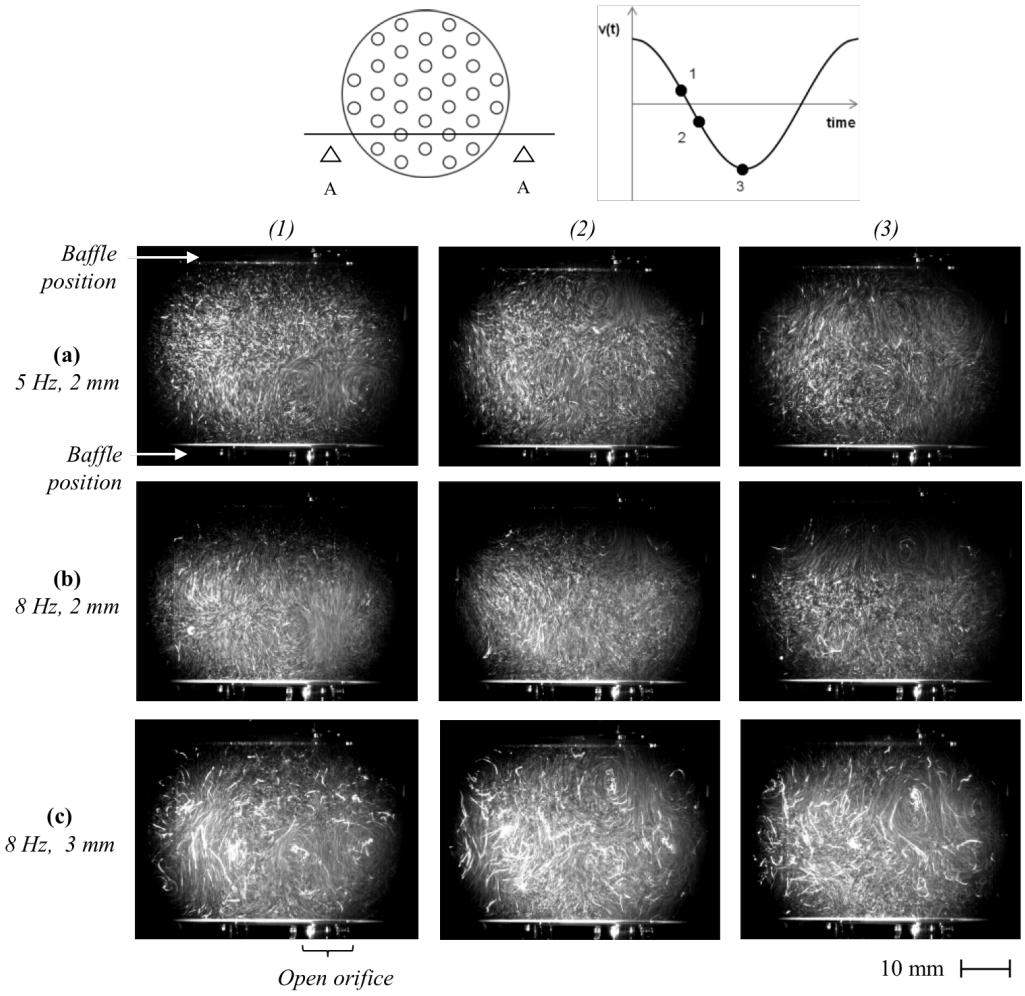

Figure 4-7 Flow visualisation of liquid mixing in the MOBC configured with baffle design 3 using tracing polyamide particles. Three different fluid oscillation conditions are shown: (a) f = 5 Hz, x_0 = 2 mm, Re_o' = 10110, St' = 1.1; (b) f = 8 Hz, x_0 = 2 mm, Re_o' = 16170, St' = 1.1; (c) f = 8 Hz, x_0 = 3 mm, Re_o' = 24260, St' = 0.7.

Figures 4-8 and 4-9 show on the left hand side a tracking of (x,y) position for a set of 4 bubbles randomly selected that could be observed rising through one inter-baffle space, and on the right hand side the instantaneous axial (vertical) velocity for each bubble corresponding to $V_y = \Delta y/\Delta t$ (mm s^{-1}). As a reference, the instantaneous mean fluid velocity imposed by the piston given by $V_y = 2\pi \cdot f \cdot x_0 \cdot \sin(2\pi \cdot f \cdot t)$ was also shown on the plots in Figures 4–8(d) and 4–9(b,d). The arrows in Figures 4–8(a,c) and 4–9(a,c) represent the direction and starting position of bubbles at the beginning of the tracking process.

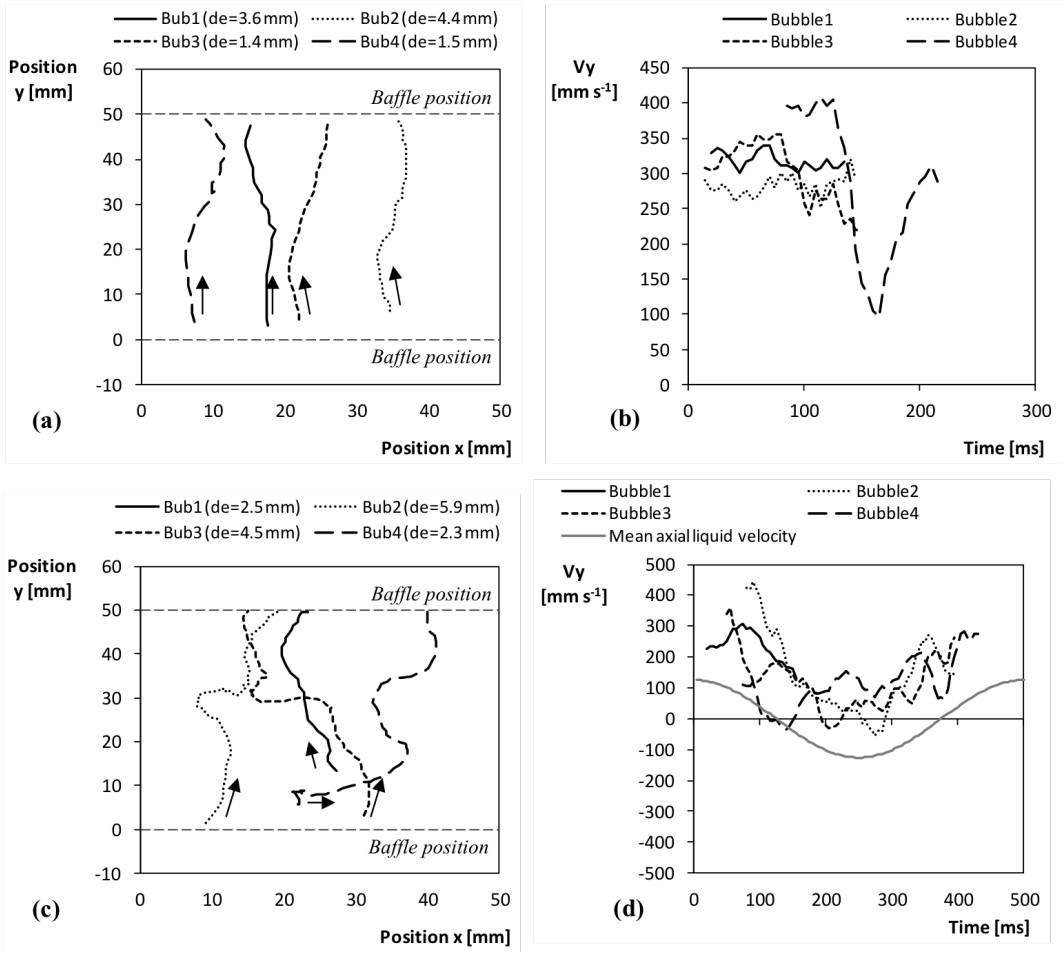

Figure 4-8 Time-tracking of (x,y) position and instantaneous vertical velocity (V_y) for 4 bubbles randomly selected in the inter-baffle region in the MOBC configured with baffle design 2. The aeration rate was kept constant at 0.04 vvm. (a) and (b) stagnant flow (i.e. Re_o' = 0); (c) and (d) fluid oscillated at f = 2 Hz, x_0 = 10 mm, Re_o' = 2310, St' = 0.1. Arrows in (a) and (c) show initial position and direction of the bubbles tracked.

Using baffle design 2 and in the absence of fluid oscillations (Figure 4-8(a-b)), bubbles ascended the column with a mean instantaneous velocity of 300–350 mm s^{-1} which agrees well with the value for terminal velocity of bubbles estimated from Stokes law in a bubble column (Talaia, 2007). In the presence of fluid oscillations (Figure 4-8(c-d)) there was some noticeable lateral displacement of the bubbles in the column which was an indicator of secondary or non-axisymmetric flow being generated in the column. Analysis to V_y during an entire oscillation cycle (Figure 4-8(d)) has revealed two important facts. First, the rising velocity of bubbles varied throughout the oscillation cycle, just like the liquid velocity did, independently of the size of bubble selected. Secondly, V_y corresponded approximately to the net difference between the

rising velocity in free flow (i.e. with no fluid oscillations – Figure 4-8(b)) and the instantaneous liquid flow velocity through the oscillation cycle. The V_y values were always positive, showing bubbles were delayed when the oscillating piston was moving downwards but accelerated as the piston moved upwards. This resulted in a net increasing in the residence time of the bubbles, therefore increased net contacting times.

In respect to baffle design 3 the bubble tracking revealed something substantially different. Two combinations of frequency and amplitude for the same Re_o' = 20220 were presented in the Figure 4-9 (f = 2 Hz, x_0 = 10 mm, St' = 0.2; f = 10 Hz, x_0 = 2 mm, St' = 1.1).

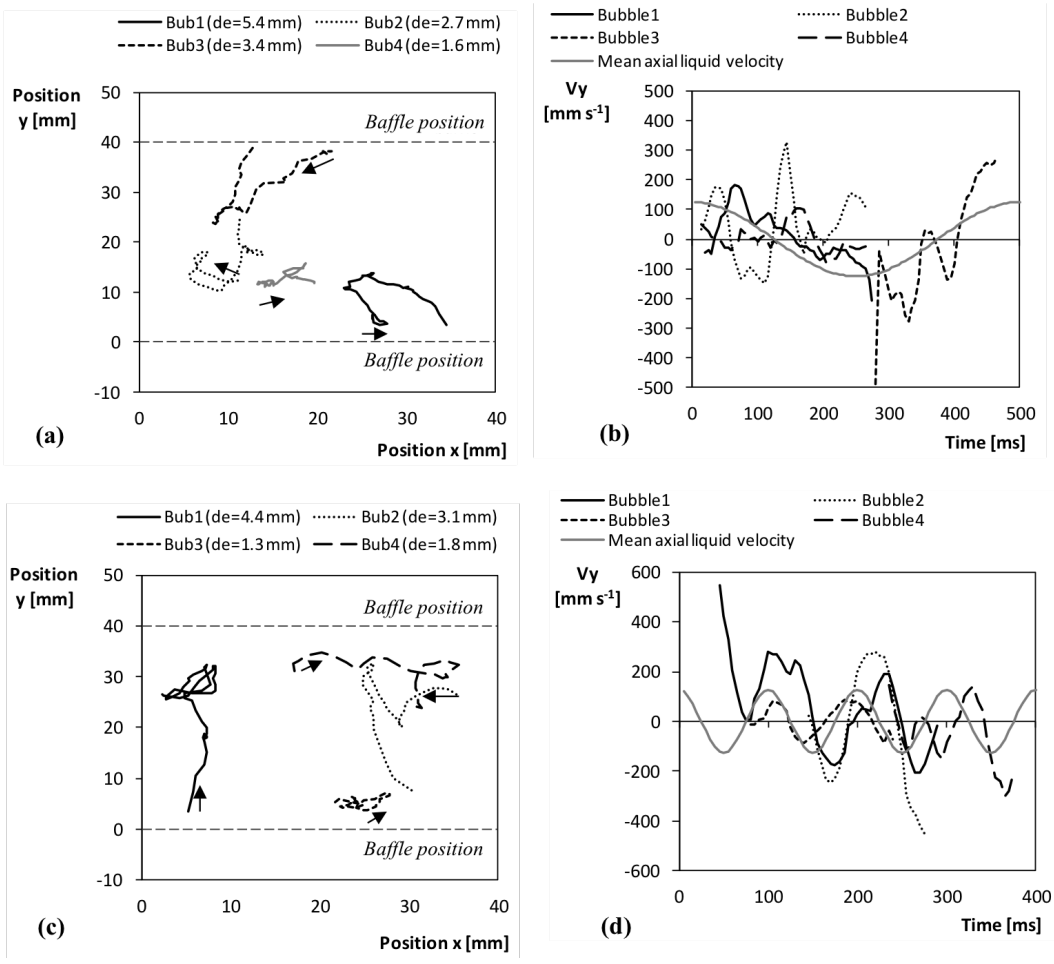

Figure 4-9 Time-tracking of (x,y) position and instantaneous vertical velocity (V_y) for 4 bubbles randomly selected in the inter-baffle region in the MOBC configured with baffle design 3. The aeration rate was kept constant at 0.01 vvm. (a) and (b) obtained at f = 2 Hz, x_0 = 10 mm, Re_o' = 20220, St' = 0.2; (c) and (d) obtained at f = 10 Hz, x_0 = 2 mm, Re_o' = 20220, St' = 1.1. Arrows in (a) and (c) show initial position and direction of the bubbles tracked.

The bubble tracking showed reduced vertical and increased lateral (radial) bubbles displacement in the inter-baffle regions. This was associated with the strong radial mixing produced in the column by the formation of strong periodic eddies that are capable of trapping bubbles and overtake the natural buoyancy. Figure 4-9(b,d) showed bubbles effectively following the liquid flow in respect to space and time.

At higher frequency, f = 10 Hz bubbles could be seen trapped in the inter-baffle regions for at least two full oscillation cycles (Figure 4-9(d)). This was due to the small open area of the baffles, which allowed effective generation of strong eddies throughout the oscillation cycle. In addition to a major reduction in $D_{3,2}$ reported in section 4.3.1 the contacting time for mass transfer of CO_2 from gas phase to the liquid phase in the column was also increased, which suggests larger mass transfer rates.

4.3.4 Effect of fluid oscillations on K_La and CO_2 dissolution efficiencies

Table 4–3 summarises K_La values obtained with the three different baffle configurations. The initial CO_2 dissolution trials using baffle designs 1 and 2 showed a marginal increase on K_La when fluid oscillation conditions were used when compared to the steady column. This was associated with the large mean bubble sizes (design 1) and poor eddy mixing (design 2) observed in the MOBC. For that reason, only CO_2 dissolution using baffle design 3 is discussed in detail in this section. Moreover, the present study aimed high CO_2 dissolution efficiencies, which involved using very low U_G values; therefore, the obtained K_La values are smaller than the ones reported in literature for CO_2 and other gases (Gagnon *et al.*, 1998; Gomaa *et al.*, 2012; Rama Rao & Baird, 2003). Figure 4-10(a) shows the impact of baffles and fluid oscillations on CO_2 dissolution in the MOBC using baffle design 3.

The required sparging time for 90 % CO_2 saturation in the un-baffled column was observed as 14.5 min, and reduced to 12.8 min in the baffled (i.e. no fluid oscillations) column, whilst the use of “mild” (5 Hz, 2 mm) or “strong” (7 Hz, 3 mm) fluid oscillations reduced it further to 10.0 min and 8.2 min, respectively. This represents up to 43 % savings on CO_2-air mixture injected into the column in order to reach same CO_2 saturation level.

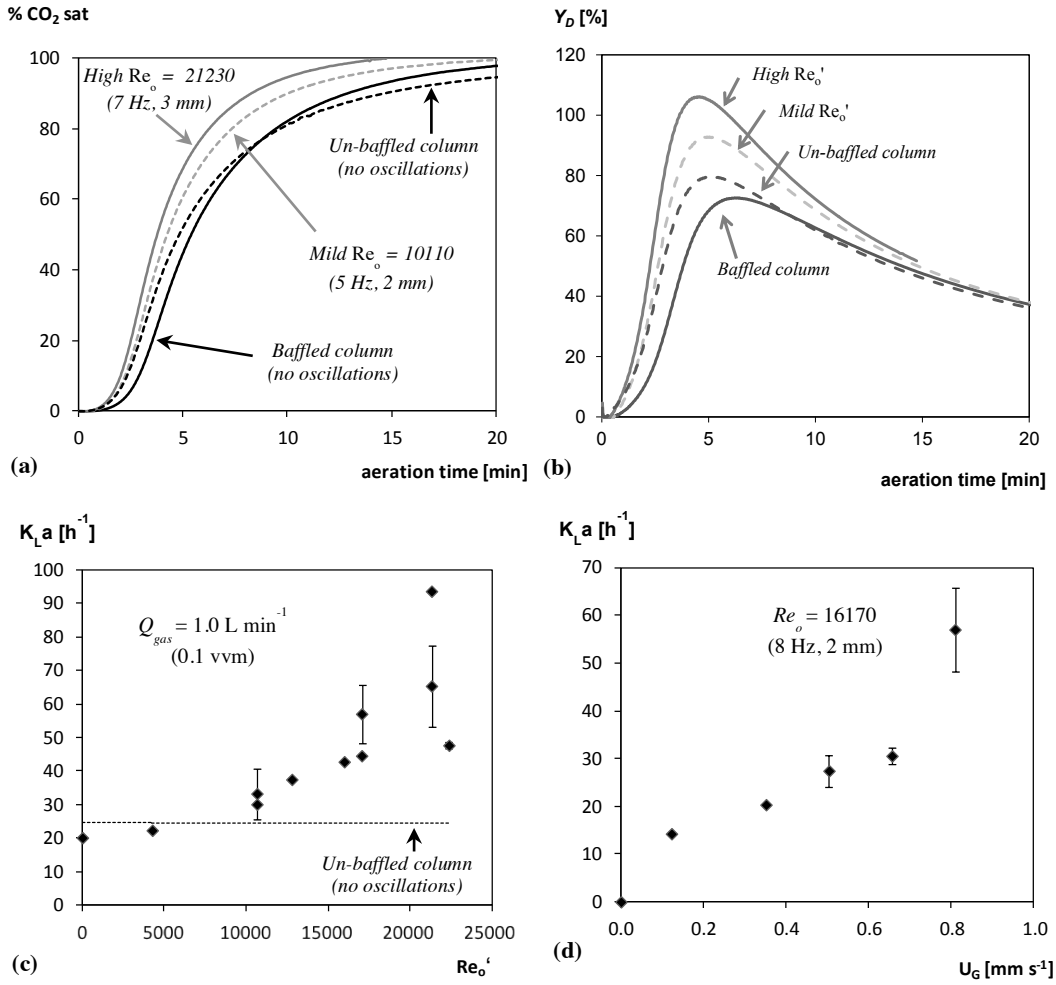

Figure 4-10 Effect of Re_o' and aeration rate, U_G on the efficiency of CO_2 dissolution and the overall volumetric mass transfer coefficient, K_La for the un-baffled and baffled multi-orifice column using baffles design 3 (see Table 4–2 for more details). (a) Example of CO_2 dissolution profiles at a constant aeration rate Q_{gas} = 1.0 L min^{-1} (0.1 vvm) for different configurations and fluid oscillation conditions in the column; (b) Time progress of cumulative CO_2 dissolution yield, Y_D at same experiments shown in (a); (c) Variation of K_La with the modified oscillatory flow Reynolds number (Re_o'), at a constant flow rate Q_{gas} = 1.0 L min^{-1} (i.e. 0.1 vvm); (d) Variation of K_La with mean superficial gas velocity (U_G) at a constant Re_o' = 16170, St' = 1.1, f =8 Hz, x_0 = 2 mm. Error bars represent two standard deviation from experimental replicas.

The cumulative mass of CO_2 supplied to the column (m_S) and CO_2 uptake in the column (m_U) at the operating conditions (20 °C and 1 atm; 5 % v/v CO_2; 0.1 vvm of gas; Henry's constant for CO_2 = 24.42 L atm mol^{-1}) is given by:

$$m_S(t) = Q_{gas} \cdot \frac{RMW}{V_M} \cdot x_{CO_2} \cdot t \qquad (4.14a)$$

$$m_U(t) = C_L(t) \cdot V_L \tag{4.14b}$$

The ratio m_U/m_S give an estimate of the cumulative efficiency or yield of CO_2 dissolution process in the column (Y_D) with the aeration time. Figure 4-10(b) shows Y_D for same experiments in Figure 4-10(a), which reveals that the maximum CO_2 dissolution efficiency increased from 79 % in the un-baffled column to 100 % in the MOBC when oscillated at f = 7 Hz and x_0 = 3 mm for a single gas passage, with a peak in CO_2 dissolution efficiency around 5 min from the beginning of time. This represented a 29 % increase in the efficiency of CO_2 dissolution achieved upon proper baffle design and the use of oscillatory flow mixing. Although generating fluid oscillations requires external energy input that represents an additional cost to be considered, this type of mixing is energetically efficient as shown by power input studies in OBCs; typical power inputs are in the range of 0.5–0.6 kW m^{-3} – see for example Baird *et al.* (1996).

The exponential increase at initial stages of dissolution curves in Figure 4-10(b) is related to the response time delay of the dissolved CO_2 probe, which underestimates C_L during the initial sparging time. CO_2 is highly soluble in water therefore Y_D for the un-baffled column is yet considerably high and related to small gas flow rate and molar fraction of CO_2 in the feeding gas stream. As the dissolved CO_2 concentration approaches the saturation concentration Y_D naturally drops and the dissolution process becomes less efficient.

In respect to K_La values, baffle design 3 revealed a major improvement in mass transfer rates when compared to the other baffle designs initially explored. The K_La increased with increasing of both Re_o' and U_G as shown in Figure 4-10(c-d). This agrees well with previous gas-liquid mass transfer studies using single-orifice OBCs (Hewgill *et al.*, 1993; Oliveira & Ni, 2004b; Reis *et al.*, 2008) and multi-perforated reciprocating plate column (Rama Rao & Baird, 2003). A maximum value for K_La of 65 ± 12 h^{-1} was obtained at f = 2 Hz and x_0 = 10 mm, which corresponded to a 3.3 and 2.7-fold increase in K_La in comparison with steady 'baffled' (K_La = 20 h^{-1}) and 'un-baffled' (K_La = 24 h^{-1}) column, respectively. The K_La values herein obtained were similar to those achieved by Taslim and Takriff (2004) for a pure CO_2-water system however with a 13 to 36-fold reduction in Q_{gas}.

It could also be observed in Figure 4-10(c) that the use of "gentle" fluid oscillations, at low values of f and x_0 (e.g. up to f = 2 Hz and x_0 = 2 mm in this study) were in general detrimental to CO_2-water mass transfer process, as the values of K_La obtained at such conditions were slightly lower than the K_La values obtained with the steady un-baffled column (dashed horizontal line in Figure 4-10(c)). This could be explained by the fact that "gentle" fluid oscillations generate very weak eddy vortices and a net acceleration of the bubbles during the piston stroke upward, as explained for bubble tracking experiments in section 3.3.3. The axial sinusoidal movement of the fluid leads to a net increase on the rising velocity of bubbles and consequently to reduced residence time of the bubbles in the column followed by a net drop on K_La. From Figure 4-10(c) it can be estimated a minimum value of Re_o' = 3000–4000 to produce an effective increase in K_La. It was however not possible to confirm experimentally that the increase in K_La in the MOBC resulted from an enhancement in the gas-liquid contacting with increasing Re_o' value (i.e. mixing intensity) or from the change in the total interfacial area, as the cloudiness of the CO_2-water dispersions at higher Re_o' obstructed the direct optical measurement of individual bubble sizes. Nevertheless, the images sequences as presented in Figure 4-5 suggested that the increase in Re_o' resulted in no additional decrease in bubble size, but rather only on an increase in the number of bubbles in the inter-baffle regions. This suggested the enhanced liquid mixing and higher velocity fluctuations on the gas-liquid interface reduced the boundary layer on the bubble's surface, as previously shown in similar studies (Oliveira & Ni, 2004a, 2004b).

In this study, it was found that K_La seems to vary linearly with Q_{gas} and U_G (Figure 4-10(d)). Other studies carried out in single-orifice OBCs of Oliveira and Ni (2004b), Hewgill *et al.* (1993), and Taslim and Takriff (2004) have shown a power law relationship between K_La and U_G, of the type obtained for bubble columns that could not be observed with baffle design 3. Al-Abduly *et al.* (2014) and Hewgill *et al.* (1993) obtained a relationship very close to the linearity. Gomaa *et al.* (2012) compiled a set of 8 correlations commonly used or K_La estimation of the type $K_La \propto U_G^b$, where b has a value in the range of 0.14–1.55. For one of those correlations b is close to unity, as it happens with the MOBC.

The high K_La values obtained for dissolution of CO_2 in water become relevant when considering the very low gas flow rates used (i.e. $Q_{gas} \leq 0.1$ vvm). For example, Hill (2006) used a stirred tank reactor and Q_{gas} in the range of 0.08–0.80 vvm (i.e. up to 8 times higher aeration rates than the

current study) and achieved K_La values in the range of 20–120 h^{-1} (despite the conditions at which the highest K_La values have been obtained could not be determined from their work). That same study mentioned the best-fitted K_La value was obtained at 27.5 °C, 0.45 vvm and 375 rpm and was equal to 41.4 h^{-1}. Taslim and Takriff (2004) performed similar CO_2 mass transfer studies in an single orifice OBC and reported similar values for K_La, although working with very large Q_{gas} in the range of 1.3–3.6 vvm using pure CO_2. The high K_La values herein reported highlights the successful scale-up and high efficiency of CO_2 dissolution upon a proper baffled design in the MOBC. The fine gas-liquid dispersion with enhanced gas-liquid contacting times and improved K_La obtained in the MOBC equipped with baffle design 3 is unique in respect to efficiency of CO_2 dissolution.

CHAPTER 5

Efficient-continuous syngas conversion in a multi-orifice oscillatory baffled bioreactor

5.1 INTRODUCTION

Gasification of biomass and other carbonaceous materials produces a gas mixture, usually known as producer gas, synthesis gas, or simply syngas. This mixture consists of carbon monoxide (CO), hydrogen (H_2), carbon dioxide (CO_2), and traces amounts of methane (CH_4), nitrogen and sulphur-containing gases, higher hydrocarbons, and particulate matter (Haryanto *et al.*, 2009). Anaerobic conversion is a biological pathway, in which mainly CO and H_2, can be assimilated by syngas-utilizing microorganisms for converting syngas into a range of bio-based compounds, such as, bioplastics, ethanol, butanol, acetic and butyric acid, and methane (Bredwell *et al.*, 1999; Kapic *et al.*, 2006). Economic and process benefits of syngas conversion over catalytic processes, such as Fisher-Tropsch, have been reported in literature (Heiskanen *et al.*, 2007; Klasson *et al.*, 1991; Munasinghe & Khanal, 2010a). Fermentation of lignocellulosic biomass, using gasification to produce syngas, is an example of this, whose process yields can theoretically be almost twice the ones achieved through sugar fermentation (Heiskanen *et al.*, 2007). In syngas conversion, CO is usually the only carbon source and H_2 acts as electron donor, and the process conversion efficiency depends on the microorganisms used and type of product desired (Henstra *et al.*, 2007). Due to the low solubility of these two compounds it is believed that CO conversion is controlled by the gas-liquid mass-transfer rates (Zhu *et al.*, 2008), which needs to be addressed in order to develop efficient alternatives to catalytic processes.

For that purpose, various approaches have been studied, using different reactor and impeller designs (Kumaresan & Joshi, 2006; Munasinghe & Khanal, 2010b; Ungerman & Heindel, 2007), applying innovative baffle design (Hewgill *et al.*, 1993; Smith & Mackley, 2006), introducing additives in the system (Zhu *et al.*, 2008, 2009), improving micro-bubble diffuser and dispersers (Kaster *et al.*, 1990; Lee *et al.*, 2012), as well as applying high gas and liquid flow rates (up to 2.14 min^{-1}, for gas) (Ungerman & Heindel, 2007), large specific gas–liquid interfacial areas, and increased gas pressures (up to 2 atm) (Munasinghe & Khanal, 2012). The most commonly used bioreactor configurations reported for syngas conversion include conventional stirred tank bioreactors, bubble columns, and membrane reactors (Abubackar *et al.*, 2011). However, these reactor configurations present some limitations in processes where highly intense gas-liquid contact and reduced bubble size are required.

Oscillatory flow mixing is an alternative mixing technology that has shown successful industrial applications on a wide range of processes, such as suspension polymerisation, crystallisation, flocculation and fermentation, in the biochemical engineering and the pharmaceutical sector (Jian & Ni, 2003; Ni & Gough, 1997). It consists in forcing sinusoidally the fluid through a set of periodic baffles or constrictions placed along a tube normally 5–50 mm in diameter, which results in the periodic formation of vortex rings at very low Reynolds numbers which is very effective in promoting radial mixing and contacting between immiscible fluids (Reis *et al.*, 2005); in an alternative design the baffles can be moved instead of the fluid. Different setups have been tested from bench to pilot scale, including constricted tubular reactor (Reis *et al.*, 2006, 2008), single-orifice tubes (Hewgill *et al.*, 1993; Oliveira & Ni, 2004b; Taslim & Takriff, 2004), multi-orifice columns (Smith & Mackley, 2006), some of them presenting unique features (e.g. type of baffle insert, orifice distribution, smooth constrictions). The baffle design usually requires a balance between minimizing frictional losses and maximizing mixing effectiveness (Harvey *et al.*, 2001). Eddy formation, promoted by the baffle sharp edges, increases the radial mixing in the column, in such a way that radial and axial velocities of the same order of magnitude can be achieved (Mackley & Ni, 1991; Ni & Pereira, 2000). The oscillatory baffled columns offer flexibility in respect to operation mode, as it can be run continuously as a near plug flow reactor or as a batch-mixing device with very gentle shear rates. In respect to gas–liquid contacting the oscillatory flow mixing results in a major reduction in bubbles size and trapping of bubbles in the inter-baffle regions, resulting in high mass transfer rates compared to other gas-liquid contacting technologies (Gaidhani *et al.*, 2003). A detailed study of the hydrodynamics and CO_2 mass transfer for a novel multi-orifice oscillatory baffled column (MOBC) was already described in work of Chapter 4.

In respect to CO conversion is it recognised that mass transfer limitations are the major bottleneck for commercialisation of this novel technology capable of producing a range of platform chemicals (Munasinghe & Khanal, 2010a). Therefore, the selection of an appropriate bioreactor configuration is important for obtaining high yields by overcoming mass transfer limitations in high cell density systems. To achieve that, an ideal bioreactor system should provide a high specific surface area for the reactions to occur, and favour high mass transfer rates (Abubackar *et al.*, 2011).

The present work aimed at studying the performance of syngas conversion using a mixed anaerobic culture inoculum in a novel multi-orifice oscillatory baffled bioreactor (MOBB) that has been specifically designed to outperform other gas-liquid contacting technologies (see Chapter 4). The effect of oscillatory mixing intensity and operation mode (batch versus continuous) was evaluated in respect to production rates of methane and other valuable intermediate products, as organic acids and alcohols, which helped addressing a major metabolic bottleneck in CO conversion.

5.2 EXPERIMENTAL METHODS AND PROCEDURES

5.2.1 Multi-orifice oscillatory baffled bioreactor (MOBB)

The basic design of the 150 mm internal diameter MOBB used in this work has been described in Chapter 4. In order to perform the syngas conversion experiments some modifications were required as shown in Figure 5-1. The MOBB was equipped with equally spaced multi-orifice baffles with unique design (see baffled design 3, in Chapter 4).

The total volume of the column was 10.6 L, with a working volume (V_L) of 9.1 L, and a total column height (h) of 540 mm. All experiments were carried out at atmospheric pressure (P_T = 1 atm). To assure maximum biological activity of the mesophilic sludge the temperature inside the bioreactor was continuously measured with a thermocouple and kept tightly in the range of 35–37 °C, using heated water recirculation thorough the water jacket in the column. The water bath used had a temperature controller and recirculation pump (TE-10A Thermoregulator, Techne, Bibby Scientific Limited, UK). The bioreactor system and tubing connections were completely sealed to maintain strict anaerobic conditions throughout the experiments.

The inlet gas stream consisted of synthetic syngas mixture (BOC Industrial Gases, UK) with the following composition (v/v): 60 % CO, 30 % H_2, and 10 % CO_2. The gas was fed directly from a pressured cylinder and sparged from the bottom of the MOBB. The gas phase was chosen based on a detailed screening of CO conversion in batch test vials (results shown in Chapter 3), as represented the syngas composition for maximum metabolic performance.

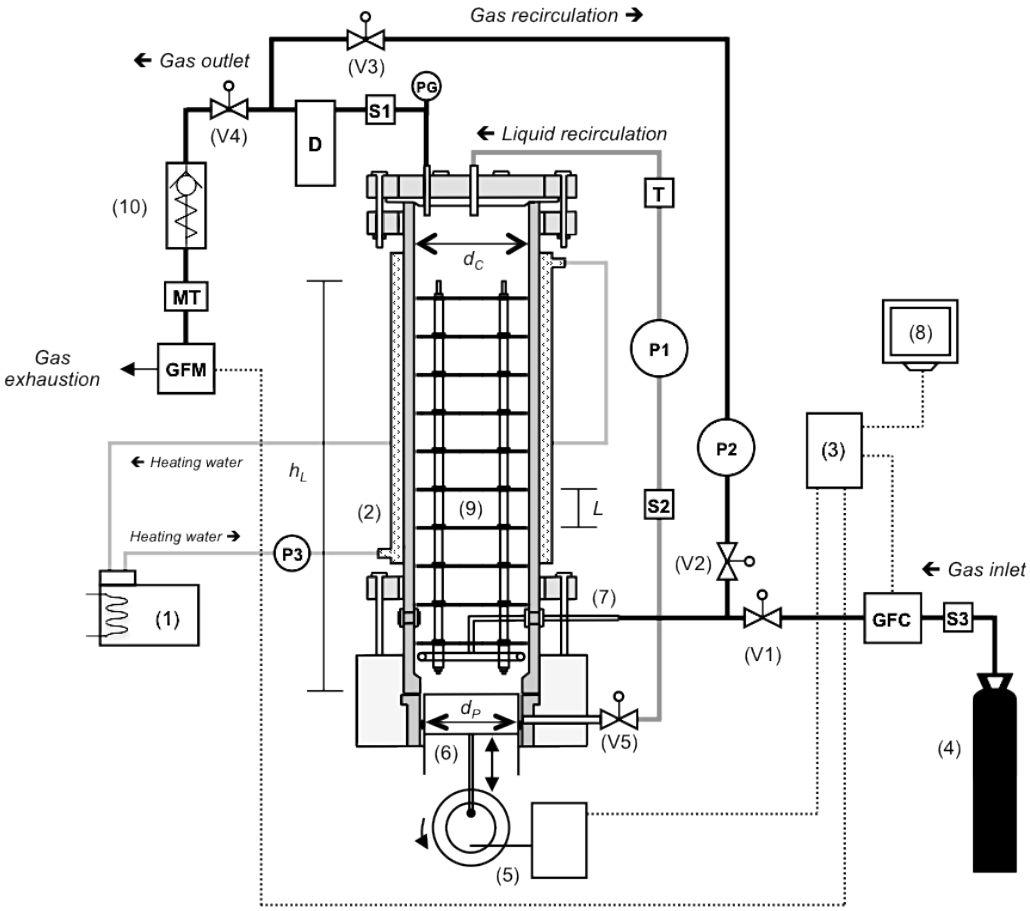

Figure 5-1 Configuration of the multi-orifice oscillatory baffled column (MOBB) used on syngas conversion studies. 1 – Water bath coupled with recirculation pump and temperature controller; 2 – Water jacket; 3 – CPU; 4 – Syngas cylinder (60 % CO, 30 % H_2, 10 % CO_2); 5 – Servo-hydraulic unit; 6 – Piston; 7 – Gas sparger; 8 – Display; 9 – Interbaffle cavity; 10 – Non-return valve. D – Dreschel bottle; GFC – Inlet gas flow controller; GFM – Outlet gas flow meter; MT – Moisture trap; P – Pumps (1 and 2, diaphragm; 3, peristaltic); PG – Pressure gauge; S – Sampling ports (1 and 3, gas; 2, liquid); T – Temperature probe and display; V – Ball valves (1 to 5). Dimensions were: liquid height in column, h_L = 450 mm; inter-baffle spacing, L = 40 mm; diameter of piston, d_P = 125 mm; maximum internal diameter of column, d_c = 150 mm.

The sparger consisted of a circular plastic tube perforated with a 0.6 mm diameter needle to deliver an even bubble formation within the column. Gas flow rate at the inlet was measured and controlled by calibrated Mass Flow Controllers (GFC 17, Aalborg®, USA), with maximum flow rates of 10 or 200 mL min^{-1}.

The outlet gas flow rate was measured using a gas flow meter (Agilent Flowmeter ADM2000, Agilent Technologies, UK), connected to a CPU, whose data was continuously acquired using the

software *HyperTerminal* (Hilgraeve, UK). A moisture trap (Chrompack Gas Clean Filter Jacket), placed in the outlet gas line right before the gas flow meter, was used to retain the moisture that could be present in gas flow and to avoid interferences with the gas meter readings.

Gas was continuously recirculated from the headspace at a constant gas flow rate of 600 mL min^{-1} using a diaphragm pump (N810FT.18, KNF, Germany), in order to enhance gas-liquid contacting and make the syngas continuously available to the anaerobic microorganisms.

The liquid phase (culture medium) was kept at a constant volume of 9.1 L. Sinusoidal fluid oscillations were imposed on the fluid using the servo-hydraulic system, controlling a 125 mm o.d. piston attached to the bottom of the column. This moving base piston is capable of delivering fluid oscillation frequency (f) and centre-to-peak amplitude (x_0) in the ranges of 1–2 Hz and 2.5–10 mm, respectively. Due to foam generation in the column, caused by the turbulent mixing in the liquid medium, a maximum oscillation of f = 2 Hz and x_0 = 10 mm was used, which according to our previous mas transfer studies should return good volumetric mass transfer coefficients (see Chapter 4). As a result of the sinusoidal movement of the fluid in the closed vessel, the gas in the headspace is also displaced, generating cycles of pressure and vacuum, according to the frequency and amplitude tested. To avoid oscillations in the outlet gas stream and ensure proper operation of the gas flow meters a Dreschel bottle was installed next to the headspace of the column. This worked as a damper to oscillations in the gas flow rate and effectively worked as an extension to the headspace in the MOBB; the total headspace volume in the system (top of MOBB and Dreschel bottle) was about 2.0 L. To keep strict anaerobic conditions and to avoid oxygen of being aspirated from the outside through the gas outlet a non-return valve (TP50P0006, Norgren, USA) was placed in the outlet gas line, between the gas flow meter and the Dreschel bottle (see Figure 5-1).

The composition of the liquid medium was the same used in study described in Chapter 3, using MES as buffer solution (see section 3.2.1 for more details). The pH of the medium was measured in liquid samples and kept in the range 5.8–6.7 throughout the experiment. At the beginning of the experiments, column was inoculated with the liquid medium and Nitrogen sparged for 30 min to remove all the oxygen eventually dissolved in the liquid or present in the headspace. When anaerobic conditions were attained, gas feeding was switched to syngas

mixture. The liquid medium was also recirculated during some periods of the experiments (mainly before sampling biomass from the MOBB) with a diaphragm pump (8005 Series, SHURflo, USA).

5.2.2 Experimental design and operational strategy

Gas composition in the inlet and outlet of the MOBB was monitored, by sampling the headspace content using a 1 mL gas-tight syringe (SGE Analytical Science, Australia). Liquid samples were taken through the liquid sampling port shown in Figure 5-1, in order to evaluate product formation as volatile fatty acids (VFA) and alcohols during the syngas conversion. After collection and prior to analysis liquid samples were centrifuged at 10,000 rpm (RCF 9,279 *x* G) for 10 min (Microcentrifuge 5415R, Eppendorf, USA), and the supernatant collected and stored at –20 °C previous to analysis.

The batch incubation assays previously described in Chapter 3, performed in 160 mL-vials were herein recalled and helped evaluating methane production potential and CO and H_2 uptake rates, in the MOBB operation, since the same anaerobic mixed culture inocula was used. These assays were performed at the same conditions of pH, P_T, gas composition, and placed on an orbital shaker to promote a gas-liquid contacting. For comparison purposes, these assays are hereby designated as test vials.

5.2.2.1 Batch syngas conversion in the MOBB

In this set of experiments, the bioreactor was initially primed with syngas (60 % CO, 30 % H_2, 10 % CO_2) for saturation of liquid medium and headspace with syngas and then operated as a closed vessel. Composition of CO and H_2 and CH_4 was monitored along the batch conversion by sampling periodically the headspace in the MOBB. All experiments started at 1 atm of total pressure (P_T).

Each experiment run started by injecting syngas into the column at 1 L min^{-1} for 20 min, which was found sufficient to achieve saturation of syngas components in the headspace. Then, the

inlet and outlet valves were closed, and from this point the batch experiment was started (this was assumed time, $t = 0$). Gas was then recirculated continuously from the headspace, until both H_2 and CO were fully consumed, and CH_4 concentration stabilised. At the end of the process, the excess volume of gas produced was determined by releasing the outlet valve and integrating the outlet flow rate with release time.

The effect of gas-liquid mixing intensity was evaluated in the batch conversions by changing the fluid oscillation conditions. Three different combinations of frequency (f) and centre-to-peak amplitude (x_0) were tested: 1 Hz, 2.5 mm; 2 Hz, 5 mm; and 2 Hz, 10 mm. These conditions corresponded to oscillatory Reynolds numbers (Re_o) equal to 2530, 10110, and 20220, respectively, calculated according to the new calculation method proposed in Chapter 4. Moreover, all references to Re_o in this Chapter 5 correspond to the "modified" Re_o calculation, although they will be further called simply Re_o. This set of experiments allowed evaluating the effect of oscillatory mixing conditions in the anaerobic syngas conversion performance, and determining the rates of uptake or production of the main gaseous compounds at the different conditions tested.

5.2.2.2 Continuous syngas conversion in the MOBB

In this set of experiments the MOBB was continuously fed with a given syngas flow rate. As the outlet and inlet gas valves remained open, the total pressure in the MOBB headspace remained constant at $P_T = 1$ atm. In addition, the recirculation of the gas and liquid medium was kept on throughout the entire set of experiments. Based on the results from the batch CO conversion experiments an oscillatory mixing condition of 2 Hz and 5 mm was selected as the settings giving the more reliable continuous operation of the MOBB (avoiding high amount of foam to be produced, as would happen with 2 Hz and 10 mm).

The range of syngas flow rates, Q_{syngas} tested for continuous experiments was 0.001–0.01 vvm (volume of gas per volume of reactor per minute), corresponding to a range of mean superficial gas velocity, U_G of 0.03–0.63 mm s^{-1}. Continuous experiments were successfully run at 5, 10, 20, 40, and 100 mL min^{-1}. The outlet gas stream was evaluated in respect to composition and

gas flow rates. As a result of the continuous syngas sparging and recirculation from the headspace, the residence time of the gas (τ_G) in the system changed depending on Q_{syngas}. This residence time was calculated according to Eq. (5.1):

$$\tau_G = \frac{V_{G,total}}{Q_{Gas}} = \frac{V_{Headspace} + \varepsilon_G \cdot V_L}{Q_{Gas}} \quad (5.1)$$

where, $V_{G,total}$ is the total volume of gas in the column, V_{HS} is the volume of headspace (including "dead" volume from the Dreschel bottle), V_L is the volume of the liquid in the column, and ε_G is the gas holdup in the column (gas volume fraction), assumed as ~1 % of V_L, based on previous measurements on the same column (see Chapter 4). Based on Eq. (5.1) τ_G values were estimated in the range of 0.3–6.8 hours, depending on the inlet syngas flow rate.

5.2.3 Analytical methods

Gaseous compounds (H_2, CO_2, CH_4, and CO) were analysed by gas chromatography (Agilent Technologies, 7890A) equipped with a TCD detector and a Carboxen®-1010 PLOT Capillary column (L × I.D. 30 m × 0.32 mm, average thickness 30 μm, Supelco, Sigma-Aldrich). Helium was used as carrier gas at a flow rate of 3 mL min^{-1}. The injector and detector temperatures were 200 and 230 °C, respectively. A split ratio of 1:5 was set in the injector. Column was run at a constant temperature of 35 °C for 7.5 min, followed by a ramp from 35 to 155 °C, at a rate of 20 °C min^{-1}. Volatile fatty acids (VFA) and alcohols were determined using the same methods described in Chapter 3.

5.3 RESULTS AND DISCUSSION

5.3.1 Enhanced syngas dissolution in the MOBB

The first step aimed at determining the uptake and mass transfer rates of H_2 and CO in the MOBB based on the dynamic gassing-out method (Fuchs *et al.*, 1971). Although CO_2 is a gaseous substrate present in the syngas mixture, it is also a product in the whole anaerobic

conversion process, and its concentration profile does not follow the same trend as for the other gaseous substrates. For that reason, it was not possible to determine the production and uptake rates for CO_2 in the MOBB. Figure 5-2 shows the concentration profiles obtained for H_2 and CO from where the volumetric gas-liquid mass transfer coefficient, K_La and uptake rates for CO and H_2 could be determined by best-fitting to the mass transfer model.

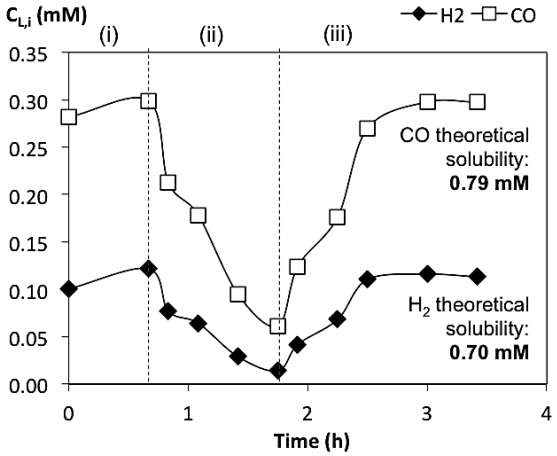

Figure 5-2 Carbon monoxide and hydrogen concentration profiles as measured in the headspace, during the dynamic gassing-out experiment performed in the MOBB. The inlet syngas flow rate used was 100 mL min^{-1} in phase (i) and (iii), and 0 mL min^{-1} in phase (ii), and mixing intensity was constant at Re_o = 10110 (f = 2 Hz, x_0 = 5 mm). Vertical dashed lines represent the time at which syngas flow was stopped and resumed.

The test started by injecting continuous syngas at 100 mL min^{-1} until steady state was attained – phase (i). Then, syngas injection was stopped and the headspace sampled at very small time intervals, from where a steady drop is expected – phase (ii). At about 20 % of the initial value, the syngas injection was resumed until steady state was reached again – phase (iii). The general mass balance calculation for a gas component *i*, is described by Eq. (5.2):

$$\frac{dC_{L,i}}{dt} = K_L a\left(C^*_{L,i} - C_{L,i}\right) - q_i \cdot X - D \cdot C_{L,i} \qquad (5.2)$$

where, the term $dC_{L,i}/dt$ (mol L^{-1} s^{-1}) is the concentration gradient of component *i* along time; K_La (s^{-1}) is the volumetric gas-liquid mass transfer coefficient; $C^*_{L,i}$ (mol L^{-1}) is the concentration of

component *i* in the liquid side of the interface in equilibrium with the partial pressure of the component in the gas phase; $C_{L,i}$ (mol L^{-1}) is the concentration of the component dissolved in the liquid; q_i (mol g_{VSS}^{-1} s^{-1}) is the specific uptake rate of the component *i*; *X* (g_{VSS} L^{-1}) is the concentration of biomass as volatile suspended solids (VSS); and *D* (s^{-1}) is the dilution rate of the liquid.

Since there is no net addition of liquid medium into the process, the last term in Eq. (5.2) is equal to zero, and the mass balance is reduced into Eq. (5.3).

$$\frac{dC_{L,i}}{dt} = K_L a\left(C_{L,i}^{*} - C_{L,i}\right) - q_i \cdot X \tag{5.3}$$

This method, typically used in biological systems, allows determining gas uptake rates and K_La, from a single experimental run in two steps. Firstly, the uptake rate is determined from the slope in phase (ii). Secondly, the dissolution profile in the liquid medium is combined with the uptake rate determined in phase (ii) allowing to estimate the K_La during phase (iii). Taking into account the different phases involved in the determination method, the final calculation for phase (ii) and (iii) are described in Eqs. (5.4) and (5.5), respectively:

$$dC_{L,i} = \left(-q_i \cdot X\right)dt \tag{5.4}$$

$$dC_{L,i} = \left[K_L a\left(C_{L,i}^{*} - C_{L,i}\right) - q_i \cdot X\right]dt \tag{5.5}$$

where, C^{*}_{i} (mol L^{-1}) is the dissolved concentration of saturation for component *i*; and C_i (mol L^{-1}) is the dissolved concentration at time *t*, along the experimental assay. The term q_i•X (mol L^{-1} s^{-1}) is described as the uptake rate of the component *i*, and will be used for further considerations. Given the difficulty of measuring the dissolved concentration for both H_2 and CO in the liquid phase, dissolved concentrations were estimated from the concentrations measured in the gas phase, according to Henry's Law (Sander, 1999). Moreover, pseudo steady-state equilibrium was assumed at all stages of the experiment and dissolution process.

Mass transfer performance of the novel MOBB evaluated by the results shown in Figure 5-2, returned K_La values of 39.9 and 24.9 h^{-1} for CO and H_2, respectively. These values are in agreement with the ones reported in literature (Munasinghe & Khanal, 2012). In fact, in a

syngas-fed bioprocess using a mixed culture, K_La values in the range of 31–104 h^{-1}, in a CSTR, and 121 h^{-1}, in a trickle bed reactor configuration have been reported for CO (Bredwell *et al.*, 1999). For H_2, in the same reported studies, K_La values reported are in the range of 75–190 h^{-1} (CSTR) and 335 h^{-1} (trickle bed), however there is no reference on those studies about the flow rates used. K_La is strongly dependent on the flow rate (Bredwell *et al.*, 1999) and the same trend is followed by this MOBB as previously demonstrated in study of Chapter 3. K_La values in the range of 72–288 h^{-1} were obtained in a CSTR, with CO flow rates of 2.4 L min^{-1}, corresponding to 0.34 vvm (Kapic *et al.*, 2006). In the present study, shown in Figure 5-2, in the MOBB a gas flow rate of 0.001 vvm was used, which is 340 times lower than the one used in literature and suggests the gas-liquid contacting is very efficient.

The uptake rates estimated from Figure 5-2 for CO and H_2 were 54.0 and 24.2 mmol L^{-1} d^{-1}, respectively. This represents to a 6-fold and 3-fold improvement for CO and H_2, respectively, in comparison with the uptake rates achieved in experiments using test vials, which were 8.3 and 6.9 mmol L^{-1} d^{-1}, respectively. These improvements in K_La and uptake rates suggest the MOBB is an appropriate platform for performing anaerobic syngas conversion studies and capable of overcoming typical gas-liquid mass transfer limitations of other gas-liquid contacting systems.

5.3.2 Batch syngas conversion: effect of oscillatory mixing intensity

Initially the MOBB was operated as a batch, fully enclosed vessel. Different oscillatory mixing conditions were tested, and its effect in respect to experimental performance fully assessed. In Figure 5-3 the amounts (mmol) of CO, H_2 and CH_4 in the headspace, normalised by the liquid volume (L), are presented for the test vials and the MOBB. It should be noticed that the initial CO and H_2 concentrations in the gas phase were similar in both experiments and, according to Henry's Law (Sander, 1999), similar dissolved CO and H_2 concentrations were predicted (equilibrium conditions were assumed). This reference to the volume of the liquid instead of volume of headspace was defined in order to facilitate comparison of results with other studies on literature.

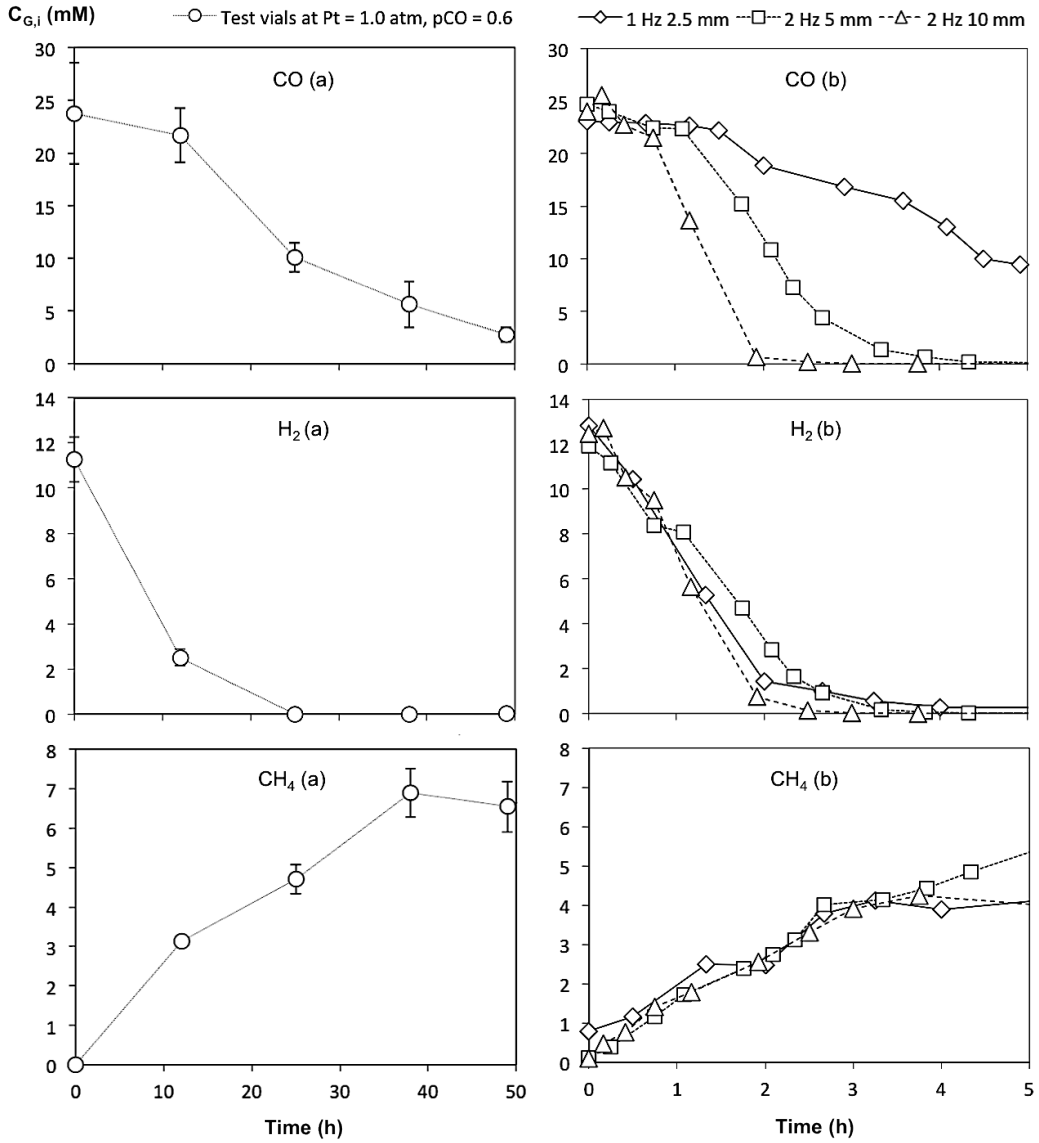

Figure 5-3 Concentration of carbon monoxide, hydrogen, and methane in the gas phase, during batch syngas conversion in (a) the 160 mL test vials, at P_T = 1.0 atm, p_{CO} = 0.6 atm (from work in Chapter 3), and in (b) the MOBB at different oscillatory mixing conditions. Vertical bars in graphs (a) represent standard deviation.

As can be observed, the initial uptake rate of CO and H_2 is strongly affected by the mixing conditions (maximum $q_{CO} \cdot X$ = 50.7 mmol L^{-1} d^{-1}, $q_{H2} \cdot X$ = 24.0 mmol L^{-1} d^{-1}, in respect to dissolved concentrations in the liquid medium). Surprisingly, initial production rate of CH_4 is not affected by the degree of mixing remaining similar to the rate of production in the test vials (range of 4.5–4.9 mmol L^{-1} d^{-1}). Despite oscillatory flow mixing is effective in improving gas-liquid contacting and increase uptake rates for CO and H_2, we failed to observe any net increase in the

CH_4 production rate which demonstrates syngas conversion using anaerobic mixed inoculum is not mass transfer limited. This has been previously suggested by several authors (Bredwell *et al.*, 1999; Klasson *et al.*, 1991; Munasinghe & Khanal, 2010a), but it remained as an unproven hypothesis before this work was carried out. Both CO and H_2 present very low solubility in water (Bredwell & Worden, 1998), therefore kinetics of CO conversion is in theory strongly dependent on the availability of these compounds in the liquid phase (Munasinghe & Khanal, 2010b; Scharlin *et al.*, 1998).

Because the inoculum used in the process is prevenient from an anaerobic process treating easily biodegradable, carbohydrates-rich wastewater from a brewery industry (Brito *et al.*, 2007; Klijnhout & Eerde, 1986), it is assumed that the culture had already good hydrogenotrophic activity. In fact, activity tests done before with the same biomass following the method described in Costa *et al.* (2012), revealed an intrinsic activity for H_2 in the range of 582–659 mL of CH_4 g_{VSS}^{-1} d^{-1}. As H_2 dissolves in the liquid medium, it is rapidly taken up by the hydrogenotrophic microorganisms, therefore reactions where H_2 is involved appear to run close to the maximum reaction rate or hydrogenotrophic activity, even at low mixing intensity (1 Hz and 2.5 mm), which is an indication that H_2 uptake is limited by mass transfer.

In respect to CO consumption it is clear that carboxydotrophic activity is not limiting to the overall conversion process. Although carboxydotrophic methanogenic activity has not been tested for this inoculum, anaerobic microorganisms can easily adapt to the use of CO as main carbon source, as long as it can be made available and dissolved in the liquid medium (Guiot *et al.*, 2011). This fact is confirmed by the data shown in Figure 5-3, where a 6-fold increase in CO uptake rate is observed when mixing intensity is increased (from 8.3 ± 2.1 up to 50.7 ± 17.1 mmol L^{-1} d^{-1}). Also a 3-fold improvement is achieved for H_2 uptake rate at such conditions (from 6.9 ± 3.9 up to 24.1 ± 4.5 mmol L^{-1} d^{-1}). At the mildest mixing intensity tested in the MOBB (Re_o = 2530) the uptake rates of CO and H_2 are slightly higher, although about the same order of magnitude. It is not clear from the data whether the CO consumption could be rather improved by testing an even higher combination of frequency and amplitude, however we have observed foam generation at high mixing intensities, which would require the addition of any anti-foaming agent that could potentially hinder the effect of Re_o on mass transfer.

Regarding CH_4 production, it was not possible to detect effect of mixing intensity on CH_4 production rate during the initial 5 hours of experiment (Figure 5-3). In fact, the CH_4 production rates obtained with the MOBB were very similar to the ones achieved in the test vials experiments (4.9 and 4.5 mmol L^{-1} d^{-1}, respectively). This confirms that in anaerobic processes, methanogenesis is the last and slowest step in the systematic chain of electron reduction down to methane. Although CH_4 production rates cannot be enhanced by means of external mixing, there are clear advantages in using intensive mixing to control gas-liquid contacting and reducing dissolution times.

Based on the initial slopes of the curves shown in Figure 5-3, initial specific rates, r_x were calculated for CO, H_2, and CH_4. The values obtained were plotted against the oscillatory Reynolds number, Re_o, corresponding to each set of oscillatory conditions tested as shown in Figure 5-4, which confirms a major effect of oscillatory mixing intensity on the main kinetics of the process.

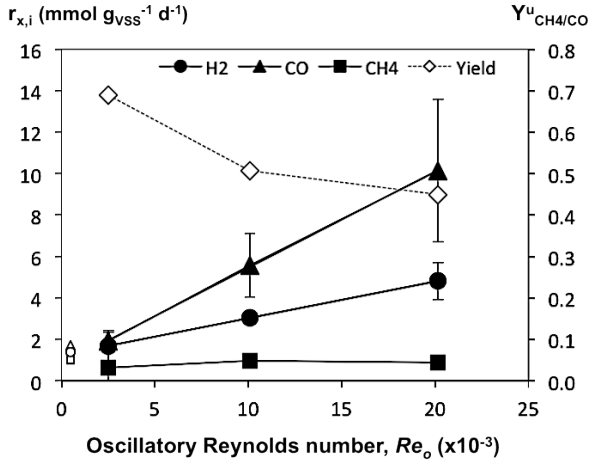

Figure 5-4 Specific rates, r_x for carbon monoxide, hydrogen and methane expressed as mmol of component per gram VSS per day, in the batch MOBB, at different fluid oscillation conditions, expressed as oscillatory Reynolds number, Re_o. The ultimate methane yield obtained from the final amount of CH_4 in headspace by consumed CO, $Y^u_{CH4/CO}$, is also represented for the same set of conditions. Vertical bars represent standard deviation.

Figure 5-4 also revealed that both CO and H_2 consumption rates are strong and linearly correlated to the mixing intensity as given by Re_o. Linear regression of each curve returned Eqs

(5.6) and (5.7) with regression coefficients, R^2 higher than 0.999 (specific uptake rates are expressed in mmol g_{VSS}^{-1} d^{-1}).

$$r_{x,CO} = 0.47 \cdot Re_o \left(\times 10^{-3}\right) + 0.79 \quad (5.6)$$

$$r_{x,H_2} = 0.18 \cdot Re_o \left(\times 10^{-3}\right) + 1.24 \quad (5.7)$$

It is also important to highlight that both Eqs. (5.6) and (5.7) have its intersection in *Y* axis (i.e. for Re_o = 0) at very similar values to those experimentally obtained for the test vials (1.7 and 1.4 mmol g_{VSS}^{-1} d^{-1} for CO and H_2, respectively); those values are also plotted in Figure 5-4. A second relevant aspect relates to the ultimate yield of CH_4 from CO, $Y^{u}_{CH4/CO}$ also summarised in Figure 5-4 for these batch experiments. This $Y^{u}_{CH4/CO}$ was calculated based on the ratio of CH_4 produced to the total amount of CO consumed, in the whole time window of the experiment. As can be observed, $Y^{u}_{CH4/CO}$ is negatively correlated with Re_o, and decreases with increasing uptake rates. This might be explained by some changes in the metabolic pathway upon the increase of the mixing intensity, which could lead to the production of other components such as volatile fatty acids or alcohols. In fact, the percentage of CH_4 in the final gas mixture present in the headspace revealed the same negative trend; final CH_4 content was 56, 50, and 38 %, for the conditions at Re_o of 2530 (1 Hz, 2.5 mm), 10110 (2 Hz, 5 mm), and 20220 (2 Hz, 10 mm), respectively. As towards the end of the experiment only CH_4 and CO_2 were detected in the headspace the remaining volume fraction should correspond to CO_2. In fact, for the tests at gradually higher mixing intensity, both substrates (CO and H_2) were totally consumed, but the metabolic pathway could be changed by directing the process to a product formation poorer in biomethane content (Munasinghe & Khanal, 2010a).

The batch conversion runs in the MOBB allowed demonstrating the positive effect of oscillatory mixing on the uptake rates for both CO and H_2, showing strong linear correlation with Re_o. Under such conditions, gas-liquid mass transfer has been improved and methanogenesis have shown to be the limiting step of the process. Surprisingly, CH_4 production rates are not affected by the improvement in mass transfer or uptake rates of CO or H_2, which are the main feedstocks for CH_4 production in anaerobic syngas conversion. This means that ultimately conversion process

times have to be extended in order to achieve higher yields; however, there is direct benefit of speeding up dissolution of these poorly soluble gases.

5.3.3 Continuous syngas conversion: effect of syngas flow rate

An additional set of experiments aimed at testing bioconversion for continuous injection of syngas in the MOBB. This was done for a range of syngas flow rates of 5–100 mL min^{-1}, and the fluid oscillations were kept constant at 2 Hz and 5 mm (Re_o = 10110). The main results of the MOBB performance along time of bioconversion are summarized in Figure 5-5.

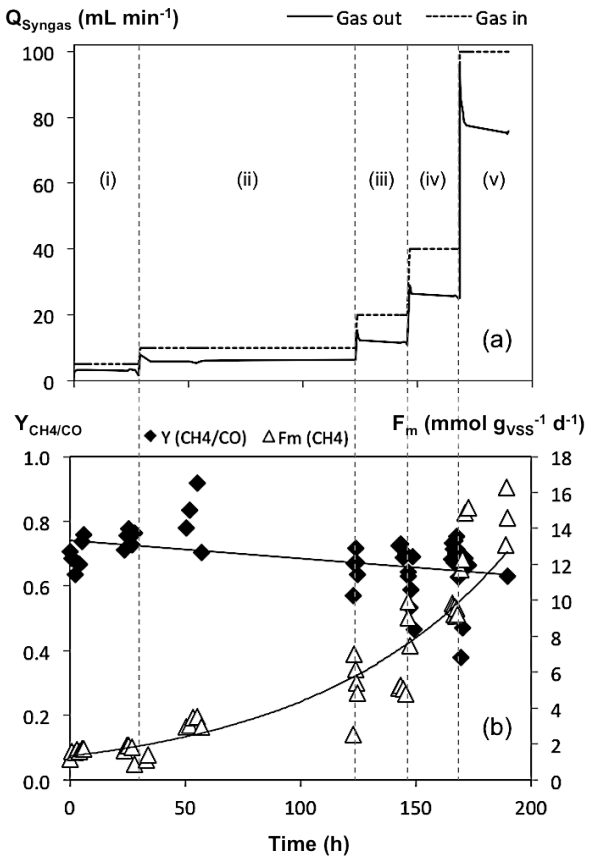

Figure 5-5 Syngas conversion performance in the MOBB during continuous operation: (a) inlet and outlet syngas flow rate ($Q_{syngas\ (in)}$, $Q_{syngas\ (out)}$); (b) instantaneous methane yield from CO ($Y_{CH4/CO}$), expressed as mmol CH_4 produced per mmol of CO consumed (averaged by straight fitting), and instantaneous methane production rate ($F_{m,CH4}$), expressed in mmol CH_4 produced per g_{VSS} in liquid medium per day (averaged by exponential line). Five different syngas flow rates were tested: (i) 5, (ii) 10, (iii) 20, (iv) 40, and (v) 100 mL min^{-1}.

In this case, both the inlet and outlet gas flow rates were monitored and plotted in Figure 5-5(a), which shows that a change in the inlet flow rate, $Q_{syngas\ (in)}$ is followed immediately by a change in the outlet flow rate, $Q_{syngas\ (out)}$. Also, steady stead was rapidly attained in the outlet. The effect of inlet syngas flow rates on both instantaneous CH_4 yields from CO ($Y_{CH4/CO}$ in brief) and CH_4 specific molar productivity ($F_{m,CH4}$ in brief) are plotted in Figure 5-5(b). In this particular set of continuous syngas injections $Y_{CH4/CO}$ was calculated as the number of moles of CH_4 produced per mole of CO consumed from the mass balances and periodic sample of the gas headspace. Similarly, $F_{m,CH4}$ was calculated based on the amount of CH_4 produced per gram of VSS in liquid medium per day. Both $Y_{CH4/CO}$ and $F_{m,CH4}$ have shown significant fluctuations during the conversion time, and it was necessary to run the bioconversion for 3–5 residence times (in respect to gas phase) in order to achieve steady state. This is presumably related to the sampling of the headspace but also to the time required to move from one steady state to another in well-mixed vessels.

The $Y_{CH4/CO}$ plot shown in Figure 5-5(b) revealed an overall negative trend with increasing syngas flow rates. Nevertheless, average values between 0.6 and 0.8 were obtained for $Y_{CH4/CO}$ in the whole range of Q_{in} tested. Conversely, the methane specific molar productivity given by $F_{m,CH4}$ (mmol g_{VSS}^{-1} d^{-1}) increased with the increase on Q_{in}, which shows the anaerobic biomass is capable of producing more CH_4 as more syngas is injected, and agrees with data reported for a three co-culture system (Klasson *et al.*, 1990a).

Based on Eq. (5.2), a mass balance to each gaseous component *i* in the headspace can be rearranged to include the syngas gas flow rates, as described in Eq. (5.8).

$$\frac{dC_i \cdot V_L}{dt} = Q_{in} \cdot C_{i,in} - Q_{out} \cdot C_{i,out} + \left(q_i \cdot X\right) \cdot V_L \tag{5.8}$$

In steady state this yields, the balance then results in Eq. (5.9).

$$-q_i \cdot X = \frac{Q_{in} \cdot C_{i,in} - Q_{out} \cdot C_{i,out}}{V_L} \tag{5.9}$$

Only a very limited set of studies previously reported continuous CO/syngas conversion using anaerobic mixed cultures (Guiot *et al.*, 2011; Luo *et al.*, 2013). One of those studies used a

600 mL continuous stirred tank reactor (CSTR) coupled with a hollow fibre membrane (HFM) module treating sewage sludge simultaneously with CO biomethanation at thermophilic conditions (Luo *et al.*, 2013). A maximum CH_4 production rate of 78 mmol L^{-1} d^{-1} was obtained, with a maximum 19 % of CH_4 content in the headspace when feeding pure CO at 0.0043 vvm, and τ_G of 2.4 h (Luo *et al.*, 2013). It was also reported that about 25 mmol L^{-1} d^{-1} of that CH_4 production rate could have come from the digestion of sludge itself. Comparing this reported result to the ones obtained in the present study, with similar CO flow rate (Q_{in} = 100 mL min^{-1}), 1.4 times higher CH_4 production rate (73.0 mmol L^{-1} d^{-1}) was herein achieved. In a second study a 30 L gas-lift reactor was used to perform biomethanation of CO with a maximum reported production rate of 4.8 mmol CH_4 g_{VSS}^{-1} d^{-1} when feeding pure CO at 23 mL min^{-1}, and τ_G of 8.9 h (Guiot *et al.*, 2011). In this present study, using similar CO flow rate (Q_{in} = 40 mL min^{-1}), 2 times higher specific CH_4 production rate (9.2 mmol g_{VSS}^{-1} d^{-1}) was attained, with 10 times lower τ_G (0.9 h). This improvement on specific CH_4 productivity in the MOBB shows that the technology is more effective than alternative gas-liquid contacting technologies, in making substrates easily available for microorganisms, so that process runs at maximum reaction rate, with no mass transfer limitation.

The overall effect of syngas flow rates over the whole "continuous" conversion can be further analysed based on the specific reaction rates, at each steady state, plotted as a function of specific CO loading rates, CO_{LR} into the MOBB, as shown in Figure 5-6. This showed that increasing CO loading rates positively benefits the uptake rates of CO and H_2, and production rate of CH_4, which agrees with limited data reported in literature (Klasson *et al.*, 1990a). In practice it also means that the molar conversion yield for CO and H_2 drops as more syngas is injected into the MOBB, so the CO loading rate will need to be fine-tuned to a particular syngas conversion efficiency requirement. This is in agreement with the literature (Vega *et al.*, 1990; Younesi *et al.*, 2008) and mass conservation principles.

Specific reaction rates, r_x for CO, H_2 and CH_4 shown in Figure 5-6 were fitted to a Monod's type model, commonly described used to describe growth kinetics in batch fermentation systems. The model herein applied is described in Eq. (5.10).

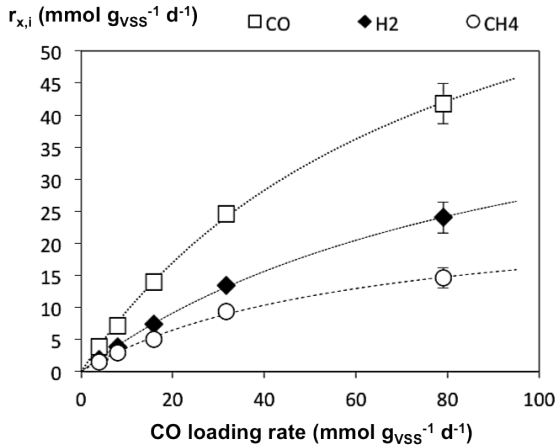

Figure 5-6 Effect of CO loading rates (mmol of CO per gram of VSS per day) on the specific reaction rates, $r_{x,i}$ for carbon monoxide, hydrogen and methane expressed as mmol of component per g_{VSS} in liquid medium per day in the MOBB, in the continuous syngas conversion experiments. Dashed lines represent the fitting of data to typical Monod's model (described in Eq. (5.10)).

$$r_{x,i} = r_{x,i}^{max} \cdot \frac{CO_{LR}}{K_x + CO_{LR}} \tag{5.10}$$

where, $r_{x,i}^{max}$ (mmol g_{VSS}^{-1} d^{-1}) and K_x (mmol g_{VSS}^{-1} d^{-1}) represent constants of the model, as a function of the CO loading rate, CO_{LR} (mmol g_{VSS}^{-1} d^{-1}), for steady state continuous operation. The dashed lines in Figure 5-6 represent data best-fitted to the model in Eq. (10). Surprisingly, very good fittings (with cross-correlation coefficients of 0.99) were obtained for all major gaseous compounds analysed. The values of the constants returned by the fitting were: ($r_{x,i}^{max}$) 83.4, 54.1, 26.0 mmol g_{VSS}^{-1} d^{-1}, and (K_x) 78.0, 98.5, 60.5 mmol g_{VSS}^{-1} d^{-1}, for CO, H_2, and CH_4, respectively. These values show that maximum CO uptake rate (or reaction rate) is almost twice the maximum H_2 uptake rate, and thrice the CH_4 production rate. On the other hand, K_x values obtained, which represent the CO loading rate matching half of the maximum reaction rates, are very similar for the three compounds. This fact indicates that the behaviour of uptake and production rates is similar and proportional. Moreover, reaction rates increase with syngas flow rate up to a maximum level in which a surplus volume of syngas will be generated. Ultimately, this excess of syngas will not be used for conversion and will create a "washing" effect in the whole system, operating at its maximum performance capacity.

Compared to the batch conversions a 8-fold and 11-fold increase in the maximum uptake rates were obtained with continuous syngas injection (417.0 and 270.5 mmol L^{-1} d^{-1}) for CO and H_2, respectively. More importantly, the increase in CO loading rate resulted in up to 27-fold improvement in CH_4 production rate (130.0 mmol L^{-1} d^{-1}) compared to the batch conversion experiments (4.8 mmol L^{-1} d^{-1}) in the same bioreactor system. Equally, this reveals that CH_4 production is affected not only by inlet gas flow rates but also by the operation mode. The reason for such improvement is not clear at the moment, but probably is related to metabolic state of the mixed anaerobes during continuous injection of syngas, which should be different from that under discontinuous (batch) syngas injection.

An interesting aspect that arises from the continuous conversion in the MOBB is that the syngas flow rate has a clear positive effect on mass transfer, as largely reported in literature (Gomaa *et al.*, 2012; Nicolella *et al.*, 1998; Riggs & Heindel, 2006), and also on reaction rates, however no effect was noticeable in respect to $Y_{CH4/CO}$ in this study or previously in literature (Guiot *et al.*, 2011; Luo *et al.*, 2013). Continuous conversion has shown to be robust and able to achieve high yields of CH_4 production with short contact times. This is presumably because process can be sustained in different metabolic stages.

5.3.4 Volatile fatty acids and alcohols production

The conversion of syngas components to methane during anaerobic conversion is not always direct, but may be rather made through the production of intermediates, as commonly occurs in the anaerobic digestion process. This occurs because, in the mixed culture involved in syngas conversion, only a few number of microbes are capable of performing direct conversion of CO or H_2/CO_2 to CH_4, while the majority of them produce organic intermediate compounds (Henstra *et al.*, 2007). Volatile fatty acids (VFA) and alcohols are two know groups of liquid compounds that can be produced as intermediates. In an efficient process well-directed to methane production, those compounds barely accumulate. Nevertheless, it is know that during anaerobic digestion processes, some limitations in the bioreactor system, either metabolic or hydrodynamics, may lead to the accumulation of those intermediates. On the other hand, by promoting the

appropriate conditions, both VFA and alcohols can be the main products of syngas conversion, as widely reported on literature (Liu *et al.*, 2014; Sim *et al.*, 2007; Worden *et al.*, 1989).

The presence of VFAs and alcohols in the liquid medium during the anaerobic syngas conversions was evaluated during both batch and continuous conversion runs. Table 5-1 summarises the amount of VFA compounds and alcohols identified in liquid samples taken at the beginning and at the end of each period of operation.

Table 5-1 Volatile fatty acids (VFA) and alcohols production measured in batch (end of run) and continuous (upon achieving the steady state) syngas conversion in the MOBB

Mode	Q_{Gas} mL min^{-1}	Re_o [-]	VFA (mM)			Alcohols (mM)		
			Formate	Acetate	Propionate	Methanol	Ethanol	*n*-Butanol
D	10	2530	(0.038) n/d	(0.115) 0.031	(0.249) 0.070	(n/d) n/d	(n/d) n/d	(n/d) n/d
D	10	10110	(n/d) 0.251	(0.247) 0.128	(0.040) 0.048	(n/d) n/d	(0.100) n/d	(n/d) n/d
D	10	20220	0.046	0.152	n/d	n/d	n/d	n/d
C	5	10110	0.027	0.034	n/d	n/d	n/d	n/d
C	10	10110	0.033	n/d	n/d	n/d	n/d	n/d
C	20	10110	0.048	n/d	n/d	n/d	n/d	n/d
C	40	10110	0.051	n/d	n/d	n/d	n/d	n/d
C	100	10110	0.087	n/d	n/d	n/d	n/d	n/d

D: Discontinuous; C: Continuous; n/d: Not detected. Note: The results represent the concentrations at the end of period time for each operation condition, taking into account that normally the end of one is the beginning of the next; whenever this condition does not match, initial concentrations are shown within brackets.

Regarding VFA content, formate, acetate and propionate were measured in the liquid samples. As can be observed in the table, VFA were detected in higher concentration during discontinuous operation. In fact, no correlation was found between the VFA accumulation and the conditions tested, with maximum concentration of about 0.25 mM of each compound being detected at different phases of operation. During continuous operation, formate was essentially the only VFA detected, which concentration increased with increasing syngas flow rates from 0.027 to 0.087 mM. Acetate was only detected during the operation at the lowest flow rate (5 mL min^{-1}) and propionate was not detected at all. Compared with other similar studies in literature, these concentrations may be considered almost negligible (Guiot *et al.*, 2011; Luo *et al.*, 2013). Regarding alcohols production, only a small concentration of ethanol (0.1 mM) was detected in the beginning of the discontinuous experiment, at Re_o = 10110 (2 Hz, 5 mm); however, such

amount was consumed before reaching the end of the experiment. No more alcohols were detected in the end of any other experiment. This fact shows there was no accumulation of alcohols during syngas conversion, in the conditions tested. Nevertheless, since there was no collecting of liquid samples during process time of each assay, the hypothesis of alcohols production as precursor of CH_4 is not excluded.

The batch and continuous anaerobic syngas conversion results herein reported using a mesophilic mixed culture in a novel MOBB give new insight in respect to syngas conversion in enhanced gas-liquid contacting conditions. There is evidence that syngas conversion process is highly constrained by metabolic limitations rather than mass transfer limitations, which remained unclear in literature. Continuous operation has shown that effective process engineering concepts can be brought together to overcome metabolic and mass transfer limitations and design efficient conversion systems.

CHAPTER 6

Flux balance analysis for modelling metabolic pathways of syngas conversion by mixed cultures

6.1 INTRODUCTION

Metabolic modelling is an important tool widely used to evaluate, optimise, and understand biological and biochemical processes. Such evaluation can allow redesigning processes to explore both fluxes of mass and energy within a metabolic network, in order to maximise growth rate or production of a certain metabolite of biotechnological interest (Orth *et al.*, 2010).

Flux balance analysis (FBA) is a metabolic modelling approach commonly used in genome-scale metabolic network reconstructions (Orth *et al.*, 2010). In this perspective, using a known encoded model, specific for a microorganism, and experimental data to constrain the model, FBA has been proven as an important tool in enhancing biochemical processes by exploiting the fluxes of metabolites (Carinhas *et al.*, 2013; Selvarasu *et al.*, 2012). Moreover, due to the simple principles behind FBA, this approach has been used in a diverse range of applications, including physiological studies, gap-filling efforts and genome-scale synthetic biology (Feist & Palsson, 2008).

FBA also presents some limitations, mainly the unsuitability to predict metabolite concentrations, as well as, to determine fluxes under unsteady state conditions. FBA predictions may not always be accurate and need to be experimentally verified to validate models (Orth *et al.*, 2010). Substrate prediction in *Escherichia coli* studies and model-based predictions of gene essentially, using FBA, have shown to be quite accurate and in agreement with experimental measurements (Edwards *et al.*, 2001; Feist *et al.*, 2007). Up to now, this FBA approach has not been widely applied to processes performed by a biological consortium containing mixed cultures. In fact, only a few number of studies have reported FBA utilisation on modelling processes based on mixed cultures (Chaganti *et al.*, 2011; Pardelha *et al.*, 2012, 2013). Nonetheless, the simplicity of the principles that support FBA approach may not prevent its application to other non-genome scale based processes, as long as a model containing all the main metabolic pathways is provided, and constrains are set based in steady state conditions. Thus, FBA application to syngas conversion studies using a mixed culture as inoculum appears as a relatively promising approach on better understanding the fluxes of compounds within the possible metabolic pathways of the process.

This study aimed at evaluating qualitatively the main metabolic pathways involved in syngas conversion by anaerobic mixed cultures, using a preliminary FBA approach based on experimental data. More than extensively characterise syngas conversion metabolic pathways, this study intends to give more insights about the whole syngas conversion process performed by mixed cultures, either on batch incubation vials or continuous bioreactor, previously studied in Chapters 3 and 5.

6.2 EXPERIMENTAL METHODS AND PROCEDURES

6.2.1 Experimental data source

Flux balance analysis (FBA) is based on specific reaction rates of metabolites involved in a reaction network. Thus, experimental data obtained during anaerobic syngas conversion, using a mixed inoculum, was used to perform the analysis. These syngas conversion studies were performed under different operational conditions and reaction vessels, consisting in three different setups: (setup A) 160 mL batch vials (studied in Chapter 3) and 10.6 L multi-orifice oscillatory baffled bioreactor (MOBB), in (setup B) batch and (setup C) continuous mode (studied in Chapters 5).

Table 6-1 summarises the averaged reaction rates of the main compounds involved in syngas conversion, CO, H_2, and CH_4, at each set of conditions. In this table, all reaction rates are described as mmol of compound per gram of inoculum (measured in volatile suspended solids, VSS) per hour. These rates represent the maximum initial rates obtained and calculated based on initial slopes of the consumption or production profiles of each compound. Negative reaction rate values are reported for consumption reactions, which was the case of CO and H_2; compounds that were totally consumed during the syngas conversion studies reported in this thesis. For production rates, values are shown positive, which in this case only refers to CH_4, as the main reaction product in the same experiments.

Table 6-1 Experimental data used for the FBA simulation. Values represent reaction rates, r_x of CO, H_2, and CH_4, expressed in mmol of gas component per gram of biomass (measured in VSS) per hour, during anaerobic syngas conversion, performed in three different setups (A, B, and C). The main conditions used in each assay are also indicated. The V_{HS}/V_L (volume of headspace per volume of liquid) ratios used in the experiments were 1 and 0.22 for vials and MOBB, respectively

Assay	Experimental conditions					Reaction rates, r_x [mmol g_{VSS}^{-1} h^{-1}]		
	Reaction vessel and operating mode	P_T [atm]	p_{CO} [atm]	Re_o [-]	CO_{LR} [mmol g_{VSS}^{-1} d^{-1}]	CO	H_2	CH_4
1	*Vials, batch*	1.0	0.2	-	-	–0.042	–0.044	0.019
2	Setup A	1.0	0.4	-	-	–0.063	–0.050	0.035
3		1.0	0.6	-	-	–0.069	–0.057	0.040
4		1.75	0.2	-	-	–0.021	–0.023	0.017
5		1.75	0.4	-	-	–0.023	–0.027	0.020
6		1.75	0.6	-	-	–0.030	–0.030	0.021
7		1.75	0.8	-	-	–0.049	–0.042	0.029
8		1.75	1.0	-	-	–0.048	–0.067	0.026
9		2.5	0.2	-	-	–0.026	–0.015	0.008
10		2.5	0.4	-	-	–0.080	–0.060	0.019
11		2.5	0.6	-	-	–0.079	–0.090	0.020
12		2.5	0.8	-	-	–0.065	–0.149	0.015
13		2.5	1.0	-	-	–0.048	–0.171	0.011
14		2.5	1.2	-	-	–0.058	–0.124	0.016
15		2.5	1.5	-	-	–0.066	–0.054	0.006
16	*MOOB, batch*	1.0	0.6	2,521	-	–0.080	–0.070	0.026
17	Setup B	1.0	0.6	10,083	-	–0.232	–0.126	0.040
18		1.0	0.6	20,166	-	–0.423	–0.200	0.037
19	*MOBB, continuous*	1.0	0.6	10,083	3.9	–0.161	–0.081	0.037
20	Setup C	1.0	0.6	10,083	7.9	–0.299	–0.158	0.122
21		1.0	0.6	10,083	15.8	–0.585	–0.307	0.199
22		1.0	0.6	10,083	31.6	–1.026	–0.561	0.384
23		1.0	0.6	10,083	79.0	–1.765	–0.991	0.609

Notes: (-) not applicable; P_T, total syngas pressure; p_{CO}, CO partial pressure; Re_o, oscillatory Reynolds number; CO_{LR}, CO loading rate.

6.2.2 Metabolic network

The metabolic model used for this analysis is based on only a few number of reactions compared to the other genomic-based studies where this approach is widely used. Nevertheless, using such a few number of reactions is not a problem, as long as the main reactions of the process are included and stoichometrically correct. Thus, Figure 6-1 represents a schematic of the metabolic network used for performing this FBA stoichiometrically.

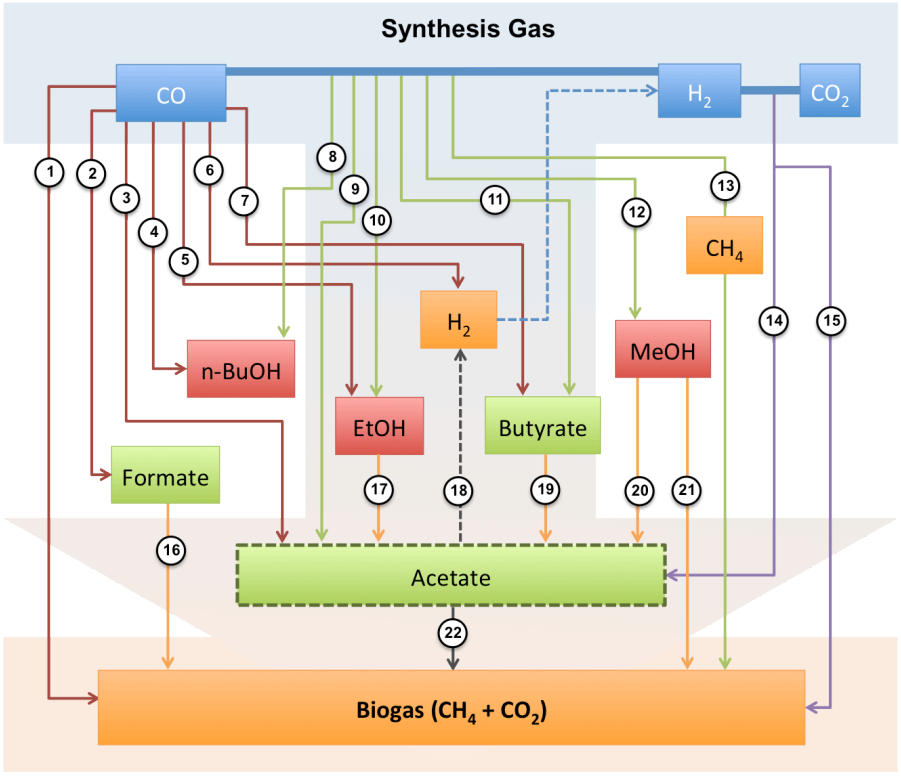

Figure 6-1 Network of main metabolic reactions during syngas conversion to biogas, used for the flux balance analysis.

This network of reactions was constructed based on possible reactions involving syngas components, and other by-products along the pathways. Some of the reactions were already studied and are reported in literature, along with the microorganisms responsible for performing them (Henstra *et al.*, 2007; Oelgeschläger & Rother, 2008; Sokolova *et al.*, 2009). Some other reactions are likely to occur, but no microorganisms able to perform them have yet been described.

6.2.3 Metabolic flux analysis

The metabolic model herein developed is composed of 52 reactions, which are described in Table 6-2. The 22 first reactions are the core reactions of the metabolic network shown in Figure 6-1. Two more reactions were added representing the CO_2 equilibrium in water.

Table 6-2 Main chemical reactions of the pathways involved in the metabolic network of syngas conversion to biogas, used for the flux balance analysis (numbers 1 to 22 match pathways shown in Figure 6-1). Other model characteristics are also described: type of reaction, reversibility, objective function and constraints, used as initial solutions for the optimisation problem

#	Reaction	Reaction type	Reversibility	LB	UB	OF
1	[c] : (4) CO + (2) H2O –> CH4 + (3) CO2	Metabolism	Irreversible	0	10	
2	[c] : CO + H2O –> Formate + H	(in cytosol)	Irreversible	0	10	
3	[c] : (4) CO + (4) H2O –> Acetate + (2) HCO3 + (3) H		Irreversible	0	10	
4	[c] : (12) CO + (5) H2O –> nBuOH + (8) CO2		Irreversible	0	10	
5	[c] : (6) CO + (3) H2O –> (4) CO2 + EtOH		Irreversible	0	10	
6	[c] : CO + H2O –> CO2 + H2		Irreversible	0	10	
7	[c] : (10) CO + (4) H2O –> Butyrate + (6) CO2 + H		Irreversible	0	10	
8	[c] : (4) CO + (8) H2 –> nBuOH + (3) H2O		Irreversible	0	10	
9	[c] : (2) CO + (2) H2 –> Acetate + H		Irreversible	0	10	
10	[c] : (2) CO + (4) H2 –> EtOH + H2O		Irreversible	0	10	
11	[c] : (4) CO + (6) H2 –> Butyrate + (2) H2O + H		Irreversible	0	10	
12	[c] : CO + (2) H2 –> MeOH		Irreversible	0	10	
13	[c] : CO + (3) H2 –> CH4 + H2O		Irreversible	0	10	
14	[c] : (2) HCO3 + (4) H2 + H –> Acetate + (4) H2O		Irreversible	0	10	
15	[c] : HCO3 + (4) H2 + H –> CH4 + (3) H2O		Irreversible	0	10	
16	[c] : (4) Formate + (4) H –> CH4 + (3) CO2 + (2) H2O		Irreversible	0	10	
17	[c] : EtOH –> Acetate + H2O		Irreversible	0	10	
18	[c] : Acetate + (4) H2O –> (4) H2 + (2) HCO3 + H		Irreversible	0	10	
19	[c] : Butyrate + (2) H2O –> (2) Acetate + (2) H2		Irreversible	0	10	
20	[c] : MeOH + CO –> Acetate		Irreversible	0	10	
21	[c] : (4) MeOH –> (3) CH4 + CO2 + (2) H2O		Irreversible	0	10	
22	[c] : Acetate + H –> CH4 + CO2		Irreversible	0	10	
23	[c] : CO2 + H2O <==> H2CO3	Metabolism	Reversible	–0.001	0.001	
24	[c] : H2CO3 + H2O <==> HCO3 + H	(in cytosol)	Reversible	–0.001	0.001	
25	Acetate[e] <==> Acetate[c]	Transport	Reversible	–10	10	
26	Butyrate[e] <==> Butyrate [c]		Reversible	–10	10	
27	CH4[e] <==> CH4[c]		Reversible	–10	10	
28	CO[e] <==> CO[c]		Reversible	–10	10	
29	CO2[e] <==> CO2[c]		Reversible	–10	10	
30	EtOH[e] <==> EtOH[c]		Reversible	–10	10	
31	Formate[e] <==> Formate[c]		Reversible	–10	10	
32	H[e] <==> H[c]		Reversible	–10	10	
33	H2[e] <==> H2[c]		Reversible	–10	10	
34	H2O[e] <==> H2O[c]		Reversible	–10	10	
35	HCO3[e] <==> HCO3[c]		Reversible	–10	10	
36	H2CO3[e] <==> H2CO3[c]		Reversible	–10	10	
37	MeOH[e] <==> MeOH[c]		Reversible	–10	10	
39	nBuOH[e] <==> nBuOH[c]		Reversible	–10	10	
39	Acetate[e] <==>	Exchange	Reversible	–10	10	
40	Butyrate[e] <==>		Reversible	–10	10	
41	CH4[e] <==>		Reversible	Min*	Max*	1[§]
42	CO[e] <==>		Reversible	–Max*	–Min*	
43	CO2[e] <==>		Reversible	–10	10	
44	EtOH[e] <==>		Reversible	–10	10	
45	Formate[e] <==>		Reversible	–10	10	
46	H[e] <==>		Reversible	–10	10	
47	H2[e] <==>		Reversible	-Max*	–Min*	
48	H2O[e] <==>		Reversible	–10	10	
49	HCO3[e] <==>		Reversible	–10	10	
50	H2CO3[e] <==>		Reversible	–10	10	
51	MeOH[e] <==>		Reversible	–10	10	
52	nBuOH[e] <==>		Reversible	–10	10	

Notes: [c] and [e] stands for cytosol (inside of "microbial system") and exchange, respectively; numbers in brackets represent reaction stoichiometries; LB: lower bound (reaction rate, in mmol g_{VSS}^{-1} h^{-1}); UB: upper bound (reaction rate, in mmol g_{VSS}^{-1} h^{-1}); OF: objective function; (*) variable values according to experimental data; ([§]) value set for objective function that represents maximization of CH_4 production; H: stands for Hydrogen protons (H^+).

All these 24 reactions are described as taking place in cytosol of cells. Since a mixed culture was herein used, instead of a single microorganism, the term cytosol represents the liquid medium surrounding the microbial consortium, considered as a whole in a black box approach. Besides, for each one of the 14 compounds involved in the metabolic reactions a respective transport and exchange reaction was considered in order to make the model consistent with FBA principles. These exchange reactions represent a global flux balance for each compound inside the network. Moreover, fluxes of compounds from the inside to the outside of the cytosol (herein medium with "microbial system") are represented by transport reactions, which allow the model to perform the flux balances.

According to FBA modelling, upper and lower bounds must be set. For most of the reactions these values are unknown and, thus, initial solutions for the algorithm calculation are defined, usually in the range from –10 to 10 mmol g_{VSS}^{-1} h^{-1}. Reversibility of the reactions also interferes in the lower bound of the model, which cannot be negative, and thus is set to a value not lower than zero. It is important to highlight here that, the bounds set for CO_2 equilibrium reactions are very low and close to zero. This was done in order to prevent these reactions of being dominant reactions in the network; since they are reversible, enormous amount of fluxes would be directed to these reactions.

The main constraints of the model are determined by the 3 experimental reaction rates used for CO, H_2 and CH_4, previously presented in Table 6-1. Since the experimental rates are based on the overall behaviour, the values must be reported to the respective exchange reactions. These experimental rates were set and chosen according to the conditions used, in order to understand if any change of metabolism is observed depending on the conditions defined. These limit bounds defined by the experimental rates, usually match minimum rates as lower bounds and maximum rates as upper bounds. This fact is true for product compounds in general, as it happens with CH_4 (Table 6-1). Nevertheless, in the case of substrates the logic is the opposite; maximum rates define the lower bounds, because they are more negative and thus mathematically lower than the minimum rates that define the upper bounds. Finally, to complete the model construction, the objective function is defined as the maximization of CH_4 production, set with the unit value in the respective exchange reaction, as can be observed in Table 6-2.

In order to solve the system, steady state flux distributions across the network were quantitatively predicted by using the constraint-based flux analysis. Flux variability analysis (FVA) was also performed in order to evaluate the accuracy of the predictions. GLPK (GNU linear programming kit) was the optimisation software used with the *glpkAPI* package and calculations were performed using *sybil* (Systems Biology Library) package (Gelius-Dietrich *et al.*, 2013), both in R-workspace (version 3.0.2) (CRAN.R-Project, 2013).

6.3 RESULTS AND DISCUSSION

6.3.1 Metabolic flux analysis of syngas conversion

Flux balance analysis of the metabolic network of syngas conversion (Table 6-2) constrained with the performance data of the three main setups tested (vials, in batch and MOBB, in batch and continuous mode) (Table 6-1) was performed. Similar flux distribution was observed, independently of the conditions selected for constraints of the model, varying only in the intensity of the fluxes. For that reason, the total amount of data (shown in Table 6-1) was reduced and only minimum and maximum values for each setup were selected. These selected constraints (reaction rates) are summarised in Table 6-3.

Table 6-3 Selected constraints (upper and lower bounds) used as initial solutions for performing FBA optimisation, for each of the three setups studied; (A) batch vials, and MOBB in (B) batch and (C) continuous mode

Setup	Constraints	Initial solutions: reaction rates (mmol g_{VSS}^{-1} h^{-1})		
		CH_4	CO	H_2
A	LB	0.006	–0.080	–0.171
	UB	0.040	–0.021	–0.015
B	LB	0.026	–0.423	–0.200
	UB	0.040	–0.080	–0.070
C	LB	0.037	–1.765	–0.991
	UB	0.609	–0.161	–0.081

Notes: LB and UB stand for lower and upper bounds (reaction rate, in mmol g_{VSS}^{-1} h^{-1}), respectively.

Method `optimizeProb` was used to perform FBA returning flux distribution, also called the phenotype of the metabolic network (Edwards *et al.*, 2002), solving the optimisation problem,

defined as maximisation of CH_4 production. Thus, the solution of the FBA analysis is schematised in Figure 6-2, as an optimisation of the initial metabolic network (Figure 6-1).

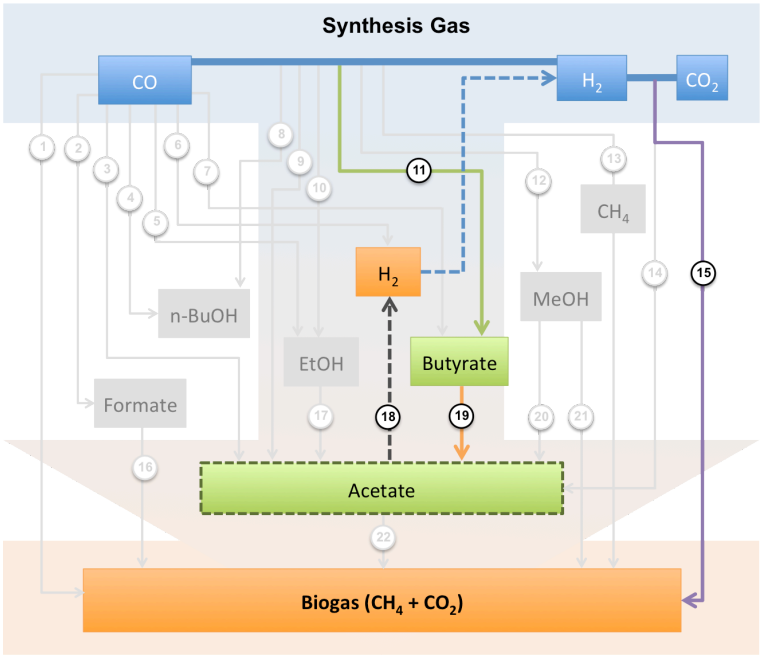

Figure 6-2 Optimised network of metabolic reactions during syngas conversion, for the three setups studied, using flux balance analysis. Reactions with resultant flux distribution are shown in coloured while remaining reactions from initial network (shown in Figure 6-1) are shown in background.

The numerical solution phenotype of the maximisation of CH_4 production, according to FBA, is shown in Table 6-4. Thus, CH_4 production is solved as the result of 4 main reactions, plus a set of other reactions corresponding to the CO_2 equilibrium in water and the respective transport and exchange reactions of the metabolites involved in the main metabolism. According to FBA solution, CH_4 is totally produced via H_2 reaction with CO_2 (reaction #15). Hydrogen molecules also react with CO producing butyrate (reaction #11). This butyrate is then oxidised to acetate (reaction #19), and acetate to CO_2 (reaction #18), both reactions generating H_2 molecules that end up being used in the production of more CH_4.

Table 6-4 Results of flux distribution (expressed in mmol g_{VSS}^{-1} h^{-1}), or phenotype, in the network after optimisation with FBA, for the three setups studied: (A) batch vials, and MOBB in (B) batch and (C) continuous mode

#	Equation	Reaction type	Flux distribution (mmol g_{VSS}^{-1} h^{-1})		
			Setup A	Setup B	Setup C
11	[c] : (4) CO + (6) H2 –> Butyrate + (2) H2O + H	Metabolism (in cytosol)	0.02	0.106	0.441
15	[c] : HCO3 + (4) H2 + H –> CH4 + (3) H2O		0.04	0.04	0.609
18	[c] : Acetate + (4) H2O + H –> (4) H2 + (2) HCO3 + (2) H		0.056	0.128	1.03
19	[c] : Butyrate + (2) H2O –> (2) Acetate + (2) H2		0.02	0.106	0.441
23	[c] : CO2 + H2O <==> H2CO3	Metabolism (in cytosol)	–0.001	–0.001	–0.001
24	[c] : H2CO3 + H2O <==> HCO3 + H		–0.001	–0.001	–0.001
25	Acetate[e] <==> Acetate[c]	Transport	0.016	–0.083	0.148
27	CH4[e] <==> CH4[c]		–0.04	–0.04	–0.609
28	CO[e] <==> CO[c]		0.08	0.423	1.765
29	CO2[e] <==> CO2[c]		–0.001	–0.001	–0.001
32	H[e] <==> H[c]		–0.035	–0.193	–0.861
33	H2[e] <==> H2[c]		0.015	0.07	0.081
34	H2O[e] <==> H2O[c]		0.103	0.391	2.291
35	HCO3[e] <==> HCO3[c]		–0.072	–0.216	–1.45
39	Acetate[e] <==>	Exchange	–0.016	0.083	–0.148
41	CH4[e] <==>		0.04	0.04	0.609
42	CO[e] <==>		–0.08	–0.423	–1.765
43	CO2[e] <==>		0.001	0.001	0.001
46	H[e] <==>		0.035	0.193	0.861
47	H2[e] <==>		–0.015	–0.07	–0.081
48	H2O[e] <==>		–0.103	–0.391	–2.291
49	HCO3[e] <==>		0.072	0.216	1.45

Notes: [c] and [e] stands for cytosol (inside of "microbial system") and exchange, respectively; numbers in brackets represent reaction stoichiometries; H: stands for Hydrogen protons (H^+).

Despite all the limitations that FBA may present on being used in a non-genome scale metabolic reconstruction problem, the metabolic pathway identified as the optimal solution of FBA might be physiologically possible in the syngas conversion process. In fact, there are microorganisms reported in literature and known as able to perform some of those reactions (Henstra *et al.*, 2007; Sipma *et al.*, 2006b). Although production of butyrate directly from CO and H_2 has not yet been reported for any microorganism, *Butyribacterium methylotrophicum* is described as able to produce butyrate from CO (Heiskanen *et al.*, 2007; Worden *et al.*, 1989). Moreover, it is known that many microorganisms are able to perform the reductive acetyl-CoA pathway, in which butyrate can be formed and both H_2 and CO are used and oxidised in the pathway for the production of reducing equivalents (Henstra *et al.*, 2007). Regarding CH_4 production from H_2 and CO_2, many hydrogenotrophic methanogenic microorganisms are known by performing this reaction, such as, *Methanosarcina barkeri* or *Methanobacterium thermoautotrophicum* (Daniels *et al.*, 1977; Henstra *et al.*, 2007; O'Brien *et al.*, 1984). This group of microorganisms has also

been reported as dominant in biogas reactors fed with defined organic substrates (Kampmann *et al.*, 2012). Nevertheless, it is very important to highlight the impact that limitations on the current experimental setup may have on the optimisation process. In fact, many components of the network (particularly those on the liquid medium) were not monitored along time, and thus many exchange reactions could not be constrained. This appeared to be the main limitation on using FBA approach, since a better-constrained network would generate a more accurate solution.

The intensity of the flux distribution is different depending on the setup studied (batch vials and MOBB, in batch and continuous mode), as can be observed in Table 6-4. This difference is related with and proportional to the range of the constraints, which are subsequently higher from setup A to C (as shown in Table 6-3). Nevertheless, all optimisation runs gave the same reaction pathway as the optimal solution. Since FBA optimisation was only based on kinetics, the optimal solution achieved does not guarantee that the preferable reactions are effectively the most favourable from a thermodynamics perspective.

6.3.2 Flux variability analysis

In linear programming problems multiple solutions can be obtained, satisfying all the constraints and giving the same optimal value. In order to evaluate the effect of the alternative optimal solutions, flux variability analysis (FVA) can be used (Mahadevan & Schilling, 2003). According to Mahadevan and Schilling (2003), although the identification of all the optimal solutions may not be possible, the maximum and minimum values of the flux, leading to the optimal objective function value can be determined. Thus, FVA was performed to the metabolic network solutions using the function `fluxVar`. This function allowed calculating minimum and maximum flux values for each reaction in the model.

The FVA returned 104 optimisation alternative solutions for the same optimal objective function, resulting in a total of 5408 fluxes analysed. Table 6-5 summarises the FVA results, showing the range of flux variation for reactions where significant variation was obtained, for the three setups studied. This range of variation is expressed as the difference between maximum and minimum fluxes that resulted from all the 104 solutions. Transport and exchange reactions of each

metabolite returned the same range of flux variation. For that reason, only exchange reactions are referred on Table 6-5. According to results of FVA, a set of metabolic reactions including production of H_2 and formate from CO (reaction #6 and #2, respectively), as well as production of methanol from CO and H_2 (reaction #12), and consequent oxidation to acetate by reaction with CO (reaction #20), have shown low significance as alternative optimal solutions for the optimisation problem, as shown by the high range variation. Moreover, even lesser significance was observed for the metabolic reactions describing production of acetate via ethanol reduction (reaction #17) and from H_2 and CO_2 reaction (reaction #14), as well as the reverse acetoclastic reaction producing H_2 from acetate (reaction #18), with very high flux variation. As a consequence, flux variation on the exchange reactions of acetate, ethanol and water are significantly high.

Table 6-5 Flux variability analysis (FVA) showing the range of variation, as the difference between maximum and minimum fluxes, obtained for each reaction within the 104 solutions generated, for the three setups studied: (A) batch vials, and MOBB in (B) batch and (C) continuous mode

#	Reaction	Range of flux variation (max – min)[§]		
		Setup A	Setup B	Setup C
2	[c] : CO + H2O –> Formate + H	0.08	0.4	1.8
6	[c] : CO + H2O –> CO2 + H2	0.08	0.4	1.8
12	[c] : CO + (2) H2 –> MeOH	0.08	0.4	1.8
14	[c] : (2) HCO3 + (4) H2 + H –> Acetate + (4) H2O	10	10	10
17	[c] : EtOH –> Acetate + H2O	10	10	10
18	[c] : Acetate + (4) H2O –> (4) H2 + (2) HCO3 + H	10	10	10
20	[c] : MeOH + CO –> Acetate	0.08	0.4	1.8
39	Acetate[e] <==>	10.1	10.2	11.5
42	CO[e] <==>	0.06	0.3	1.6
43	CO2[e] <==>	0.2	0.5	3.6
44	EtOH[e] <==>	10.0	10.2	10.9
45	Formate[e] <==>	0.3	0.6	4.2
46	H[e] <==>	0.3	0.7	4.9
48	H2O[e] <==>	10.2	10.8	14.1
49	HCO3[e] <==>	0.2	0.7	3.7
51	MeOH[e] <==>	0.2	0.9	4.4

Notes: [c] and [e] stands for cytosol (inside of "microbial system") and exchange, respectively; numbers in brackets represent reaction stoichiometries; H: stands for Hydrogen protons (H^+); [§] all values were rounded to the first significant figure or to the decimal, in case value is greater than unit.

Flux balance analysis was successfully applied on modelling main metabolic pathways involved in syngas conversion. Moreover, although an optimal solution was obtained, further experimental

studies and data from the physiology of the process are required to validate the metabolic model herein proposed. Additionally, it is important to highlight the fact, that FBA optimisation has been demonstrated as accurate for processes characterised in steady state conditions. In this study, the data used to characterise the constraints of the metabolic model and optimisation process were experimentally obtained in unsteady-state conditions, as the maximum initial reaction rates in the conversion process. Furthermore, the low number of determined rates, compared to the number of reactions and metabolites, is a disadvantage in achieving accuracy.

Ultimately, the study herein described has shown the potential of using FBA approach for modelling metabolic systems, characterised by using a mixed culture as "microbial system", with poorly defined metabolic models, in contrast with its wide application in other research fields, as genome-scale metabolic reconstruction systems. The application of other alternative metabolic approaches, such as the energy-based approach proposed by Rodríguez *et al.* (2008), may also open good perspectives on the attempt to bring novel insights in the characterisation of syngas conversion process.

6.4 ACKNOWLEDGMENTS

The insightful help and scientific support given by Dr Cleo Kontoravdi and Sarantos Kyriakopoulos, from the Department of Chemical Engineering, Faculty of Engineering, Imperial College London (UK), for performing FBA described in this chapter is gratefully acknowledged.

CHAPTER 7

Conclusions and future perspectives

7.1 MAIN CONCLUSIONS FROM PRESENTED WORK

Biological anaerobic syngas conversion for the production of biofuels or chemicals is regarded as a promising area in industrial biotechnology. Ethanol production from syngas is already developed and close to commercialisation; INEOS Bio, Lanzatech, and Coskata are companies that offer technology for hybrid (gasification and fermentation) cellulosic biomass conversion to ethanol. However, biological production of alternative biofuels and valuable chemicals from syngas still needs to be further researched and explored. The research presented in this thesis is centred in the utilisation of anaerobic mixed cultures for the conversion of syngas to biofuels and/or chemicals. In a first study, metabolic and kinetic aspects of syngas bioconversion by anaerobic sludge were studied in batch assays. Then, technological alternative for intensified syngas bioconversion were explored by the utilisation of gas-liquid mixing enhancement system. A preliminary approach to metabolic modelling was also performed in the thesis.

Methane was the main product resulting from syngas conversion by the methanogenic mixed cultures. Conversion was mainly affected by syngas pressure, being more efficient at low pressure. This is likely due to CO concentration, as this compound is known to inhibit methanogens. The relation P_{total}/p_{CO} and its influence on methane production were found relevant, since methane production rates along time exhibited a similar behaviour to the Monod fermentation models. Inhibition was obtained, showing that there is a critical value of p_{CO} for each P_T, in which methane production rate has its maximum. Lower pH was found to be optimal to obtain better methane productivity, during biological syngas conversion. When methanogenesis was inhibited, acetate, propionate and butyrate were the main products resulting from syngas conversion and only residual concentration of alcohols were detected.

Major improvements in K_La and efficiency for CO_2 dissolution in water were reported for a multi-orifice oscillatory baffled column (MOBC) working under oscillatory flow mixing and stagnant conditions. The main achievements were:

- Low gas flow rate was enough to achieve K_La values, in the range of the ones reported for other gas-liquid contacting systems operating at gas flow rates 10 to 40-fold higher;
- Baffle design showed a major impact in the performance of the gas-liquid contacting system in respect to $D_{3,2}$, BSD and K_La control;

- The scale-up of baffle configurations from single-orifice OBCs requires an even distribution of small diameter orifices and small aperture areas in order to generate a high degree of secondary mixing in the column, therefore the main dimensionless numbers that govern oscillatory flow mixing have been redefined;
- The shear caused by the oscillatory flow in the highly constricted baffles resulted in the formation of monodispersed microbubbles, and for the first time, it was visually shown microbubble trapping by the strong toroidal vortices;
- The increased residence times and gas hold-ups caused by the retention of fine bubbles in the column combined with intensive oscillatory gas-liquid contacting were the main parameters responsible for major increase obtained in K_La for CO_2;
- Up to 100 % efficiency in CO_2 transport from the gas to the liquid phase was obtained with a single gas passage, which suggested the MOBC is an advantageous system for large-scale use in gas-liquid reactions and multiphase biotransformations.

The results presented in this work are of general relevance to gas-liquid mass transfer in sparged systems and of particular relevance to bioreactor design.

Methane production from syngas conversion, using anaerobic mixed cultures, was enhanced in a novel multi-orifice oscillatory baffled bioreactor (MOBB). Mixing intensity, CO loading rate and reactor operating mode, have shown greater influence in the efficiency of the process. The main conclusions are:

- The MOBB has proven to be very efficient in promoting gas-liquid contacting, using gas flow rates 340 times lower than the common used in literature, showing that MOBB is an appropriate platform for performing anaerobic syngas conversion, capable of overcoming typical gas-liquid mass transfer limitations of other gas-liquid contacting systems;
- The discontinuous operation in the MOBB evidenced the positive effect of oscillatory flow mixing on the uptake rates of CO and H_2, but no effect on CH_4 production (compared to studies in serum bottles), and the process has shown to be controlled by metabolism (methanogenesis) rather than mass transfer limitations;

- Continuous operation of the MOBB enhanced CH_4 production rates (up to 27-fold) and CO and H_2 uptake rates (up to 8-fold), compared to the discontinuous operation, leading to increased reaction rates, which played as driving force in the kinetics of the process;
- Robust continuous syngas bioconversion was achieved with high yields of CH_4 production and short contact times, whose reaction rates changed from first order to order zero with increasing in CO loading rates, similar to Monod type kinetics.

Syngas bioconversion to methane, using mixed cultures, has been enhanced in the novel MOBB, opening perspectives for future technological development and industrial applications.

A metabolic network of the biological syngas conversion was defined and flux balance analysis (FBA) used for metabolic modelling as a preliminary approach. A reduced network was achieved from the optimisation process, despite the significant low amount of experimental data that limited the application on achieving accuracy. This preliminary approach applied to biological syngas conversion by mixed cultures opens good perspectives for future developments in enhancing process efficiency.

7.2 PERSPECTIVES FOR FUTURE WORK

The work described in this thesis evidences the potential of enhancing biological syngas conversion to biogas, using anaerobic mixed cultures. Nevertheless, further research is required for making the process more robust for technological application. With respect to this, some guidelines for future research on this topic are presented.

Anaerobic syngas conversion could be further investigated in terms of kinetics and metabolic networks. Although, FBA approach applied in this work has shown potential benefits for better understanding the metabolic behaviour of the process, an alternative energy-based metabolic modelling (Rodríguez *et al.*, 2008) could also be used and explored. This alternative modelling approach would integrate both kinetics and energetics of the process, with potential for bringing new insights about the existing model and/or on developing new metabolic models.

Mixed cultures, as a low cost biocatalyst, allow keeping the production and maintenance costs of the whole process in a low level. In the present work methane was the main product from the process at mesophilic conditions. Nevertheless, the potential for producing a wider range of valuable products could be further evaluated. A thermophilic process approach could be studied, since syngas stream generated during gasification leaves the process at high temperatures. Although syngas stream always needs to be cooled before the biological process, the utilisation of thermophilic mixed cultures as inoculum for the process could be exploited with no extra energy input costs. Some microorganisms, such as *Carboxydothermus hydrogenoformans* (Svetlitchnyi *et al.*, 2001) and *Moorella stamsii* sp. nov. (Alves, 2013), could be explored to produce H_2 and acetate from carbon monoxide present in syngas. Batch incubations and bioreactor applications could be also applied. Although higher temperatures reduce the solubility of the gases, the utilisation of the MOBC studied in this work, could be advantageous to overcome that limitation.

Regarding gas-liquid mass transfer in the interface of the bubbles, and its effect on the surface of the microbial cells or agglomerates, further fundamental studies could be developed using computational fluid dynamics. Numerical simulations could be applied to study the interaction of micro-bubbles generated in the MOBB over the flow patterns of the solid-liquid mixture phase (liquid medium with the anaerobic mixed culture agglomerates). The integrity and susceptibility of the microbial agglomerates to intense oscillatory mixing could also be studied.

7.3 SCIENTIFIC OUTPUTS OF THIS THESIS

The work presented in this thesis has been object of some publications in proceedings of scientific conferences and some manuscripts for submission to scientific international journals, either already submitted or in preparation. The list of the outputs is following presented.

Papers in scientific international peer-reviewed journals:

Pereira F M, Sousa D Z, Alves M M, Mackley M R, Reis N M (2014). CO_2 dissolution and design aspects of a multi-orifice oscillatory baffled column. Industrial & Engineering Chemistry Research. *(Manuscript submitted)*

Pereira F M, Sousa D Z, Alves M M, Reis N M (2014). Efficient-continuous syngas conversion in a multi-orifice oscillatory baffled bioreactor. *(Manuscript in preparation)*

Pereira F M, Reis N M, Alves M M, Sousa D Z (2014). Head pressure directs syngas conversion by anaerobic microbial communities towards methane or fatty acids production. *(Manuscript in preparation)*

Publication in proceedings of scientific conferences:

Pereira F M, Alves M M, Sousa D Z. Effect of pH and pressure on syngas fermentation by anaerobic mixed cultures. 13th World Congress on Anaerobic Digestion, Santiago de Compostela, Spain, June 25–28, 2013. **(Oral communication)**

Alves J I, **Pereira F M**, Sousa D Z, Alves M M. Mixed culture biotechnology for syngas conversion. 34th Symposium on Biotechnology for Fuels and Chemicals, New Orleans, USA, April 30–May 3, 2012. (Poster communication)

Pereira F M, Mackley M R, Sousa D Z, Alves M M, Reis N M. Effect of orifice diameter in CO_2-water mass transfer in an oscillatory baffled column. GLS10 – 10th International Conference on Gas-Liquid and Gas-Liquid-Solid Reactor Engineering, Braga, Portugal, 26–29 June, 2011. **(Poster communication)**

REFERENCES

Abubackar, H. N., Veiga, M. C., & Kennes, C. (2011). Biological conversion of carbon monoxide: rich syngas or waste gases to bioethanol. *Biofuels, Bioproducts & Biorefining*, *5*(1), 93–114.

Abubackar, H. N., Veiga, M. C., & Kennes, C. (2012). Biological conversion of carbon monoxide to ethanol: Effect of pH, gas pressure, reducing agent and yeast extract. *Bioresource Technology*, *114*(6), 518–522.

Ahmed, A., & Lewis, R. S. (2007). Fermentation of biomass-generated synthesis gas: effects of nitric oxide. *Biotechnology and Bioengineering*, *97*(5), 1080–1086.

Al-Abduly, A., Christensen, P., Harvey, A., & Zahng, K. (2014). Characterization and optimization of an oscillatory baffled reactor (OBR) for ozone-water mass transfer. *Chemical Engineering and Processing: Process Intensification*, in press.

Almaas, E., Kovács, B., Vicsek, T., Oltvai, Z. N., & Barabási, A.-L. (2004). Global organization of metabolic fluxes in the bacterium Escherichia coli. *Nature*, *427*(6977), 839–843.

Alves, J. I. (2013). *Microbiology of thermophilic anaerobic syngas conversion*. University of Minho, Portugal.

Alves, J. I., van Gelder, A. H., Alves, M. M., Sousa, D. Z., & Plugge, C. M. (2013). Moorella stamsii sp. nov., a new anaerobic thermophilic hydrogenogenic carboxydotroph isolated from digester sludge. *International Journal of Systematic and Evolutionary Microbiology*, *63*(11), 4072–4076.

Baird, M. H. I., & Stonestreet, P. (1995). Energy dissipation in oscillatory flow within a baffled tube. *Chemical Engineering Research & Design*, *73*(5), 503–511.

Baird, M. H. I., Rama Rao, N. V, & Stonestreet, P. (1996). Power dissipation and holdup in a gassed reciprocating baffle-plate column. *Chemical Engineering Research & Design*, *74*(4), 463–470.

Boogerd, F. C., Bos, P., Kuenen, J. G., Heijnen, J. J., & van Der Lans, R. G. J. M. (1990). Oxygen and carbon dioxide mass transfer and the aerobic, autotrophic cultivation of moderate and extreme thermophiles: a case study related to the microbial desulfurization of coal. *Biotechnology and Bioengineering*, *35*(11), 1111–1119.

Bredwell, M. D., & Worden, R. M. (1998). Mass-transfer properties of microbubbles. 1. Experimental studies. *Biotechnology Progress*, *14*(1), 31–8.

Bredwell, M. D., Srivastava, P., & Worden, R. M. (1999). Reactor design issues for synthesis-gas fermentations. *Biotechnology Progress*, *15*(5), 834–844.

Bridgwater, A. V. (1995). The technical and economic feasibility of biomass gasification for power generation. *Fuel*, *74*(5), 631–653.

Brito, A. G., Peixoto, J., & Oliveira, J. M. (2007). Brewery and winery wastewater treatment: some focal points of design and operation. In V. Oreopoulou & W. Russ (Eds.), *Utilization of By-Products and Treatment of Waste in the Food Industry* (pp. 109–131). Springer US.

Brunold, C. R., Hunns, J. C. B., Mackley, M. R., & Thompson, J. W. (1989). Experimental observations on flow patterns and energy losses for oscillatory flow in ducts containing sharp edges. *Chemical Engineering Science*, *44*(5), 1227–1244.

Calderbank, P. H., & Lochiel, A. C. (1964). Mass transfer coefficients, velocities and shapes of carbon dioxide bubbles in free rise through distilled water. *Chemical Engineering Science*, *19*(7), 485–503.

Carinhas, N., Duarte, T. M., Barreiro, L. C., Carrondo, M. J. T., Alves, P. M., & Teixeira, A. P. (2013). Metabolic signatures of GS-CHO cell clones associated with butyrate treatment and culture phase transition. *Biotechnology and Bioengineering*, *110*(12), 3244–3257.

Chaganti, S. R., Kim, D.-H., & Lalman, J. A. (2011). Flux balance analysis of mixed anaerobic microbial communities: effects of linoleic acid (LA) and pH on biohydrogen production. *International Journal of Hydrogen Energy*, *36*(21), 14141–14152.

Chatterjee, S., Grethlein, A. J., Worden, R. M., & Jain, M. K. (1996). Evaluation of support matrices for an immobilized cell gas lift reactor for fermentation of coal derived synthesis gas. *Journal of Fermentation and Bioengineering*, *81*(2), 158–162.

Cherubini, F. (2010). The biorefinery concept: using biomass instead of oil for producing energy and chemicals. *Energy Conversion and Management*, *51*(7), 1412–1421.

Chew, C. M., Ristic, R. I., Reynolds, G. K., & Ooi, R. C. (2004). Characterisation of impeller driven and oscillatory mixing by spatial and temporal shear rate distributions. *Chemical Engineering Science*, *59*(7), 1557–1568.

Claassen, P. A. M., van Lier, J. B., Lopez Contreras, A. M., van Niel, E. W. J., Sijtsma, L., Stams, A. J. M., de Vries, S. S., & Weusthuis, R. A. (1999). Utilisation of biomass for the supply of energy carriers. *Applied Microbiology and Biotechnology*, *52*(6), 741–755.

Costa, J. C., Gonçalves, P. R., Nobre, A., & Alves, M. M. (2012). Biomethanation potential of macroalgae Ulva spp. and Gracilaria spp. and in co-digestion with waste activated sludge. *Bioresource Technology*, *114*(6), 320–326.

Covert, M. W., Schilling, C. H., Famili, I., Edwards, J. S., Goryanin, I. I., Selkov, E., & Palsson, B. O. (2001). Metabolic modeling of microbial strains in silico. *Trends in Biochemical Sciences*, *26*(3), 179–186.

Cowger, J. P., Klasson, K. T., Ackerson, M. D., Clausen, E. C., & Gaddy, J. L. (1992). Mass-transfer and kinetic aspects in continuous bioreactors using Rhodospirillum rubrum. *Applied Biochemistry and Biotechnology*, *34/35*(1), 613–624.

CRAN.R-Project. (2013). The comprehensive R archive network. *http://cran.r-project.org/*.

Dalai, A. K., & Davis, B. H. (2008). Fischer–Tropsch synthesis: a review of water effects on the performances of unsupported and supported Co catalysts. *Applied Catalysis A: General*, *348*(1), 1–15.

Daniel, S. L., Hsu, T., Dean, S. I., & Drake, H. L. (1990). Characterization of the H2- and CO-dependent chemolithotrophic potentials of the acetogens Clostridium thermoaceticum and Acetogenium kivui. *Journal of Bacteriology*, *172*(8), 4464–4471.

Daniels, L., Fuchs, G., Thauer, R. K., & Zeikus, J. G. (1977). Carbon monoxide oxidation by methanogenic bacteria. *Journal of Bacteriology*, *132*(1), 118–126.

Dashekvicz, M. P., & Uffen, R. L. (1979). Identification of a carbon monoxide-metabolizing bacterium as a strain of Rhodopseudomonas gelatinosa (Molisch) van Niel. *International Journal of Systematic Bacteriology*, *29*(2), 145–148.

Datar, R. P., Shenkman, R. M., Cateni, B. G., Huhnke, R. L., & Lewis, R. S. (2004). Fermentation of biomass-generated producer gas to ethanol. *Biotechnology and Bioengineering*, *86*(5), 587–594.

Demirbas, A. (2007). Progress and recent trends in biofuels. *Progress in Energy and Combustion Science*, *33*(1), 1–18.

Demirbas, M. F. (2009). Biorefineries for biofuel upgrading: a critical review. *Applied Energy*, *86*(1), S151–S161.

Demirel, B., & Scherer, P. (2008). The roles of acetotrophic and hydrogenotrophic methanogens during anaerobic conversion of biomass to methane: a review. *Reviews in Environmental Science and Bio/Technology*, *7*(2), 173–190.

Drake, H. L. (1994). Acetogenesis, acetogenic bacteria, and the acetyl-CoA "Wood/Ljungdahl" pathway: past and current perspectives. In *Acetogenesis* (pp. 3–60). New York: Chapman & Hall.

Duarte, N. C., Becker, S. A., Jamshidi, N., Thiele, I., Mo, M. L., Vo, T. D., Srivas, R., & Palsson, B. Ø. (2007). Global reconstruction of the human metabolic network based on genomic and bibliomic data. *Proceedings of the National Academy of Sciences of the United States of America*, *104*(6), 1777–1782.

Ebrahimi, S., Picioreanu, C., Xavier, J. B., Kleerebezem, R., Kreutzer, M. T., Kapteijn, F., & Moulijn, J. A. (2005). Biofilm growth pattern in honeycomb monolith packings: effect of shear rate and substrate transport limitations. *Catalysis Today*, *105*(3/4), 448–454.

Edwards, J. S., Covert, M., & Palsson, B. (2002). Metabolic modelling of microbes: the flux-balance approach. *Environmental Microbiology*, *4*(3), 133–140.

Edwards, J. S., Ibarra, R. U., & Palsson, B. Ø. (2001). In silico predictions of Escherichia coli metabolic capabilities are consistent with experimental data. *Nature Biotechnology*, *19*(2), 125–130.

Feist, A. M., & Palsson, B. Ø. (2008). The growing scope of applications of genome-scale metabolic reconstructions: the case of E. coli. *Nature Biotechnology*, *26*(6), 659–667.

Feist, A. M., Henry, C. S., Reed, J. L., Krummenacker, M., Joyce, A. R., Karp, P. D., Broadbelt, L. J., Hatzimanikatis, V., & Palsson, B. Ø. (2007). A genome-scale metabolic reconstruction for Escherichia coli K-12 MG1655 that accounts for 1260 ORFs and thermodynamic information. *Molecular Systems Biology*, *3*(121), 1–18.

Fischer, C. R., Klein-Marcuschamer, D., & Stephanopoulos, G. (2008). Selection and optimization of microbial hosts for biofuels production. *Metabolic Engineering*, *10*(6), 295–304.

Fischer, E., & Donath, B. (1938). Improvements in or relating to the synthesis of hydrocarbons under ultra-pressure. United Kingdom.

Fitch, A. W., Jian, H., & Ni, X. (2005). An investigation of the effect of viscosity on mixing in an oscillatory baffled column using digital particle image velocimetry and computational fluid dynamics simulation. *Chemical Engineering Journal*, *112*(1-3), 197–210.

Fuchs, R., Ryu, D. D. Y., & Humphrey, A. E. (1971). Effect of surface aeration on scale-up procedures for fermentation processes. *Industrial & Engineering Chemistry Process Design and Development*, *10*(2), 190–196.

Gaddy, J. L. (2000). Biological production of ethanol from waste gases with Clostridium ljungdahlii. United States of America: US Patent No. 6,136,577.

Gaddy, J. L., & Clausen, E. C. (1992). Clostridium ljungdahlii, an anaerobic ethanol and acetate producing microorganism. United States of America: US Patent No. 5,173,429.

Gagnon, H., Lounès, M., & Thibault, J. (1998). Power consumption and mass transfer in agitated gas-liquid columns: a comparative study. *The Canadian Journal of Chemical Engineering*, 76(3), 379–389.

Gaidhani, H. K., Mcneil, B., & Ni, X.-W. (2003). Production of pullulan using an oscillatory baffled bioreactor. *Journal of Chemical Technology and Biotechnology*, *78*(2-3), 260–264.

Gelius-Dietrich, G., Desouki, A. A., Fritzemeier, C. J., & Lercher, M. J. (2013). sybil – Efficient constraint-based modelling in R. *BMC Systems Biology*, *7*(125), 1–8.

Genthner, B. R. S., & Bryant, M. P. (1982). Growth of Eubacterium limosum with carbon monoxide as the energy source. *Applied and Environmental Microbiology*, *43*(1), 70–74.

Genthner, B. R. S., & Bryant, M. P. (1987). Additional characteristics of one-carbon-compound utilization by Eubacterium limosum and Acetobacterium woodii. *Applied and Environmental Microbiology*, *53*(3), 471–476.

Gomaa, H. G., Hashem, N., & Al-Taweel, A. M. (2012). Dispersion characteristics and mass transfer in a pilot-scale gas-liquid oscillatory-plate column. *Chemical Engineering & Technology*, *35*(7), 1300–1311.

Gough, P., Ni, X., & Symes, K. C. (1997). Experimental flow visualisation in a modified pulsed baffled reactor. *Journal of Chemical Technology and Biotechnology*, *69*(3), 321–328.

Grassi, G., & Bridgwater, A. V. (1991). The European Community Energy from Biomass Research and Development Programme. *International Journal of Solar Energy*, *10*(3-4), 127–136.

Grethlein, A. J., Worden, R. M., Jain, M. K., & Datta, R. (1991). Evidence for production of n-butanol from carbon monoxide by Butyribacterium methylotrophicum. *Journal of Fermentation and Bioengineering*, *72*(1), 58–60.

Guiot, S. R., Cimpoia, R., & Carayon, G. (2011). Potential of wastewater-treating anaerobic granules for biomethanation of synthesis gas. *Environmental Science and Technology*, *45*(5), 2006–2012.

Harvey, A. P., Mackley, M. R., & Stonestreet, P. (2001). Operation and optimization of an oscillatory flow continuous reactor. *Industrial & Engineering Chemistry Research*, *40*(23), 5371–5377.

Haryanto, A., Fernando, S. D., Pordesimo, L. O., & Adhikari, S. (2009). Upgrading of syngas derived from biomass gasification: a thermodynamic analysis. *Biomass and Bioenergy*, *33*(5), 882–889.

Heiskanen, H., Virkajärvi, I., & Viikari, L. (2007). The effect of syngas composition on the growth and product formation of Butyribacterium methylotrophicum. *Enzyme and Microbial Technology*, *41*(3), 362–367.

Henstra, A. M., Sipma, J., Rinzema, A., & Stams, A. J. M. (2007). Microbiology of synthesis gas fermentation for biofuel production. *Current Opinion in Biotechnology*, *18*(3), 200–206.

Hewgill, M. R., Mackley, M. R., Pandit, A. B., & Pannu, S. S. (1993). Enhancement of gas-liquid mass transfer using oscillatory flow in a baffled tube. *Chemical Engineering Science*, *48*(4), 799–809.

Hill, G. A. (2006). Measurement of overall volumetric mass transfer coefficients for carbon dioxide in a well-mixed reactor using a pH probe. *Industrial & Engineering Chemistry Research*, *45*(16), 5796–5800.

Howes, T., Mackley, M. R., & Roberts, E. P. L. (1991). The simulation of chaotic mixing and dispersion for periodic flows in baffled channels. *Chemical Engineering Science*, *46*(7), 1669–1677.

Hu, P., Bowen, S. H., & Lewis, R. S. (2011). A thermodynamic analysis of electron production during syngas fermentation. *Bioresource Technology*, *102*(17), 8071–8076.

Hurst, K. M., & Lewis, R. S. (2010). Carbon monoxide partial pressure effects on the metabolic process of syngas fermentation. *Biochemical Engineering Journal*, *48*(2), 159–165.

Jackson, B. E., & McInerney, M. J. (2002). Anaerobic microbial metabolism can proceed close to thermodynamic limits. *Nature*, *415*(6870), 454–456.

Jansson, C., & Northen, T. (2010). Calcifying cyanobacteria – the potential of biomineralization for carbon capture and storage. *Current Opinion in Biotechnology*, *21*(3), 365–371.

Jian, H., & Ni, X.-W. (2003). On modelling turbulent flow in an oscillatory baffled column – RANS model or large-eddy simulation? *Journal of Chemical Technology and Biotechnology*, *78*(2-3), 321–325.

Jones, D. (2005). Evolutionary theory: personal effects. *Nature*, *438*(7064), 14–16.

Jung, G. Y., Jung, H. O., Kim, J. R., Ahn, Y., & Park, S. (1999). Isolation and characterization of Rhodopseudomonas palustris P4 which utilizes CO with the production of H2. *Biotechnology Letters*, *21*(6), 525–529.

Kampmann, K., Ratering, S., Baumann, R., Schmidt, M., Zerr, W., & Schnell, S. (2012). Hydrogenotrophic methanogens dominate in biogas reactors fed with defined substrates. *Systematic and Applied Microbiology*, *35*(6), 404–413.

Kapic, A., Jones, S. T., & Heindel, T. J. (2006). Carbon monoxide mass transfer in a syngas mixture. *Industrial & Engineering Chemistry Research*, *45*(26), 9150–9155.

Kaster, J. A., Michelsen, D. L., & Velander, W. H. (1990). Increased oxygen transfer in a yeast fermentation using a microbubble dispersion. *Applied Biochemistry and Biotechnology*, *24/25*(1), 469–484.

Kerby, R. L., Ludden, P. W., & Roberts, G. P. (1995). Carbon monoxide-dependent growth of Rhodospirillum rubrum. *Journal of Bacteriology*, *177*(8), 2241–2244.

Klasson, K. T., Ackerson, M. D., Clausen, E. C., & Gaddy, J. L. (1991). Bioreactor design for synthesis gas fermentations. *Fuel*, *70*(5), 605–614.

Klasson, K. T., Ackerson, M. D., Clausen, E. C., & Gaddy, J. L. (1993a). Biological conversion of coal and coal-derived synthesis gas. *Fuel*, *72*(12), 1673–1678.

Klasson, K. T., Cowger, J. P., Ko, C. W., Vega, J. L., Clausen, E. C., & Gaddy, J. L. (1990a). Methane production from synthesis gas using a mixed culture of R. rubrum, M. barkeri, and M. formicicum. *Applied Biochemistry and Biotechnology*, *24/25*(1), 317–328.

Klasson, K. T., Elmore, B. B., Vega, J. L., Ackerson, M. D., Clausen, E. C., & Gaddy, J. L. (1990b). Biological production of liquid and gaseous fuels from synthesis gas. *Applied Biochemistry and Biotechnology*, *24/25*(1), 857–873.

Klasson, K. T., Gupta, A. K., Clausen, E. C., & Gaddy, J. L. (1993b). Evaluation of mass-transfer and kinetic parameters for Rhodospirillum rubrum in a continuous stirred tank reactor. *Applied Biochemistry and Biotechnology*, *39/40*(1), 549–557.

Kleerebezem, R., & van Loosdrecht, M. C. M. (2007). Mixed culture biotechnology for bioenergy production. *Current Opinion in Biotechnology*, *18*(3), 207–212.

Klijnhout, A. F., & Eerde, P. V. (1986). Some characteristics of brewery effluent. *Journal of the Institute of Brewing*, *92*(5), 426–434.

Knott, G. F., & Mackley, M. R. (1980). On eddy motions near plates and ducts, induced by water waves and periodic flows. *Philosophical Transactions of the Royal Society of London. Series A, Mathematical and Physical Sciences*, *294*(1412), 599–623.

Kreutzer, M. T., Kapteijn, F., Moulijn, J. A., Ebrahimi, S., Kleerebezem, R., & van Loosdrecht, M. C. M. (2005). Monoliths as biocatalytic reactors: smart gas-liquid contacting for process intensification. *Industrial & Engineering Chemistry Research*, *44*(25), 9646–9652.

Krumholz, L. R., & Bryant, M. P. (1985). Clostridiurn pfennigii sp. nov. uses methoxyl groups of monobenzenoids and produces butyrate. *International Journal of Systematic Bacteriology*, *35*(4), 454–456.

Kumaresan, T., & Joshi, J. B. (2006). Effect of impeller design on the flow pattern and mixing in stirred tanks. *Chemical Engineering Journal*, *115*(3), 173–193.

Kundu, S., Premer, S. A., Hoy, J. A., Trent III, J. T., & Hargrove, M. S. (2003). Direct measurement of equilibrium constants for high-affinity hemoglobins. *Biophysical Journal*, *84*(6), 3931–3940.

Lee, C. T., Mackley, M. R., Stonestreet, P., & Middelberg, A. P. J. (2001). Protein refolding in an oscillatory flow reactor. *Biotechnology Letters*, *23*(22), 1899–1901.

Lee, K.-C., & Rittmann, B. E. (2002). Applying a novel autohydrogenotrophic hollow-fiber membrane biofilm reactor for denitrification of drinking water. *Water Research*, *36*(8), 2040–2052.

Lee, P.-H., Ni, S.-Q., Chang, S.-Y., Sung, S., & Kim, S.-H. (2012). Enhancement of carbon monoxide mass transfer using an innovative external hollow fiber membrane (HFM) diffuser for syngas fermentation: experimental studies and model development. *Chemical Engineering Journal*, *184*(3), 268–277.

Liou, J. S.-C., Balkwill, D. L., Drake, G. R., & Tanner, R. S. (2005). Clostridium carboxidivorans sp. nov., a solvent-producing clostridium isolated from an agricultural settling lagoon, and reclassification of the acetogen Clostridium scatologenes strain SL1 as Clostridium drakei sp. nov.. *International Journal of Systematic and Evolutionary Microbiology*, *55*(5), 2085–2091.

Liu, K., Atiyeh, H. K., Stevenson, B. S., Tanner, R. S., Wilkins, M. R., & Huhnke, R. L. (2014). Continuous syngas fermentation for the production of ethanol, n-propanol and n-butanol. *Bioresource Technology*, *151*(1), 69–77.

Ljungdahl, L. G., & Wiegel, J. (1986). Anaerobic fermentations. In A. L. Demain & N. A. Solomon (Eds.), *Manual of Industrial Microbiology and Biotechnology* (pp. 84–96). Washignton DC: ASM Press.

Lorowitz, W. H., & Bryant, M. P. (1984). Peptostreptococcus productus strain that grows rapidly with CO as the energy source. *Applied and Environmental Microbiology*, *47*(5), 961–964.

Luo, G., Wang, W., & Angelidaki, I. (2013). Anaerobic digestion for simultaneous sewage sludge treatment and CO biomethanation: process performance and microbial ecology. *Environmental Science & Technology*, *47*(18), 10685–10693.

Lynd, L. R. (1996). Overview and evaluation of fuel ethanol from cellulosic biomass: technology, economics, the environment, and policy. *Annual Review of Energy and the Environment*, *21*(1), 403–465.

Lynd, L., Kerby, R., & Zeikus, J. G. (1982). Carbon monoxide metabolism of the methylotrophic acidogen Butyribacterium methylotrophicum. *Journal of Bacteriology*, *149*(1), 255–263.

Mackley, M. R., & Ni, X. (1991). Mixing and dispersion in a baffled tube for steady laminar and pulsatile flow. *Chemical Engineering Science*, *46*(12), 3139–3151.

Mackley, M. R., & Ni, X. (1993). Experimental fluid dispersion measurements in periodic baffled tube arrays. *Chemical Engineering Science*, *48*(18), 3293–3305.

Mackley, M. R., & Stonestreet, P. (1995). Heat transfer and associated energy dissipation for oscillatory flow in baffled tubes. *Chemical Engineering Science*, *50*(14), 2211–2224.

Mackley, M. R., Dickens, A. W., & Williams, H. R. (1989). Experimental residence time distribution measurements for unsteady flow in baffled tubes. *Chemical Engineering Science*, *44*(7), 1471–1479.

Mackley, M. R., Smith, K. B., & Wise, N. P. (1993). The mixing and separation of particle suspensions using oscillatory flow in baffled tubes. *Chemical Engineering Research & Design*, *71A*(6), 649–656.

Mackley, M. R., Stonestreet, P., Thurston, N. C., & Wiseman, J. S. (1998). Evaluation of a novel self-aerating, oscillating baffle column. *The Canadian Journal of Chemical Engineering*, *76*(1), 5–10.

Mackley, M. R., Tweddle, G. M., & Wyatt, I. D. (1990). Experimental heat transfer measurements for pulsatile flow in baffled tubes. *Chemical Engineering Science*, *45*(5), 1237–1242.

Mahadevan, R., & Schilling, C. H. (2003). The effects of alternate optimal solutions in constraint-based genome-scale metabolic models. *Metabolic Engineering*, *5*(4), 264–276.

Menon, S., & Ragsdale, S. W. (1996). Unleashing hydrogenase activity in carbon monoxide dehydrogenase/acetyl-CoA synthase and pyruvate: ferredoxin oxidoreductase. *Biochemistry*, *35*(49), 15814–15821.

Mohammadi, M., Najafpour, G. D., Younesi, H., Lahijani, P., Hekarl, M., & Rahman, A. (2011). Bioconversion of synthesis gas to second generation biofuels: a review. *Renewable and Sustainable Energy Reviews*, *15*(9), 4255–4273.

Mojovic, L., Pejin, D., Grujic, O., Markov, S., Pejin, J., Rakin, M., Vukasinovic, M., Nikolic, S., & Savic, D. (2009). Progress in the production of bioethanol on starch-based feedstocks. *Chemical Industry and Chemical Engineering Quarterly*, *15*(4), 211–226.

Munasinghe, P. C., & Khanal, S. K. (2010a). Biomass-derived syngas fermentation into biofuels: opportunities and challenges. *Bioresource Technology*, *101*(13), 5013–5022.

Munasinghe, P. C., & Khanal, S. K. (2010b). Syngas fermentation to biofuel: evaluation of carbon monoxide mass transfer coefficient (kLa) in different reactor configurations. *Biotechnology Progress*, *26*(6), 1616–1621.

Munasinghe, P. C., & Khanal, S. K. (2012). Syngas fermentation to biofuel: Evaluation of carbon monoxide mass transfer and analytical modeling using a composite hollow fiber (CHF) membrane bioreactor. *Bioresource Technology*, *122*(10), 130–136.

National Energy Board of Canada. (2006). *Canada's oil sands opportunities and challenges to 2015: an update*. *Energy* (p.72). Canada.

Ni, X., & Gao, S. (1996). Scale-up correlation for mass transfer coefficients in pulsed baffled reactors. *The Chemical Engineering Journal*, *63*(3), 157–166.

Ni, X., & Gough, P. (1997). On the discussion of the dimensionless groups governing oscillatory flow in a baffled tube. *Chemical Engineering Science*, *52*(18), 3209–3212.

Ni, X., & Mackley, M. R. (1993). Chemical reaction in batch pulsatile flow and stirred tank reactors. *The Chemical Engineering Journal*, *52*(3), 107–114.

Ni, X., & Pereira, N. E. (2000). Parameters affecting fluid dispersion in a continuous oscillatory baffled tube. *AIChE Journal*, *46*(1), 37–45.

Ni, X., Cosgrove, J. A., Arnott, A. D., Greated, C. A., & Cumming, R. H. (2000a). On the measurement of strain rate in an oscillatory baffled column using particle image velocimetry. *Chemical Engineering Science*, *55*(16), 3195–3208.

Ni, X., de Gélicourt, Y. S., Neil, J., & Howes, T. (2002a). On the effect of tracer density on axial dispersion in a batch oscillatory baffled column. *Chemical Engineering Journal*, *85*(1), 17–25.

Ni, X., Gao, S., Cumming, R. H., & Pritchard, D. W. (1995a). A comparative study of mass transfer in yeast for a batch pulsed baffled bioreactor and a stirred tank fermenter. *Chemical Engineering Science*, *50*(13), 2127–2136.

Ni, X., Jian, H., & Fitch, A. W. (2002b). Computational fluid dynamic modelling of flow patterns in an oscillatory baffled column. *Chemical Engineering Science*, *57*(14), 2849–2862.

Ni, X., Liu, S., Joyce, M. J., Grewal, P. S., & Greated, C. A. (1995b). A study of velocity vector profile and strain rate distribution for laminar and oscillatory flows in a baffled tube using particle image velocimetry. *Journal of Flow Visualization and Image Processing*, *2*(2), 135–147.

Ni, X., Mackley, M. R., Harvey, A. P., Stonestreet, P., Baird, M. H. I., & Rao, N. V. R. (2003). Mixing through oscillations and pulsations – a guide to achieving process enhancements in the chemical and process industries. *Environmental Science & Technology*, *81*(3), 373–383.

Ni, X., Nelson, G., & Mustafa, I. (2000b). Flow patterns and oil-water dispersion in a 0.38 m diameter oscillatory baffled column. *The Canadian Journal of Chemlcal Engineering*, *78*(2), 211–220.

Ni, X., Zhang, Y., & Mustafa, I. (1998). An investigation of droplet size and size distribution in methylmethacrylate suspensions in a batch oscillatory-baffled reactor. *Chemical Engineering Science*, *53*(16), 2903–2919.

Ni, X., Zhang, Y., & Mustafa, I. (1999). Correlation of polymer particle size with droplet size in suspension polymerisation of methylmethacrylate in a batch oscillatory-baffled reactor. *Chemical Engineering Science*, *54*(6), 841–850.

Nicolella, C., van Loosdrecht, M. C. M., van Der Lans, R. G., & Heijnen, J. J. (1998). Hydrodynamic characteristics and gas-liquid mass transfer in a biofilm airlift suspension reactor. *Biotechnology and Bioengineering*, *60*(5), 627–35.

O'Brien, J. M., Wolkin, R. H., Moench, T. T., Morgan, J. B., & Zeikus, J. G. (1984). Association of hydrogen metabolism with unitrophic or mixotrophic growth of Methanosarcina barkeri on carbon monoxide. *Journal of Bacteriology*, *158*(1), 373–375.

Oberhardt, M. A., Palsson, B. Ø., & Papin, J. A. (2009). Applications of genome-scale metabolic reconstructions. *Molecular Systems Biology*, *5*(1), 320.

Oelgeschläger, E., & Rother, M. (2008). Carbon monoxide-dependent energy metabolism in anaerobic bacteria and archaea. *Archives of Microbiology*, *190*(3), 257–269.

Oliveira, M. S. N., & Ni, X. (2001). Gas hold-up and bubble diameters in a gassed oscillatory baffled column. *Chemical Engineering Science*, *56*(21-22), 6143–6148.

Oliveira, M. S. N., & Ni, X.-W. (2004a). Characterization of a gas-liquid OBC: bubble size and gas holdup. *AIChE Journal*, *50*(12), 3019–3033.

Oliveira, M. S. N., & Ni, X.-W. (2004b). Effect of hydrodynamics on mass transfer in a gas-liquid oscillatory baffled column. *Chemical Engineering Journal*, *99*(1), 59–68.

Oliveira, M. S. N., Fitch, A. W., & Ni, X. (2003a). A study of bubble velocity and bubble residence time in a gassed oscillatory baffled column – effect of oscillation frequency. *Chemical Engineering Research and Design*, *81*(2), 233–242.

Oliveira, M. S. N., Fitch, A. W., & Ni, X.-W. (2003b). A study of velocity and residence time of single bubbles in a gassed oscillatory baffled column: effect of oscillation amplitude. *Journal of Chemical Technology and Biotechnology*, *78*(2-3), 220–226.

Orth, J. D., Thiele, I., & Palsson, B. Ø. (2010). What is flux balance analysis? *Nature Biotechnology*, *28*(3), 245–248.

Pardelha, F., Albuquerque, M. G. E., Carvalho, G., Reis, M. A. M., Dias, J. M. L., & Oliveira, R. (2013). Segregated flux balance analysis constrained by population structure/function data: the case of PHA production by mixed microbial cultures. *Biotechnology and Bioengineering*, *110*(8), 2267–2276.

Pardelha, F., Albuquerque, M. G. E., Reis, M. A. M., Dias, J. M. L., & Oliveira, R. (2012). Flux balance analysis of mixed microbial cultures: application to the production of polyhydroxyalkanoates from complex mixtures of volatile fatty acids. *Journal of Biotechnology*, *162*(2-3), 336–345.

Parshina, S. N., Kijlstra, S., Henstra, A. M., Sipma, J., Plugge, C. M., & Stams, A. J. M. (2005). Carbon monoxide conversion by thermophilic sulfate-reducing bacteria in pure culture and in co-culture with Carboxydothermus hydrogenoformans. *Applied Microbiology and Biotechnology*, *68*(3), 390–396.

Phillips, J. R., Clausen, E. C., & Gaddy, J. L. (1994). Synthesis gas as substrate for the biological production of fuels and chemicals. *Applied Biochemistry and Biotechnology*, *45/46*(1), 145–157.

Ragauskas, A. J., Williams, C. K., Davison, B. H., Britovsek, G., Cairney, J., Eckert, C. A., Frederick Jr, W. J., Hallett, J. P., Leak, D. J., Liotta, C. L., Mielenz, J. R., Murphy, R., Templer, R., & Tschaplinski, T. (2006). The path forward for biofuels and biomaterials. *Science*, *311*(5760), 484–489.

Rama Rao, N. V., & Baird, M. H. I. (2006). Gas-liquid mass transfer in a 15 cm diameter reciprocating plate column. *Journal of Chemical Technology and Biotechnology*, *78*(2-3), 134–137.

Reis, N. M. (2006). *Novel oscillatory flow reactors for biotechnological applications*. University of Minho, Portugal.

Reis, N., Gonçalves, C. N., Vicente, A. A., & Teixeira, J. A. (2006). Proof-of-concept of a novel micro-bioreactor for fast development of industrial bioprocesses. *Biotechnology and Bioengineering*, *95*(4), 744–753.

Reis, N., Harvey, A. P., Mackley, M. R., Vicente, A. A., & Teixeira, J. A. (2005). Fluid mechanics and design aspects of a novel oscillatory flow screening mesoreactor. *Chemical Engineering Research and Design*, *83*(4), 357–371.

Reis, N., Mena, P. C., Vicente, A. A., Teixeira, J. A., & Rocha, F. (2007). The intensification of gas-liquid flows with a periodic, constricted oscillatory-meso tube. *Chemical Engineering Science*, *62*(24), 7454–7462.

Reis, N., Pereira, R. N., Vicente, A. A., & Teixeira, J. A. (2008). Enhanced gas-liquid mass transfer of an oscillatory constricted-tubular reactor. *Industrial & Engineering Chemistry Research*, *47*(19), 7190–7201.

Reis, N., Vicente, A. A., Teixeira, J. A., & Mackley, M. R. (2004). Residence times and mixing of a novel continuous oscillatory flow screening reactor. *Chemical Engineering Science*, *59*(22-23), 4967–4974.

Riggs, S. S., & Heindel, T. J. (2006). Measuring carbon monoxide gas-liquid mass transfer in a stirred tank reactor for syngas fermentation. *Biotechnology Progress*, *22*(3), 903–906.

Rodríguez, J., Kleerebezem, R., Lema, J. M., & van Loosdrecht, M. C. M. (2006). Modeling product formation in anaerobic mixed culture fermentations. *Biotechnology and Bioengineering*, *93*(3), 592–606.

Rodríguez, J., Lema, J. M., & Kleerebezem, R. (2008). Energy-based models for environmental biotechnology. *Trends in Biotechnology*, *26*(7), 366–374.

Rother, M., & Metcalf, W. W. (2004). Anaerobic growth of Methanosarcina acetivorans C2A on carbon monoxide: an unusual way of life for a methanogenic archaeon. *Proceedings of National Academy of Sciences*, *101*(48), 16929–16934.

Sander, R. (1999). Compilation of Henry 's Law constants for inorganic and organic species of potential importance in environmental chemistry (http://www.mpch-mainz.mpg.de/~sander/res/henry.html).

Savage, M. D., Wu, Z., Daniel, S. L., Lundie Jr, L. L., & Drake, H. L. (1987). Carbon monoxide-dependent chemolithotrophic growth of Clostridium thermoautotrophicum. *Applied and Environmental Microbiology*, *53*(8), 1902–1906.

Scharlin, P., Battino, R., Silla, E., Tuñón, I., & Pascual-Ahuir, J. L. (1998). Solubility of gases in water: correlation between solubility and the number of water molecules in the first solvation shell. *Pure & Applied Chemistry*, *70*(10), 1895–1904.

Schink, B., & Stams, A. J. M. (2006). The prokaryotes: an evolving electronic resource for the microbiological community. In *Syntrophism among prokaryotes* (pp. 309–335). New York: Springer-Verlag.

Selvarasu, S., Ho, Y. S., Chong, W. P. K., Wong, N. S. C., Yusufi, F. N. K., Lee, Y. Y., Yap, M. G. S., & Lee, D.-Y. (2012). Combined in silico modeling and metabolomics analysis to characterize fed-batch CHO cell culture. *Biotechnology and Bioengineering*, *109*(6), 1415–1429.

Shen, G.-J., Sheih, J.-S., Grethlein, A. J., Jain, M. K., & Zeikus, J. G. (1999). Biochemical basis for carbon monoxide tolerance and butanol production by Butyribacterium methylotrophicum. *Applied Microbiology and Biotechnology*, *51*(6), 827–832.

Shuler, M. L., & Kargi, F. (2002). *Bioprocess engineering basic principles* (2nd Ed.). Upper Saddle River, NJ: Prentice Hall PTR.

Sim, J. H. (2006). *Bioconversion of carbon monoxide gas to acetic acid using clostridium aceticum in batch and continuous fermentations*. Universiti Sains Malaysia.

Sim, J. H., Kamaruddin, A. H., Long, W. S., & Najafpour, G. (2007). Clostridium aceticum – a potential organism in catalyzing carbon monoxide to acetic acid: application of response surface methodology. *Enzyme and Microbial Technology*, *40*(5), 1234–1243.

Sinada, F., & Karim, A. G. A. (1984a). A quantitative study of the phytoplankton in the Blue and White Niles at Khartoum. *Hydrobiologia*, *110*(1), 47–55.

Sinada, F., & Karim, A. G. A. (1984b). Physical and chemical characteristics of the Blue Nile and the White Nile at Khartoum. *Hydrobiologia*, *110*(1), 21–32.

Sipma, J., Henstra, A. M., Parshina, S. N., Lens, P. N., Lettinga, G., & Stams, A. J. (2006a). Microbial CO conversions with applications in synthesis gas purification and bio-desulfurization. *Critical Reviews in Biotechnology*, *26*(1), 41–65.

Sipma, J., Lens, P. N. L., Stams, A. J. M., & Lettinga, G. (2003). Carbon monoxide conversion by anaerobic bioreactor sludges. *FEMS Microbiology Ecology*, *44*(2), 271–277.

Sipma, J., Lettinga, G., Stams, A. J. M., & Lens, P. N. L. (2006b). Hydrogenogenic CO conversion in a moderately thermophilic (55 °C) sulfate-fed gas lift reactor: competition for CO-derived H2. *Biotechnology Progress*, *22*(5), 1327–1334.

Sivakumar, A., Srinivasaraghavan, T., Swaminathan, T., & Baradarajan, A. (1994). Extended monod kinetics for substrate inhibited systems. *Bioprocess Engineering*, *11*(5), 185.

Slepova, T. V, Sokolova, T. G., Lysenko, A. M., Tourova, T. P., Kolganova, T. V, Kamzolkina, O. V, Karpov, G. A., & Bonch-osmolovskaya, E. A. (2006). Carboxydocella sporoproducens sp. nov., a novel anaerobic CO-utilizing/H2-producing thermophilic bacterium from a Kamchatka hot spring. *International Journal of Systematic and Evolutionary Microbiology*, *56*(4), 797–800.

Smith, K. B. (1999). *The scale-up of oscillatory flow mixing*. University of Cambridge, UK.

Smith, K. B., & Mackley, M. R. (2006). An experimental investigation into the scale-up of oscillatory flow mixing in baffled tubes. *Chemical Engineering Research and Design*, *84*(11), 1001–1011.

Sokolova, T. G., Henstra, A. M., Sipma, J., Parshina, S. N., Stams, A. J. M., & Lebedinsky, A. V. (2009). Diversity and ecophysiological features of thermophilic carboxydotrophic anaerobes. *FEMS Microbiology Ecology*, *68*(2), 131–141.

Sokolova, T. G., Jeanthon, C., Kostrikina, N. A., Chernyh, N. A., Lebedinsky, A. V, Stackebrandt, E., & Bonch-Osmolovskaya, E. A. (2004). The first evidence of anaerobic CO oxidation coupled with H2 production by a hyperthermophilic archaeon isolated from a deep-sea hydrothermal vent. *Extremophiles*, *8*(4), 317–23.

Sokolova, T. G., Kostrikina, N. A., Chernyh, N. A., Tourova, T. P., Kolganova, T. V, & Bonch-Osmolovskaya, E. A. (2002). Carboxydocella thermautotrophica gen. nov., sp. nov., a novel anaerobic, CO-utilizing thermophile from a Kamchatkan hot spring. *International Journal of Systematic and Evolutionary Microbiology*, *52*(6), 1961–1967.

Stams, A. J. M., van Dijk, J. B., Dijkema, C., & Plugge, C. M. (1993). Growth of syntrophic propionate-oxidizing bacteria with fumarate in the absence of methanogenic bacteria. *Applied and Environmental Microbiology*, *59*(4), 1114–1119.

Steinbusch, K. J. J., Hamelers, H. V. M., & Buisman, C. J. N. (2008). Alcohol production through volatile fatty acids reduction with hydrogen as electron donor by mixed cultures. *Water Research*, *42*(15), 4059–4066.

Stonestreet, P., & Harvey, A. P. (2002). A mixing-based design methodology for continuous oscillatory flow reactors. *Chemical Engineering Research and Design*, *80*(1), 31–44.

Stonestreet, P., & van der Veeken, P. M. J. (1999). The effects of oscillatory flow and bulk flow components on residence time distribution in baffled tube reactors. *Chemical Engineering Research and Design*, *77*(8), 671–684.

Svetlitchnyi, V., Peschel, C., Acker, G., & Meyer, O. (2001). Two membrane-associated NiFeS-carbon monoxide dehydrogenases from the anaerobic carbon-monoxide-utilizing Eubacterium Carboxydothermus hydrogenoformans. *Journal of Bacteriology*, *183*(17), 5134–5144.

Talaia, M. A. R. (2007). Terminal velocity of a bubble rise in a liquid column. *World Academy of Science, Engineering and Technology*, *28*(5), 264–268.

Tanner, R. S., Miller, L. M., & Yang, D. (1993). Clostridium ljungdahlii sp. nov., an acetogenic species in clostridial rRNA homology group I. *International Journal of Systematic Bacteriology*, *43*(2), 232–236.

Taslim, & Takriff, M. S. (2004). Gas-liquid mass transfer in continuous oscillatory flow in a baffled column. *AJChE Journal*, *4*(2), 1–6.

Temudo, M. F., Muyzer, G., Kleerebezem, R., & van Loosdrecht, M. C. M. (2008). Diversity of microbial communities in open mixed culture fermentations: impact of the pH and carbon source. *Applied Microbiology and Biotechnology*, *80*(6), 1121–1130.

Tirado-Acevedo, O., Chinn, M. S., & Grunden, A. M. (2010). Production of biofuels from synthesis gas using microbial catalysts. *Advances in Applied Microbiology*, *70*, 57–92.

Uffen, R. L. (1976). Anaerobic growth of a Rhodopseudomonas species in the dark with carbon monoxide as sole carbon and energy substrate. *Proceedings of the National Academy of Sciences of the United States of America*, *73*(9), 3298–3302.

Ugwu, C. U., Aoyagi, H., & Uchiyama, H. (2008). Photobioreactors for mass cultivation of algae. *Bioresource Technology*, *99*(10), 4021–4028.

Ungerman, A. J., & Heindel, T. J. (2007). Carbon monoxide mass transfer for syngas fermentation in a stirred tank reactor with dual impeller configurations. *Biotechnology Progress*, *23*(3), 613–620.

Vasconcelos, J. M. T., Rodrigues, J. M. L., Orvalho, S. C. P., Alves, S. S., Mendes, R. L., & Reis, A. (2003). Effect of contaminants on mass transfer coefficients in bubble column and airlift contactors. *Chemical Engineering Science*, *58*(8), 1431–1440.

Vasic, B., Bankovic-Ilic, I. B., Lazic, M. L., Veljkovic, V. B., & Skala, D. U. (2007). Oxygen mass transfer in a 16.6 cm i.d. multiphase reciprocating plate column. *Journal of Serbian Chemical Society 72*(5), 523–531.

Vega, J. L., Clausen, E. C., & Gaddy, J. L. (1990). Design of bioreactors for coal synthesis gas fermentations. *Resources, Conservation and Recycling*, *3*(2/3), 149–160.

Worden, R. M., Grethlein, A. J., Jain, M. K., & Datta, R. (1991). Production of butanol and ethanol from synthesis gas via fermentation. *Fuel*, *70*(5), 875–884.

Worden, R. M., Grethlein, A. J., Zeikus, J. G., & Datta, R. (1989). Butyrate production from carbon monoxide by Butyribacterium methylotrophicum. *Applied Biochemistry and Biotechnology*, *20/21*(1), 687–698.

Xu, D., & Lewis, R. S. (2012). Syngas fermentation to biofuels: effects of ammonia impurity in raw syngas on hydrogenase activity. *Biomass and Bioenergy*, *45*(10), 303–310.

Younesi, H., Najafpour, G., & Mohamed, A. R. (2005). Ethanol and acetate production from synthesis gas via fermentation processes using anaerobic bacterium, Clostridium ljungdahlii. *Biochemical Engineering Journal*, *27*(2), 110–119.

Younesi, H., Najafpour, G., Ismail, K. S. K., Mohamed, A. R., & Kamaruddin, A. H. (2008). Biohydrogen production in a continuous stirred tank bioreactor from synthesis gas by anaerobic photosynthetic bacterium: Rhodopirillum rubrum. *Bioresource Technology*, *99*(7), 2612–2619.

Zhang, Y., Ni, X., & Mustafa, I. (1996). A study of oil-water dispersion in a pulsed baffled reactor. *Journal of Chemical Technology and Biotechnology*, *66*(3), 305–311.

Zhu, H., Shanks, B. H., & Heindel, T. J. (2008). Enhancing CO-water mass transfer by functionalized MCM41 nanoparticles. *Industrial & Engineering Chemistry Research*, *47*(20), 7881–7887.

Zhu, H., Shanks, B. H., & Heindel, T. J. (2009). Effect of electrolytes on CO-water mass transfer. *Industrial & Engineering Chemistry Research*, *48*(6), 3206–3210.